NASA-CR-195547

STIFFENING OF DEPLOYABLE SPACE BOOMS

AUTOMATED PROTEIN CRYSTAL GROWTH FACILITY

NASW-4435

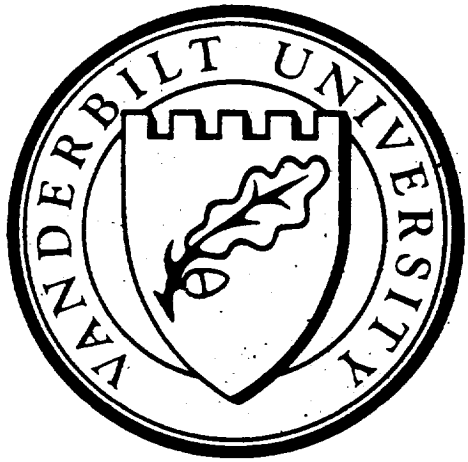

Vanderbilt University
Department of Mechanical Engineering

June 1993

UNIVERSITIES SPACE RESEARCH ASSOCIATION
NASA/USRA ADVANCED DESIGN PROGRAM
MARSHALL SPACE FLIGHT CENTER

1993 USRA/ADP Design Projects

STIFFENING OF DEPLOYABLE SPACE BOOMS

AUTOMATED PROTEIN CRYSTAL GROWTH FACILITY

Vanderbilt University
Department of Mechanical Engineering
Nashville, Tennessee

Dr. Thomas Cruse
Susan E. Ward, Teaching Assistant

Student Teams:

1A - Stiffening System for a Lanyard Deployed Boom
Craig Driscoll, Jay Dyer, Spencer Lisenby,
Wayne Oetinger, Chris Rehberg, Scott Shepard

1B - Stiffening System for a Nut Deployed Boom
Lynne Coleman, Kevin Graham, Don Nordin,
John Rich, David Sims, Brett Susany

1C - System Integration for Stiffened Deployable Booms
Vincent Baria, David Everson, Greyson Gallaher,
Ken Johns, Jason Seay, Rebecca Turner

2A - Protein Crystal Growth Experimental Facility
Clayton Alves, Christopher Chandler, Andrew Cocks,
Stephen Erdmann, Allegra Lewis, Sabina Mohyuddin

2B - Robot End Effector for Automated Protein Crystal Growth
David Anderson, Mike Fowler, Ken Givens,
Robbie Loveless, Joe Martinez, Brian Weston

2C - System Integration for Automated Protein Crystal Growth
Chris Apple, David Beckham, John Bryan,
Melissa Cross, Jason Pierson, Braxton Sealy

Table Of Contents

1 Vanderbilt University Mechanical Engineering Design

Part of the curriculum for the seniors at Vanderbilt University in the Mechanical Engineering Program is to take a design class. The purpose of the class is to expose the students to the open ended problems which working engineers are involved with every day. In the past, the students have been asked to work in a variety of projects developed by the professor. This year Vanderbilt was admitted into the Advanced Design Program (ADP) sponsored by the Universities Space Research Association (USRA) and the National Aeronautics and Space Association (NASA). The grant sponsored undergraduate design and research into new and innovative areas in which NASA is involved. The grant sponsors the Teaching Assistant as well as provides monies for travel and other expenses. This paper documents the design and research of the seniors of the 1992-1993 school year in association with NASA and USRA.

1.1 Program

The USRA ADP program was established to encourage design and research among the undergraduates of member universities. Vanderbilt was accepted into the program in the fall of 1992 and began the designs that following fall. The designs were found by discussing the needs of the class with NASA employees at Marshall Space Flight Center. The engineers and MSFC were very helpful in developing feasible, interesting designs for the class.

1.2 Summer Internship

During the summer of 1992 the teaching assistant for the class the following year, Ms. Susan E. Ward, worked at Marshall Space Flight Center in the Controls and Dynamics Branch (ED 12). Henry Waites, Angie Bukley, and Alan Patterson were developed a research project for the summer of a Linear Momentum Exchange Device (LMED) for the ACES experiment being run at MSFC. The ACES experiment is studying the active control of a continuous longeron deployable boom with a simulated satellite dish on the end. The purpose is to use closed loop dynamic control systems to quickly damp out the vibrations imparted upon the boom. The LMEDs that were being used on the system were only dependable up to 10 Hz. To increase the effectiveness of the system, Dr. Waites suggested increasing the bandwidth of the LMED to 25 Hz. This was the task assigned to Ms Ward for the summer. She studied the LMED and the circuitry involved in the control system. After modifying the circuits and studying the effects upon the response, it was determined that the entire circuit needed to be redesigned to meet the new needs of the LMED.

At this point, Ms Ward was asked to find the design projects for the class from engineers at NASA. She investigated the design projects in the Dynamics area and found the Boom stiffening problem discussed in chapters 3 through 5. Discussions with the Preliminary design groups produced the Protein Crystal Growth experiment for the Space Station design project. With the projects developed for the class, Ms Ward returned to Vanderbilt to begin the school year.

1.3 Fall Term (ME 202 Design Synthesis)

The fall semester was spent teaching the students about design through known methods. The students used the book "The Mechanical Design Process" by David G. Ullman. Dr. Cruse instructed the students on Quality Function Deployment and its application to design, functional decompositions, feasibility judgements, decision matrices, as well as other methods. The students were also to work on

a design individually for the semester. There were three designs from which they were to choose.

The first was to design a new connection system for a washer and dryer which made the maintenance of the appliances easy for a single person. The design could either address the system for moving the appliances so that the connections could be easily reached, or the connections were redesigned for ease of access.

The second was to redesign a water pump which is used by back packers. The current model was hard to hold and operate and required a great deal of manpower to operate. The purpose was to design a more user friendly system which would filter the water to a defined level of purity. Human interaction was a key element of this design.

The third was the design of a hand hygiene system for the restrooms in the engineering building. The students were to account for maintenance, waste, cost and effectiveness of the system.

All three of the designs were redesigns of current systems for improved use. The next semester asked the students to design a system essentially from scratch.

1.4 Spring Term (ME 203 Design Projects)

The spring semester split the class into two different sections. The students applied to the section and team of their choice and presented the skills which they had which would benefit the team. The students were then assigned to the teams accordingly. The two design projects met on different days. Within the groups, the students were split into three different teams. There were 36 students in the class and therefore 6 students on each team. Within the two groups, the team projects were split differently according to the best division of the design. For group 1, the boom stiffening project (chapters 2-5), the teams were broken into two teams which were to design stiffening systems for the two different types of booms , lanyard and nut deployed booms, and then the third team was the system integration team. For the second group, the protein crystal growth project, one team was responsible for design of the science aspect including the crystal growth chamber and interior of the space station rack. The second team was responsible for the utilization of the robot and the interaction of the robot with the experiment through the end effector. The third team was responsible for system integration with the space station.

The class was expected to meet once a week and report on the progress of the team. Oral reports were made to the class via transparencies. Each team member was required to be the group leader at least one week in the semester. Interaction between the groups was greatly encouraged to add to the completeness of the design and reality of the working situation.

Peer evaluations were completed twice within the semester. Once at the mid-semester and once at the end. The students evaluated the other five members of the team on leadership, work accomplished, effort, and group interaction. The evaluations provided information on student performance as well as identifying students who gave extra effort to the projects. The evaluations were averaged and comprised 30% of the individual's final grades.

Each student was required to keep a journal which was to document all actions taken on the design throughout the semester. The journal was to be used to record all telephone conversations, meetings and decisions made. This journal was an additional basis for individual grading.

The design teams were also gave a final presentation. The presentation summarized the work of each group for the semester. The presentations were an hour long and summarized the designs of the three teams in each group. The NASA personnel involved, the faculty of the mechanical engineering department, the dean of the school and the ME freshman class were invited to the presentations.

Each team was also required to write a final report on the work completed for the semester. The reports were to completely document the final design completed by each group. The six team reports comprise the bulk of this final report.

2 Stiffening of Deployable Space Booms

2.1 Abstract

In the future, Earth observation, interferometry, and solar physics experiments will require highly stable and remote platforms on which to operate. One such platform utilizes a deployable boom. Low fundamental frequencies of vibrations in the boom coupled with vibration inducing mechanisms in the experiment as well as movement in the boom base are potentially hazardous for experimentation. One method of minimize the effects of these vibrations the boom is by stiffening, thereby increasing its fundamental frequency. The objective is to provide enough stiffness to increase the fundamental frequency of the boom 5 to 10 times and raise the first mode above 10 - 20 Hz.

Similar to sailboat masts and rigging, the most promising concept for boom stiffening is the use of tensioned cables and spreaders. The boom is transported in a collapsed position and deployed once in orbit, and therefore the stiffening mechanism should be deployable as well. The mechanical engineering design students at Vanderbilt have developed deployable spreader and cable mechanisms for two booms with different deployment mechanism - a lanyard deployed continuous longeron boom (Fig. 2.1) and a nut deployed boom (Fig. 2.2), which are shown without the spreader/cable mechanisms attached.

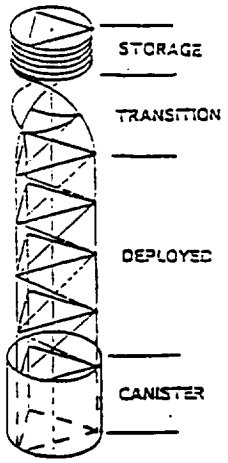

Figure 2.1 : Lanyard Deployed Boom

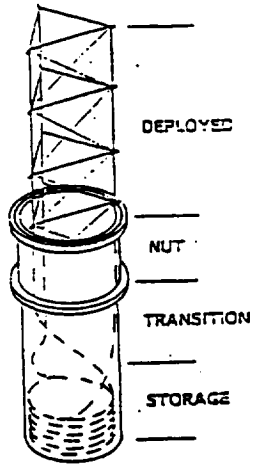

Figure 2.2 : Nut Deployed Boom

The spreader/cable stiffening mechanisms and boom are deployed from a protective storage canister. This canister is designed to attach to an Eagle space module which acts as the base for the boom after deployment. The tip of the boom is designed to accommodate an excitation mechanism capable of exciting the first ten modes of the boom. Accelerometers record vibrational information and relay it to the base, which will in turn relays it to Earth.

NASA will use this experiment for system identification and experimentation. An identical boom and spreader/cable stiffening system will be built at the Marshall Space Flight Center in Huntsville, AL. The experiment will identify differences in vibrational behavior of structures in microgravity and the 1-g environment on Earth. These differences can then be reduced to a set of algorithms which would aid future boom experimentation and application.

2.2 Introduction

Control of large space structures will be important in the future of space applications. These space structures will be the building block of the space program and space structures. The LSS can be constructed or may be self-deploying. The self-deploying trusses require very little astronaut interaction, and are therefor more desirable for certain applications. Unfortunately, the high flexibility of the structures creates problems in application. Therefore, controlling the vibrations of the these trusses is very beneficial.

2.3 Background

The Controls and Dynamics Branch (ED 12) at Marshall Space Flight Center has been working on closed loop control of deployable booms. These boom resonate at very low frequencies and therefore impart a great deal of deflection to the end of the boom. Currently, the branch is working on two booms with an active control system or momentum exchange devices and a computer controlled closed loop. A new concept for reducing the deflection is to increase the fundamental frequency. Similar to sailboat masts, the use of spreader bars and a cable tensioning system would increase the lowest modes and decrease deflection.

2.3 Assumptions and Requirements/Customer Requirements

The customer requirement information session was held at the NASA Marshall Space Flight Center (MSFC) on the date of January 21, 1993. In this meeting, it was learned that the design task involved developing a Controls/Structures Integration (CSI) experiment which would be lightweight, low cost, and support future science missions in interferometry and solar physics, specifically, the overall design project is called the Low-cost Active Structural Control (LASC) flight experiment. The proposition is that a deployable boom be configured so that it is compatible with a spacecraft such as the STP bus. The boom and bus combination will then be sent into orbit for system identification and simple controls experiments, and an identical test will be setup in the ground test facility at MSFC. The main purpose is the comparison of vibrational behavior exhibited by the orbited experiment to that of the 1-g Earth environment.

The role of the two different deployment sub-group is to design a deployable spreader and cable configurations to effectively stiffen the deployable boom. This design task stems from the fact that the deployable booms are rigid structures yet they can have vibrations at very low frequency, and these vibrations tend to interfere with experiments. The concept for vibration actuation through the use of tensioned cables and spreader bars was suggested by NASA.

The overall design objective are:

(1) Design deployable spreaders for the two deployed boom systems (Lanyard Deployed and Nut Deployed).

(2) Determine the spreader/cable configuration such that the fundamental frequency of the sample boom is increased approximately five to ten times. The desired level of vibration is frequencies over 20 Hz. It is important to note that cable configuration refers to the number, placement, and length of spreaders.

(3) Design a cable deployment mechanism which can be integrated into the above concept. Cable tension must have the ability to be adjusted and sensed to 0.5 Newton increments.

(4) Determine accelerometer placement on the deployed boom such that the first ten modes of the structure with and without the cable in tension can be determined. Placement refers to both

number and position of accelerometers.

(5) The operating temperature range is defined as -100° to 100° C.

Other design requirements were developed during the question period following the presentation of the original design specifications. NASA engineers expressed a distinct interest in making the spreader/cable system scalable from a 12 to 18 foot experimental boom to booms up to 300 ft long. They stated that the nominal lifetime of the experiment would be one year, and shielding of the booms with deployable stiffening mechanisms should not be a concern to the overall design. A five pound mass was assumed to be placed at the end of the boom. Finally, the NASA engineers suggested that off-the-shelf items be used in all applicable situations because they are readily available and cheaper.

3 Deployable Stiffening System for a Lanyard Deployed Boom

3.1 Summary

3.1.1 Design Objective

To raise the natural frequency five to ten times of the Lanyard Deployed Boom through deployable stiffening mechanisms for Space Test Program (STP) bus based experiments.

3.1.2 Abstract

The purpose of this design project was to raise the fundamental natural frequency of the lanyard deployed space boom five to ten times through deployable stiffening mechanisms. The boom is intended for use in STP bus-based space experiments. The original boom was modeled using a finite element code to determine the natural frequencies and mode shapes of the space boom. A deployable cable/spreader mechanism was then developed. The system was optimized with respect to the cable configurations, spreader locations, and spreader lengths using a mathematical beam analysis. The design was then modified to meet the deployability requirements. Finite element analysis was then completed on the stiffening system. The vibrational frequencies and mode shapes were determined for the modified system. Knowing the modes of vibration of the stiffened and unstiffened system, proper instrumentation locations were determined. This instrumentation will monitor boom dynamics on station and will allow for determination of experimental mode shapes.

3.2 Glossary

ANSYS	- a finite element code
CSI	- Controls/Structures Integration
FEA	- Finite Element Analysis
GTF	- Ground Test Facility
LASC	- Low-cost Active Structural Control, flight experiment
LDB	- Lanyard Deployed Boom
MDOF	- Master Degree of Freedom
MSFC	- Marshall Space Flight Center
STP	- Space Test Program

3.3 Background

3.3.1 Customer Requirements

The design group met with Angie Bukley, Melody Herrmann, and Henry Waites from the Controls and Dynamics group at Marshall Space Flight Center in Hunstville, AL on January 21, 1993. At the meeting, the specifications of the program were developed. The overall specifications for the design group (1A, 1B,and 1C) are found in section 2.3. The specific considerations of the Lanyard Deployed Boom design group were also developed.

1) Design deployable spreader and cabling system for an Astro Aerospace Corporation lanyard

deployed boom.

2) A 5 meter lanyard deployed boom model with a 23 centimeter diameter form Astro Aerospace Corporation was available for prototype and testing.

3.3.2 Lanyard Deployed Boom Background Information

The lanyard deployed boom differs from the nut deployed boom only in the method of deployment and canister design. The LDB is held in place by the lanyard which holds the boom in its various positions. As the lanyard is unwound by the motor found in the base, the boom deploys. The canister for the NDB is only for shielding and containment. The boom will deploy with out the canister in place. Figure 3.13 shows the deployment of the lanyard boom from its canister. The design of the stiffening system must take into consideration the deployment of the lanyard system. The longeron rotates about 90 degrees during deployment and therefore adds difficulty to the design. The change in diameter of the deploying structure also must be considered.

The deployed boom must be analyzed first to determine the best stiffening system. With the stiffening system developed, the deployment of the stiffened can then be addressed.

3.4 Analyses

The boom was analyzed in several ways. These methods included finite element analyses of both the unstiffened and stiffened booms, a mathematical examination and optimization of the spreader and cable system, and an experimental analysis of the unstiffened boom. Each of these subjects are covered in detail in the following sections.

3.4.1 Finite Element Analyses

3.4.1.1 Unstiffened Boom

Initially, a simple cantilever beam model was constructed using ANSYS 4.4A to model the unstiffened boom. The beam consisted of 35 nodes and 34 3-D beam elements. Node 1 was constrained in all directions and master degrees of freedom (MDOFs) were included for all other nodes. Effective boom values were used for material and geometric properties (shown in Table 3.1). A modal analysis of the model was performed, and natural frequencies and mode shapes were determined. The fundamental frequency was determined to be 2.85 Hz.

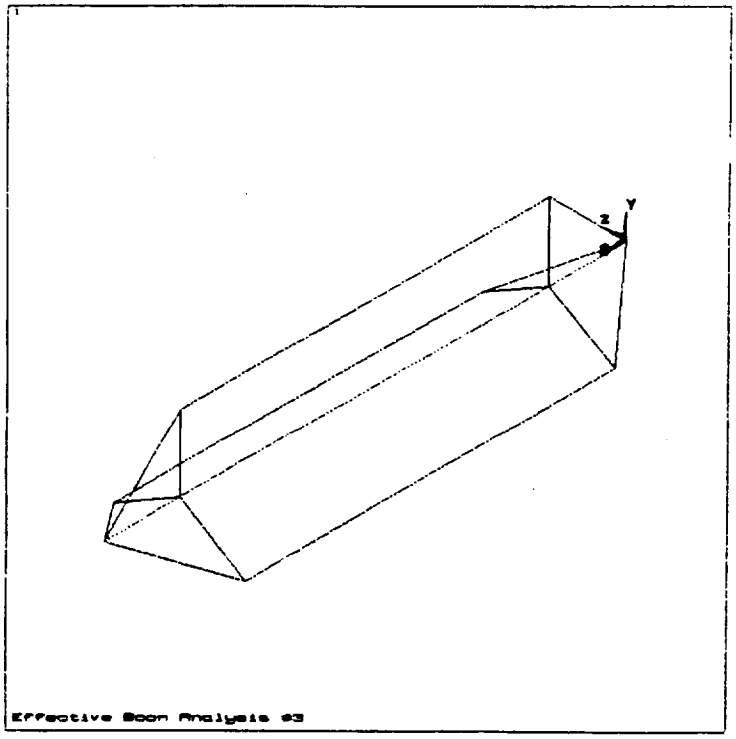

Figure 3.1 : Stiffened Finite Element Model

3.4.2.1 Stiffened Boom

The stiffened boom was then analyzed by the FEM by adding spreaders, cables, and lumped masses for rings. The spreaders were modeled using 3-D beam elements and were rigidly mounted to the beam. The cables were modeled as compression-only bi-linear truss elements. Figure 3.1 is a plot of this model. Prestress was applied to the cables to model the tension in the system.

The first ten mode shapes of the stiffened system were examined. Also, prestress was varied from no tension to 200 N (45 lb) tension. The 200 N tension was used because it was determined that 200 N/cable was necessary to achieve half of the buckling load of the boom. The first, third, fifth, and seventh bending modes were then examined as a function of prestress or tension. These were chosen due to the ANSYS model interpretation which pairs the natural frequencies by giving a bending mode in the y and z directions for each frequency. As Section 3.4.2 will show, the actual boom exhibits this quality in triples due to the boom's three faces. Figure 3.2 depicts the boom's dynamic behavior as a function of cable tension from 0 to 200 N. These values are included in Table 3.2 in the appendix (section 3.10). Mode shapes were obtained for the first four bending frequencies and are included in Figures 3.18 through 3.21 in the appendix (section 3.10.1) respectively.

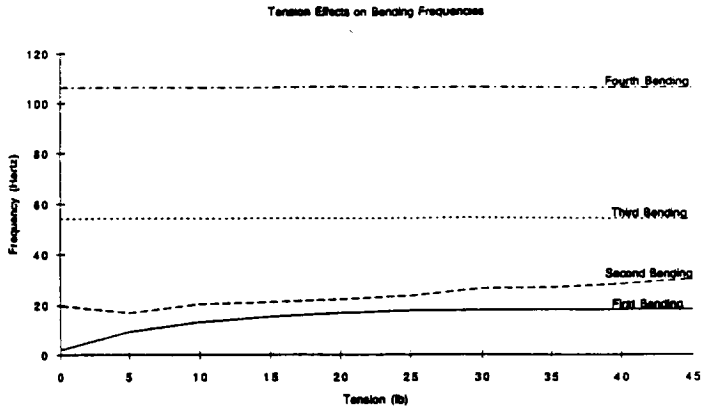

Figure 3.2 : Effects of Cable Tension on Bending Modes

3.4.2 Mathematical Analyses

A numerical analysis was performed using Mathcad. The increased boom stiffness needed to be calculated for varying spreader positions and lengths. An initial analysis proved that the maximum increased stiffness using one spreader only occurs at a spreade r position of L/2 (where L is boom length) on the boom and a spreader length of equal magnitude. This configuration is shown in Figure 3.3, and a plot of increased stiffness versus spreader length is included in Figure 3.4.

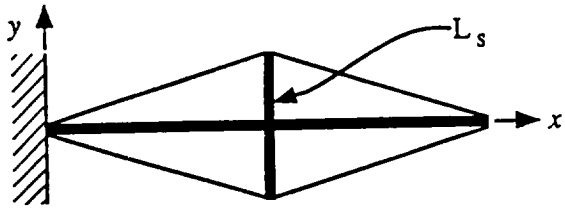

Figure 3.3 : One Spreader Configuration

This boom/spreader configuration resembles a symmetric triangle, and trigonometric and static relations prove that the stiffness is indeed maximized whenever the angle between the cable and the boom is 45°. However, a spreader length of L/2 is large and impractical for larger booms. This insight led to a double spreader design shown in Figure 3.5.

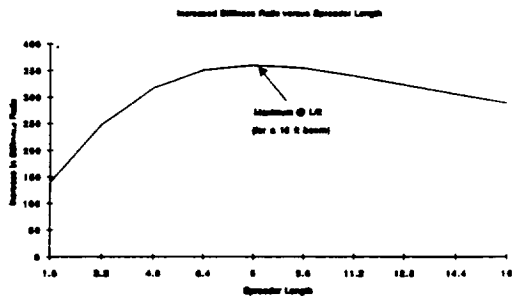

Figure 3.4 : Increased Stiffness versus Spreader Lengths

The spreaders were to start at the midpoint of the boom (resembling the one spreader design) and move incrementally to the ends of the beam. At each increment of spreader movement, the spreader lengths were varied from L/10 to L in increments of L/10. Matrices

containing the spreader lengths and positions along the boom were created, and an iterative solution was used to find the increased stiffness at each spreader length and position. The stiffness is calculated by first finding the original length of the cables between the boom ends and passing over the spreader tips (see Figure 3.22 in Appendix 3.10). Then a force P displaces the boom end and causes the boom to deflect, resulting in a change in length of all of the cables. This change in length is multiplied by the spring constant of the cables (EA/L) to find the tension in the cables. Using static and trigonometric relations, the tension in the cables can be resolved into a resulting force acting on the end of the boom. The normal (to the boom) component of the new force is opposite of the original force P. The deflection of the boom is now recalculated by redefining P as P-f. The ratio of the old and the new boom deflections is the stiffness ratio. Mathcad iterated stiffness ratios for each spreader position and spreader length and produced a stiffness matrix (Figure 3.23b in Appendix 3.10.1). Note that the values for stiffness when the spreaders are at the midpoint of the boom peak at a spreader length of L/2. This corresponds to the previous analysis of the one-spreader design.

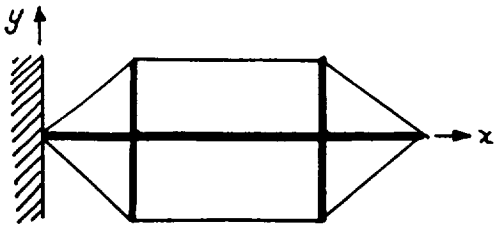

Figure 3.5 : Double Spreader Configuration

The effective mass of the boom in each case of the spreader length and spreader position is calculated by the method shown in Figure 3.24. The effective mass matrix is shown graphically in Figure 3.23a. The x-axis is varying spreader length, the y-axis is varying spreader position, and the z-axis is the resulting mass value. Notice that the effective mass is critical when the spreaders are moved toward the end of the boom.

The natural frequency of the boom and spreader system is calculated to be the square root of the stiffness to mass ratio. This is shown in Figure 3.23c. This surface plot peaks at a value of L/10 for the spreader lengths, and spreaders positioned at L/10 from the ends of the boom. This configuration gives the 45° between the boom and the cables.

The Mathcad iterative solution tries to maximize stiffness while minimizing the effective mass in order to increase the natural frequency. Further examination of the model shows that the length of the spreader must be equal to the distance of the spreader to the end of the boom, thus ensuring the 45° angle between the cables and the boom and a maximum normal force component of the tension in the cables. The analysis minimizes the effective mass by minimizing the spreader length and by maximizing the position of the spreaders. A final constraint considered is the cable length, which is minimized in the analysis (boom deflection is proportional to the cable length). A minimized cable length means minimized spreader length and minimized spreader positions as previously discussed.

3.4.3 Experimental Rap Test

Experimental data was gathered in the form of a rap test. In this test, the Astro LDB was fully deployed and energy was imparted to the structure in the form of an impact. A roll of masking tape was used to impact the boom in order to excite the low frequencies, rather than using a harder material which would excite higher frequencies. The boom's response was monitored with accelerometers. Two accelerometers were placed at the top of one of the longerons. Assuming the axes to be as shown in Figure 3.6, the accelerometers were positioned as shown to measure the accelerations in the x and y directions.

A typical response is shown in Figure 3.7. This is an accelerometer trace of the x (3.7a) and y (3.7b) accelerometer signals. Both plots show three peaks from 2.45 to 2.85 Hz. These are the first

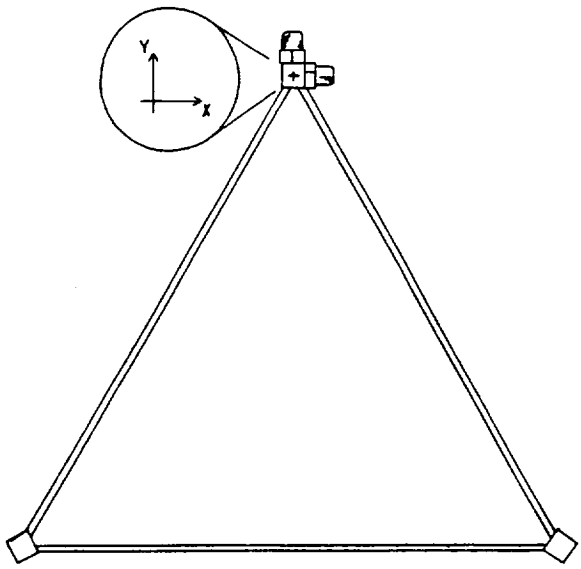

Figure 3.6 : Rap Test Accelerometer Placement

bending mode about the three faces of the boom. The 2.65 Hz peak is very strong in the x plot and

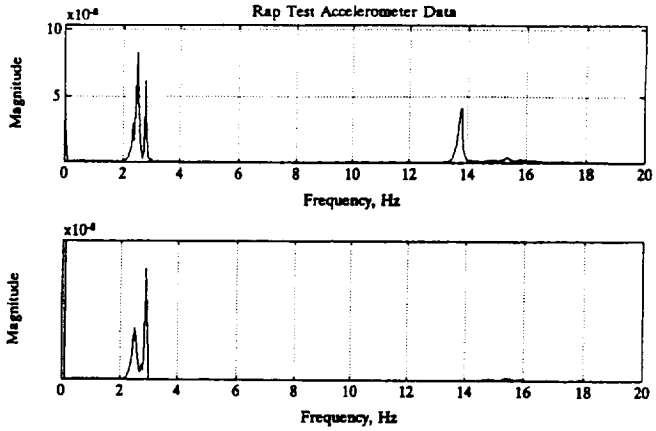

Figure 3.7 : Rap Test Accelerometer Data

very weak in the y plot. This is to be expected and signifies relatively high dynamics in the x direction at 2.65 Hz. This same type of behavior can be seen in the peak at 13.8 Hz in the x direction. This peak does not exist in the y direction, and due to the relative placements of the accelerometers, can be assumed to be a torsional mode. As seen in Figure 3.6, the accelerometer in the x direction will measure torsion while that in the y direction will not. This test shows that the boom has both bending and torsional modes under 20 Hz. Both must be raised to over 20 Hz to achieve the design objective.

3.5 Design Concept

In developing the cable/spreader configuration proposed by NASA, it was determined that cables would run the length of the boom between the spreaders to stiffen the LDB. The boom has a triangular cross section and bends about each face. The cables are tensioned by motors and are attached to the ends of spreaders mounted to the boom in a triangular orientation (Figure 3.8).

During bending in one direction, the cable on the opposite side of the boom will be brought into tension and thus reduce the actual bending of the boom. By this method, the cable tension will reduce the amount of bending the boom undergoes and thus raise the vibrational frequencies.

The major considerations in developing the above system include the following:

Ability to be deployed with the LDB, scaleability, ability to be stored in flight, lightweight design to reduce added mass, method of attachment of the stiffening system to the boom, spreader length and positions, cable dispensing to eliminate the possibility of fouling, method of tensioning the cables. These points are detailed in the following sections.

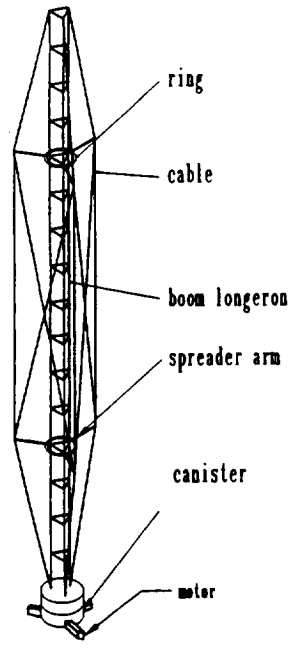

Figure 3.8 : Stiffening System for LDB

3.5.1 Rings

Rings were developed as the mounting interface between the spreaders and the boom. Each ring has three spreaders mounted to it, and it in turn is mounted to the boom (Figure 3.9).

The purpose of this arrangement is to establish a rigid connection between the spreaders and the boom without affecting the structural integrity of the boom.

The shape of the ring serves two purposes. The first is that during storage, the mounting interface must be circular to fit around the coiled longerons. The second is that, when used as mounting devices, the rings are stressed due to cable tension. When the cables are tensioned, forces are directed along the spreaders toward the boom. The rings distribute the stress created by these forces within themselves, rather than allow it to be transferred to the boom. In addition, a circular ring has no stress concentrators which would reduce the strength of the ring itself. Therefore, the boom is not weakened or otherwise adversely affected by the tension in the cables.

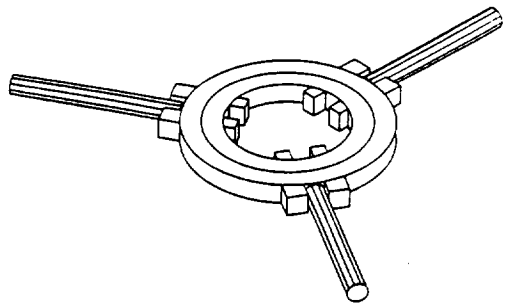

Figure 3.9 : Ring with Spreaders

These rings are mounted to the boom by simple pins. Hinges on the longerons of the boom at designated positions will have pins projecting outward. These pins will interface with holes in the inner edge of the mounting ring (Figure 3.10).

In addition to providing a rigid mount for the rings, the pins allow for the reduction of the cross section of the boom as it deploys.

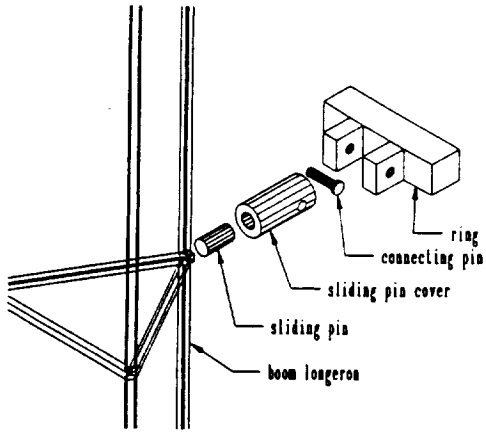

Figure 3.10 : Boom-Inner Ring Interface

The spreaders are mounted to the rings in a pinned hinge arrangement (Figure 3.11).

The pins are attached to the ring by simply-hinged tabs, and allow the spreaders to rotate 90°. The spreaders rotate from parallel to the boom's longitudinal axis during storage to perpendicular to the boom while deployed (Figure 3.12).

A complication encountered in boom deployment involves a transition phase (Figure 3.13) in which the longerons rotate from their horizontal stored position to their vertical deployed position. During this twisting of the boom, the cross section shrinks and then reopens to its full size when the boom locks into its deployed position. The mounting pins slide within the holes (Figure 3.10) when the longerons are drawn inward, and allow the ring to remain attached to the boom.

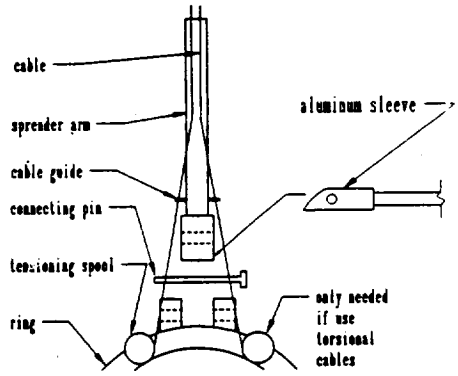

Figure 3.11 : Spreader-Outer Ring Interface

Another kinematic complication occurred when the cables were rigidly attached to the top plate of the boom. The top plate and stored portion of the longerons rotate during deployment. The cables, connected to the tensioning mechanisms, are directed

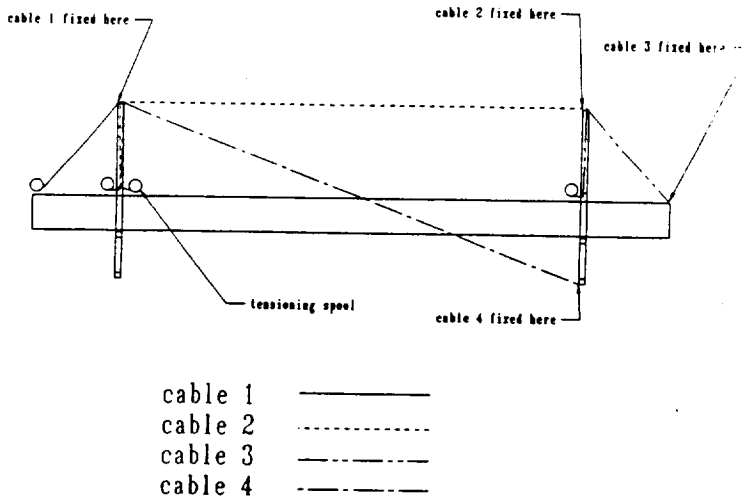

Figure 3.12 : Spreader and Cable Deployment

spreaders are mounted. The ring concept was modified to be composed of two concentric rings connected by bearings (Figure 3.14). In this manner the inner ring remains attached to the boom, and rotates with it during deployment. The outer ring, to which the spreaders are connected, swivels on the bearings to allow the cables to deploy in a straight line. In this arrangement, the spreaders and cables follow a linear path during deployment which eliminates the possibility of line entanglement.

The benefits of the stiffening system would not be realized if the rings were allowed to rotate once the boom is deployed. Therefore, a locking mechanism was added to the rings and top plate to prevent the swivel mechanisms from rotating. This locking device consists of a solenoid and a toothed ring (Figure 3.14). The solenoid is driven by a current and pushes a toothed pin against the toothed ring on the opposite side of the swivel mechanism. The solenoid was orientated to lock the swivel by creating a radial force against the outer ring. Three solenoids are to be used in each ring, one at each pin location, and will effectively lock the outer ring to the inner ring to eliminate any rotation between the two. Wiring for these devices will be run along each longeron and be attached with a lacquer film. The diameter of these wires is very small and will not affect the boom's deployment.

The rings will be made of a graphite/epoxy matrix or some other stiff and strong composite. If using a composite, it would be necessary to use a space-qualified coating to adequately protect the rings from atomic oxygen breakdown. A metal ring would not need to be coated, but would in most cases significantly raise the mass added to the boom which would be detrimental to the effectiveness of the stiffening system. An exception to this would be the use of a titanium which is both light and very strong, but more difficult to manufacture.

through holes in the baseplate, and therefore would get twisted as the boom deploys and the top plate rotates. A swivel collar was developed for the top plate to which the cables were attached using the same basic concepts in Figures 3.9 and 3.14. This collar allows the boom to rotate during deployment and the cables to remain in-line with their through-holes. In this manner, the cables are simply payed out during deployment and follow a straight line.

This swivel mechanism was also applied to the rings to which the

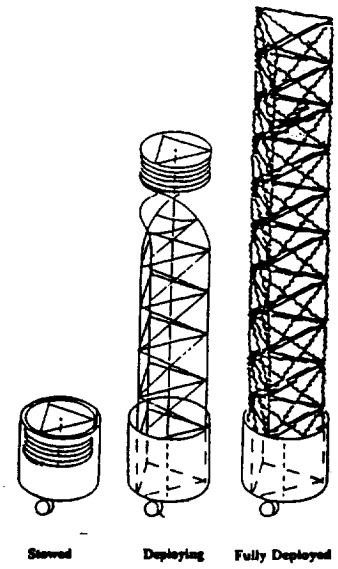

Figure 3.13 : LDB Deployment Stages

3.5.2 Spreaders

The spreaders are long thin tubes of graphite. They are stiff, and hollow to allow for cable routing inside. The outboard ends of the spreaders have teflon inserts to allow for smooth passage of the cables through the tips. The inboard end of the spreaders are mounted in aluminum sleeves for added support and strength while pinned to the mounts on the outer ring (Figure 3.10). The curved surface on the pinned end of the sleeve allows the spreader to rotate 90° during deployment, but no further.

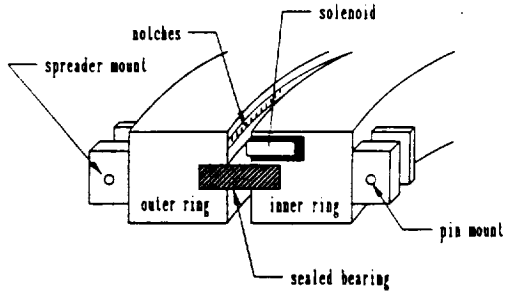

Figure 3.14 : Swivel Ring Cross Section

3.5.3 Cables

The cables are made of Kevlar, a space-proven material high in strength and very low in weight, creep and elasticity. The Kevlar cables are susceptible to atomic oxygen removal, as are the spreaders and rings, so a proper coating would also have to be used to protect the cables. Data on Kevlar can be found in Table 3.2 in the Appendix (3.10.2).

3.5.4 Cable Tensioning Method

The cables are rigidly mounted as described above. The shortest cables, at the base of the boom, are connected to the tensioning devices. Each cable has its own take-up spool/tensioning motor. Having three different motors allows for independent control of each cable. Each mechanism has instrumentation to monitor the tension in its cable and can be driven to match the tension in the other cables. See Figure 3.15 for a schematic of the tensioning mechanism configuration.

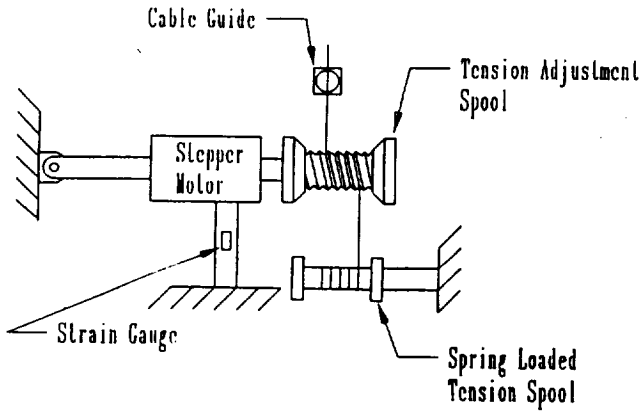

Figure 3.15 : Tensioning Mechanism Configuration

In the LASC program, NASA plans to evaluate boom dynamics at various boom stiffness values, and these different stiffness will be achieved by varying the tension in the cables. The tensioning mechanisms will be used to set a specific tension in the cables in order to establish a desired boom stiffness. Once this tension is achieved, the cables will be locked at the through-holes in the baseplate. A solenoid will be used to clamp each of the cables at these points.

A stepper motor is used to tension the cables. By stepping the rotation of the take-up spool, the cable can be tensioned in known increments. The tensioning device consists of a Hurst Geared SAS (Type SAS4004-001) stepper motor with a step angle of 0.0125°. By driving a take-up spool (threaded for constant diameter) with a 1 cm diameter in 0.0125° increments, the cable tension will be varied by 12 N/step (2.7 lb/step). This motor is capable of producing 1.41 N*m (200 oz-in) torque, which exceeds the 1.02 N*m (144 oz-in) torque required for 203.7 N (45.8 lb) tension in the cables. The maximum cable tension is 282.9 N (63.6 lb) in order to not exceed 69% of the Euler buckling load of the boom.

It is important to note that control of cable tension will not be active in the sense that the motors will change the amount of tension in the cables to damp dynamics during boom excitation.

3.6 Stiffening Mechanism Deployment

3.6.1 Stiffening Mechanism Kinematics

The method of deployment developed involved a parallelogram-type pivoting action. While stored, the spreaders are folded against the boom to minimize the diameter of the stored payload. During deployment, the spreaders are rotated 90° into their deployed positions, perpendicular to the boom. This is accomplished by tensioning the cables at their bases, thus pulling the spreaders from a "flattened parallelogram" state into a rectangle.

The cable arrangement designed to allow this type of deployment involves multiple cables on each side of the boom. The first cable (Cable 1, Figure 3.12) is located at the base of the boom. It is rigidly attached to the tip of the first spreader, and payed out by the tensioning mechanism. The parallelogram deployment action is driven through this cable by the tensioning device. The second cable (Cable 2, Figure 3.12) is rigidly attached to the second spreader tip, runs into the tip of the first spreader, and is wound on a torsion-driven spool. Additional cables and spreaders can be included along the boom as dictated by boom length. Cable deployment will be the same for those, as the design is scalable. The top cable (Cable 3, Figure 3.12) is rigidly attached to the swiveling top plate, feeds into the top spreader tip, and onto a spool as previously discussed.

The cables are contained on the spools while the boom is stowed. The spools are driven by torsional springs which provide light torsional resistance and allow for long cable travel (deployment). The resistance is such that it retracts the cable when slack, but allows the cable to be pulled out during deployment. Due to the latter, the resistance must be very light so as not to hinder boom deployment.

The cable lengths are critical. They must be sized so that the cables draw tight just before the spreaders are pulled into their deployed positions, perpendicular to the boom. In this way, the tensioning of Cable 1 (Figure 3.12) will eliminate any slack and stretch in the cables by pulling the spreaders into their final positions.

3.6.2 Prototype - proving deployment kinematics

A prototype of the deployable stiffening concept was constructed to test the kinematics of deployment of the spreaders and cables. The prototype was built on a 22.86 cm (9 in.) diameter, 4.856 m (191.25 in.) long Astro lanyard deployed boom. The prototype was mechanically similar to the design concept in almost every way, with one outstanding exception.

The model included two rings with three spreaders each, and axial cables (Figure 3.17 in section 3.10.1). PVC tubing was sectioned into 1.27 cm (0.5 in.) long rings to which the spreaders were pinned. These pinned hinges included the aluminum sleeves discussed in Section 3.5.2. Pins were epoxied to the three hinges at two bays to mount the rings. Plexiglas mounting blocks were machined to connect the pins to the rings. The hole in one end was slid onto the pins on the boom, and the groove in the other end provided a track in which the rings could rotate. A swivel plate was mounted to the boom's top plate to allow the rigid cable mount to rotate with the rings and spreaders. Graphite tubing was used for spreaders, and tape measure spools were used to contain the lines. Dacron fishing line was run through the spreaders as included in the design concept.

The prototype worked for the most part. A few rough edges in the model necessitated human intervention during deployment and retraction of the boom. The majority of the problems occurred in

the boom/ring interface, where the greatest deviation from the design concept occurred. This variation involved the substitution of the plexiglas mounting blocks for the concentric swivel rings with bearings. First, the rings did not rotate in the plexiglas blocks as well as the bearings will allow the design concept to do. Therefore, the spreaders and rings had to be rotated by hand occasionally to keep the cables straight. Second, and most importantly, the tolerance necessary for the plexiglas mounting blocks to always work correctly was not met and sometimes the rings would slip off the blocks. This was to be expected since dealing with the kinematics of the transition period was the most difficult aspect of successful boom deployment and retraction. Therefore, it should be noted that the dimensions of the boom/ring interface are critical and must be sized carefully. In summary, the prototype proved that the design concept will work, and the proper boom/ring interface is crucial.

3.7 Instrumentation

The instrumentation with which this design is concerned is comprised of triaxial accelerometers and strain gauges. The accelerometers are to be mounted approximately every fifth bay along the length of the boom, and will be used to map out the mode shapes of the boom during excitation. The strain gauges will be mounted on the tensioning motor support and will be used to derive the tension in the cables. The relationship for the tension in the cables as a function of the strain gauge output is given in the Appendix (section 3.10.3).

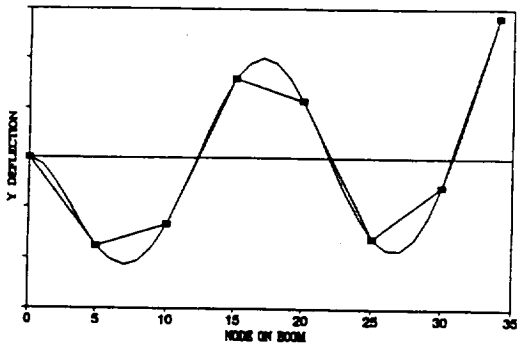

Figure 3.16 : Accelerometer Placement for Mode Shape Determination up to the Ninth Mode

The desired locations of the accelerometers on the boom were determined using a rudimentary method of approximating the mode shapes output by the FEA model. To identify mode shapes, it is desirable to record data on each side of every peak for the highest vibrational mode of concern. Figure 3.16 indicates that for the ninth mode of the unstiffened model, this spacing requirement is approximately every fifth bay. This convention of one accelerometer every fifth bay will allow a quick determination of a given mode of vibration, but will not yield detailed information on the modes themselves. Wiring for the accelerometers will be run down one continuous boom longeron and will pass through the canister at the point designated by the systems integration group.

3.8 Conclusions

The stiffening system design proposed here is as detailed and complete as was possible with the time and resources at hand. The complexity of the boom deployment made it difficult to attach any sort of spreader/cable system, but the swiveling rings and top plate proved to be successful concepts.

Modeling the boom with the ANSYS finite element code was performed as accurately as possible to give an idea of how the boom would act with the spreaders and cables attached. It was found that the simple model did show an increase in the boom's vibrational frequencies with the addition of the cables and spreaders. This supported the proposed design goal.

Finally, the motors and instrumentation provided the means to adjust and determine the resulting stiffness of the boom. This was a requirement that was successfully achieved for the LASC program supported by NASA.

3.9 Recommendations

It is recommended that NASA tailor the design proposed here to raise the natural vibrational frequencies of the LDB. The principle concepts suggested in this stiffening system design are sound, but variations in materials and modeling might be necessary. For instance, a three-dimensional model would yield a much more accurate representation of the non-planar LDB having a triangular cross-section. Related to difficulty in modeling is the fact that the LDB has pre-twist when fully deployed. This poses a much more complex problem when attempting to accurately model it and improve dynamics. In addition, the scaleability of the stiffening system is finite, which means that for longer booms, alterations and adjustments to the stiffening system would have to be made. Finally, work should be done in the area of actively controlling the boom to raise the vibrational frequencies as necessary for experimentation being done on the boom.

3.10 Appendices

3.10.1 Figures

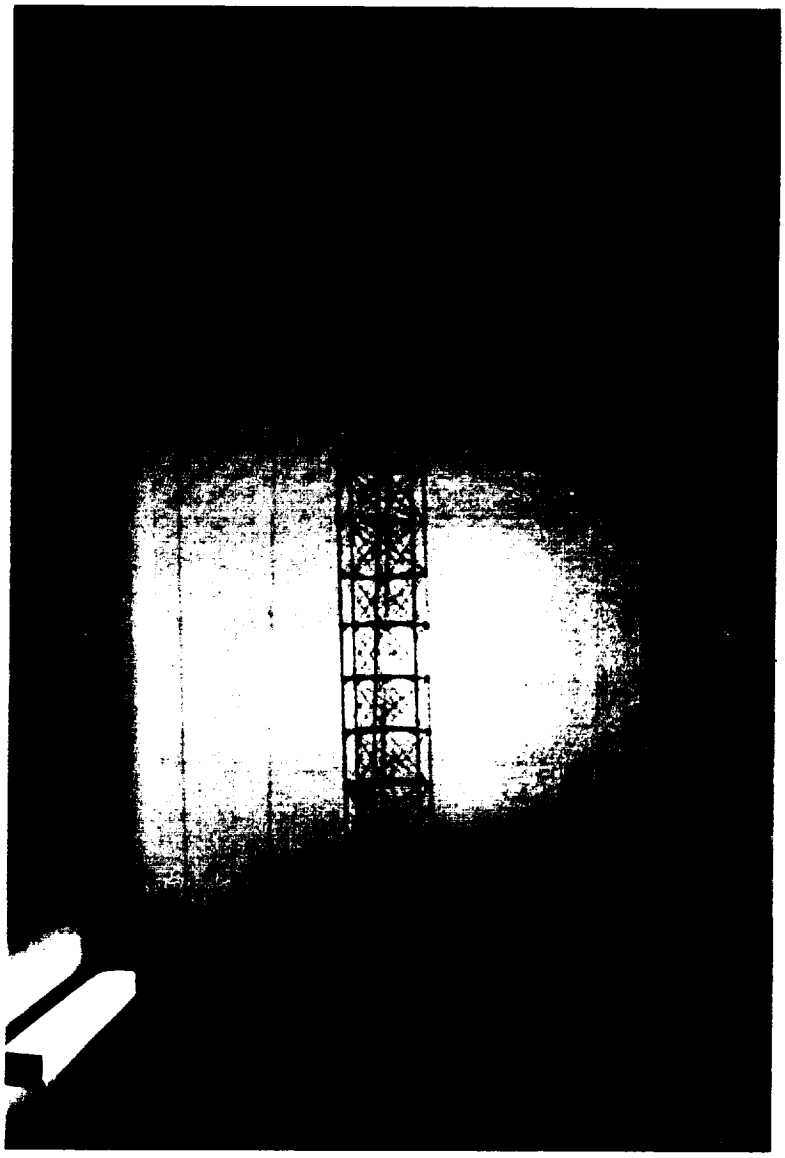

Figure 3.17a : Prototype

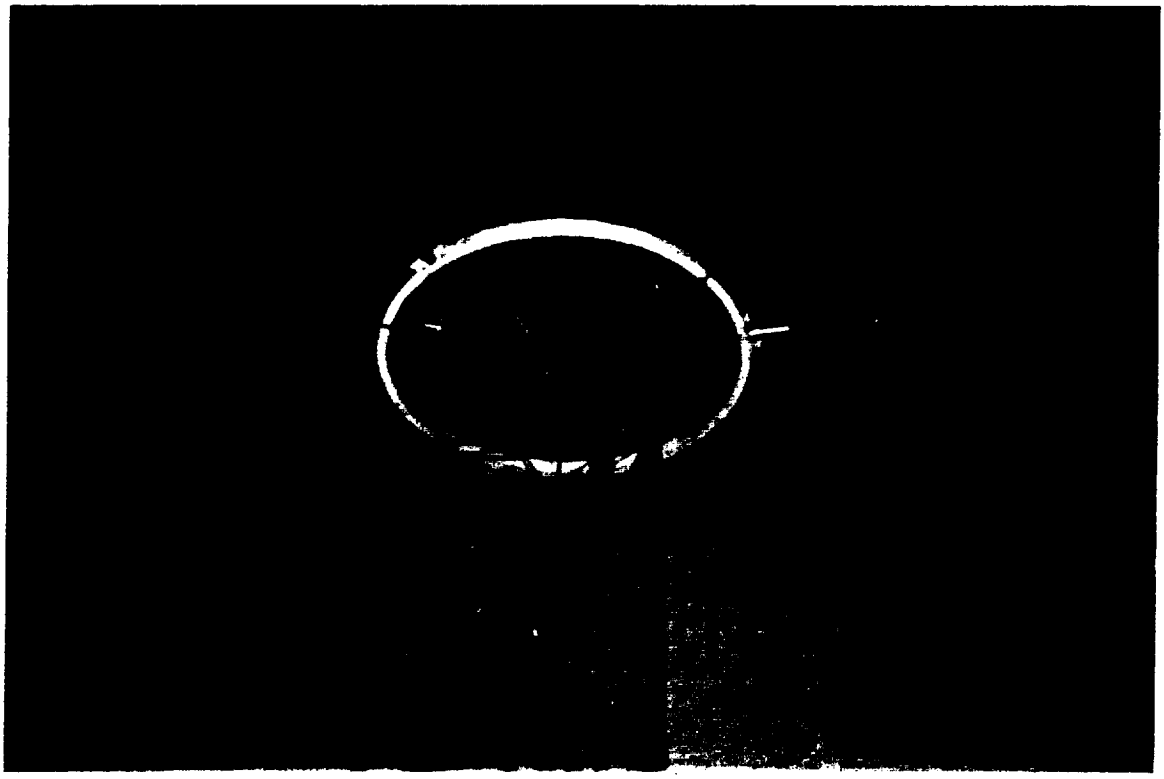

Figure 3.17b : Prototype

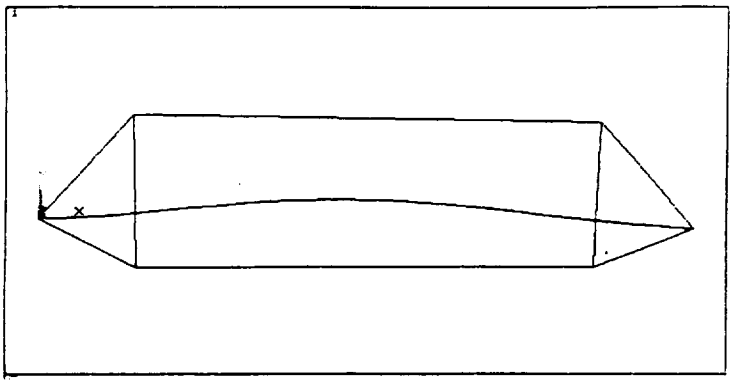

Figure 3.18 : First Mode of Stiffened Boom

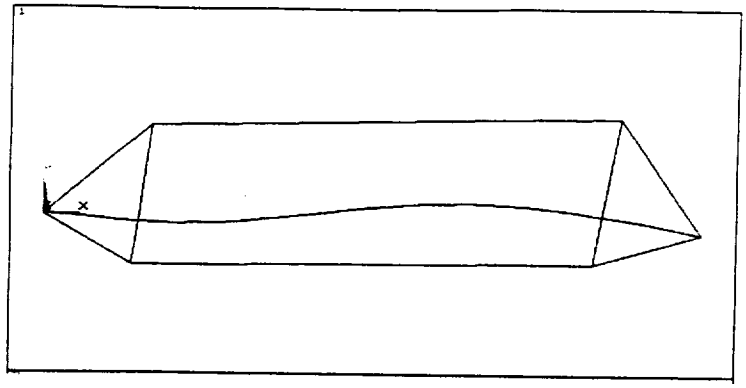

Figure 3.19 : Second Mode of Stiffened Boom

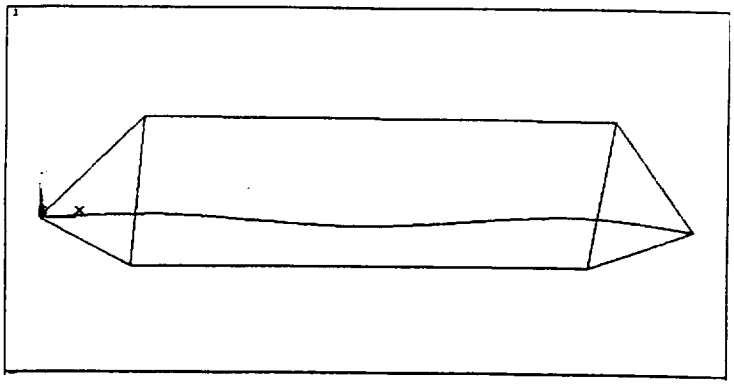

Figure 3.20 : Third Mode of Stiffened Boom

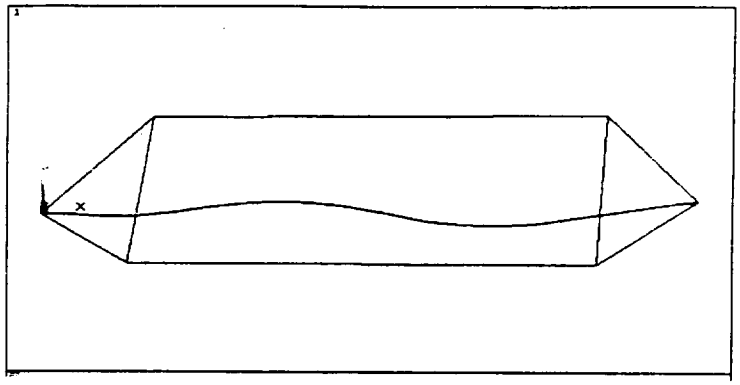

Figure 3.21 : Fourth Mode Of Stiffened Boom

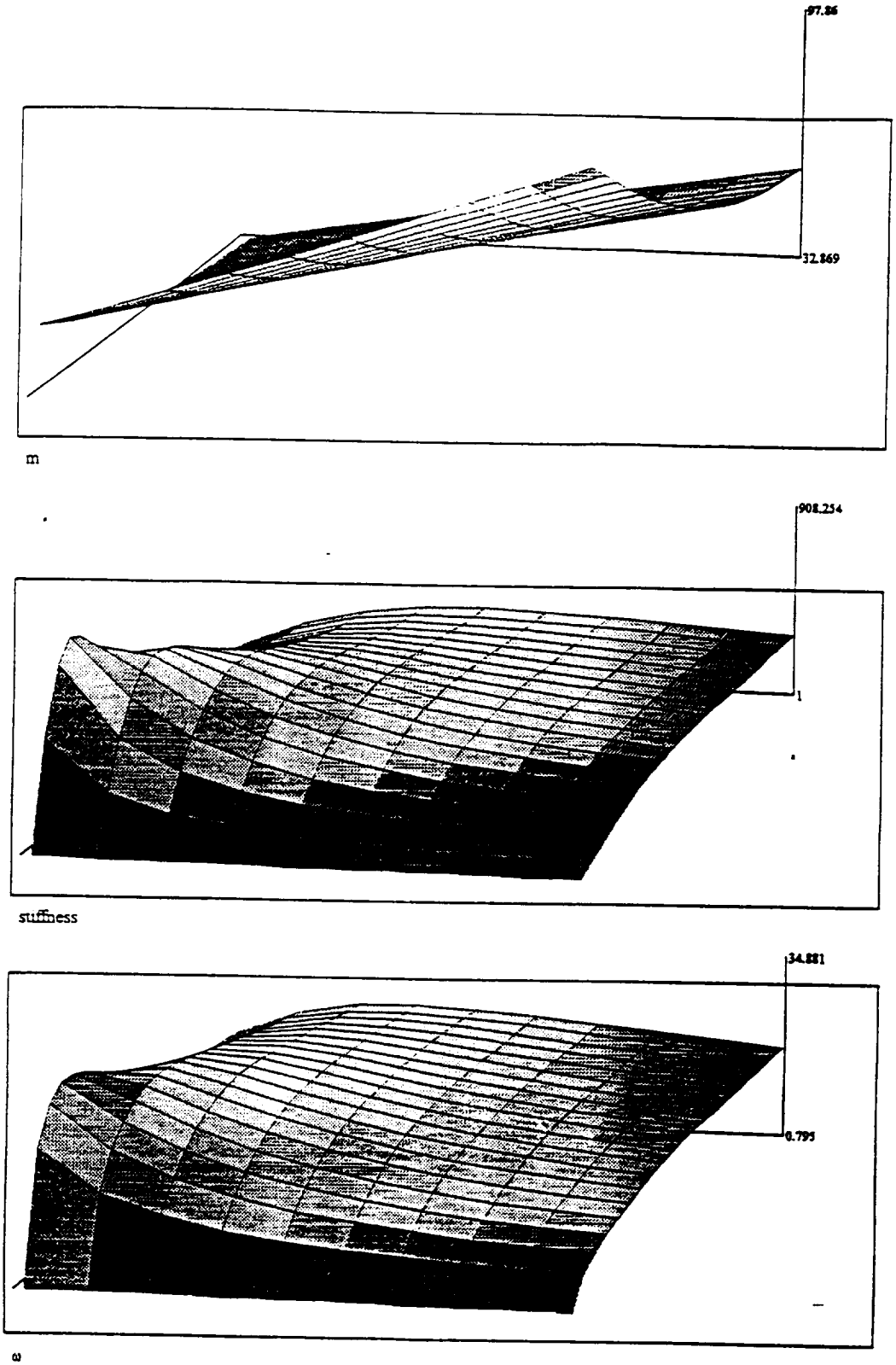

Figure 3.22 : Mass (a), Stiffness (b), and Natural Frequency (c) Surface Plots

3.11.2 Tables

Table 3.1 : Geometric and Material Properties of 23 cm (9 in) Astro LDB

	SI Units	English Units
Diameter	23 cm	9 in
Length per Bay	14.3 cm	5.625 in
Weight per Length	1.764 N/m	0.01 lb/in
E longeron	48.75 GPa	7.07E6 psi
EI	8382 Nm^2	2.9E6 $lb\text{-}in^2$
EA	1.27 MN	0.286E6 lb
GJ Theoretical	243 Nm^2	0.84E5 $lb\text{-}in^2$
GJ Experimental	207 Nm^2	0.716E5 $ln\text{-}in^2$
GA	31.5 kN	7.08E3 lb
M max	27.1 Nm	240 lb-in
T max	2.15 Nm	19 lb-in
V max	18.7 N	4.2 lb

Table 3.2 : Stiffened Boom Frequencies

Bending Frequencies (Hz)				
Tension (lb)	First	Second	Third	Fourth
0	2.01	19.81	54.20	106.35
5	9.21	16.90	54.22	106.36
10	13.17	20.49	54.25	106.36
15	15.31	21.16	54.27	106.37
20	16.87	22.45	54.30	106.37
25	17.87	23.84	54.33	106.38
30	18.02	26.64	54.36	106.39
35	18.33	27.15	54.39	106.39
40	18.38	28.61	54.42	106.40
45	18.52	30.57	54.45	106.41

Table 3.3 : Material Properties of Components

	Kevlar		Graphic Composite	
	SI units	English Units	Si Units	English Units
Tensile Break Strength	3.5 GPa	0.5E6 psi	1.7 GPa	0.25E6 psi
Young's Modulus	130 GPa	19E6 psi	255 GPa	37E6 psi
Coefficient of Thermal Expansion	-2E-6 /°C	-1.1E-6 /°F	NA	NA

3.11.3 Calculations

Undeformed and Deformed Boom and Spreader Positions

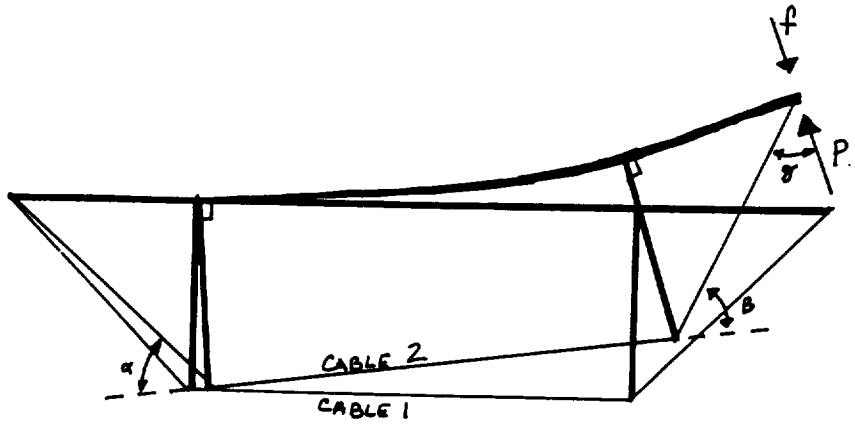

P causes tension in cables that result in force f
Resulting in the parametric equations:

$$f=[(T_1\sin(\alpha)+T_2)\cos(\beta)+T_3]\cos(\gamma)$$

where

$$T_{cableX}=(new\ length_{cableX}-old\ length_{cableX})k_{cable}$$

$$y(x)=\frac{(P-f)x^2}{48\ EI}(x-3L) \qquad 0\le x<L$$

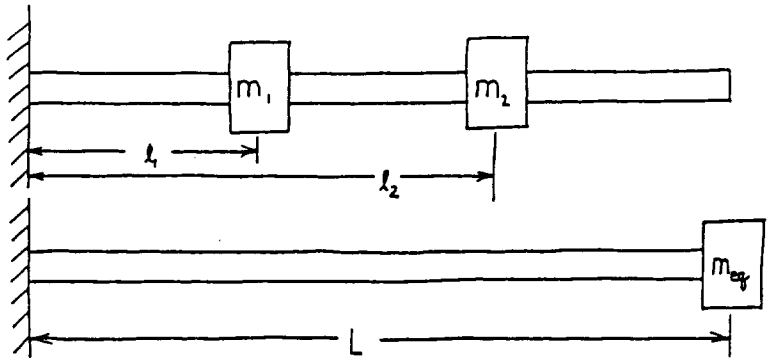

Mass Calculations

Obtaining equivalent mass of cantilever beam:
Use Kinetic Energy equation:

$$T=\frac{1}{2}mv^2$$

Therefore for the beam :

$$\frac{1}{2}m_{eq}x_{deq}^2=\frac{1}{2}m_1x_{d1}^2+\frac{1}{2}m_2x_{d2}^2$$

Relating deflection to rotation:

$$x=r\theta$$

Using ratio of distances:

$$m_{eq}=m_1(\frac{l_1}{L})^2+m_2(\frac{l_2}{L})^2$$

For a mass at the end of a cantilever beam:

$$m_{eq}'=M + 0.23\ m_{beam}$$

Therefore the final equation is:

$$m_{eq}' = m_{eq} + 0.23\ m_{beam}$$

4 Deployable Stiffening Mechanism for a Nut Deployable Boom

4.1 Summary

4.1.1 Design Objective

To raise the natural frequency five to ten times of the Nut Deployed Boom through deployable stiffening mechanisms for STP bus based space experiments.

4.1.2 Abstract

This design report will describe in detail the findings of the design team associated with the nut deployed boom (NDB). The main focus is to design deployable spreader and cable configurations to stiffen the boom, thereby raising the natural frequency five to ten times. This report will explain the final design concepts (including the mathematical modeling, locking and spreader plates, cabling, and instrumentation), conclusions, and recommendations.

4.2 Glossary

accelerometer	- an instrument for measuring acceleration
bay	- portion of the boom between adjacent frames
CSI	- Controls/Structures Integration
FEM	- Finite Element Model
LASC	- Low-cost Active Structural Control
LDB	- Lanyard Deployed Boom
longeron	- segment of the boom which is articulated at the batten frame with universal hinge fittings
MSFC	- Marshall Space Flight Center
NDB	- Nut Deployed Boom

4.3 Background for NDB

Deployable booms can be used for a variety of purposes. They have been used to deploy and support solar-cell arrays, magnetometers, hydrophones, spectrometers, antennas, interferometers or gravity gradient masses. Their light weight and compact stowage make them highly suitable for space applications.

AEC-ABLE ENGINEERING COMPANY, INC. (AEC-ABLE) has developed two types of continuous longeron deployable booms, the nut deployed boom (NDB) and the lanyard deployed boom (LDB). Once deployed, there is no difference in these two booms. The uniqueness of the booms comes from their deployment mechanisms. While the LDB is deployed under its own energy, with the lanyard regulating its rate of deployment, the NDB is deployed with a motorized mechanism.

The canister of the NDB contains four basic regions, as shown in Figure 4.1. The bottom region is the storage region. This is where the boom is stored when it is undeployed. Above this is the transition region. In this region the longerons are guided from their stowed position to a vertical position.

The next region is the nut region. This is the motorized region of the canister. Contained in this region is a three-threaded nut and three vertical guide rails. The three threaded nut rotates, lifting the longerons up through the guide rails via the guide pins on the boom.

Once a section of the boom has left the canister, it is a fully functional boom. There is no rotating of the boom above the canister. This allows the boom to be deployed to any length up to its maximum while maintaining its rigidity. This is an advantage over the LDB, which deploys from the bottom first, and twists as it goes up.

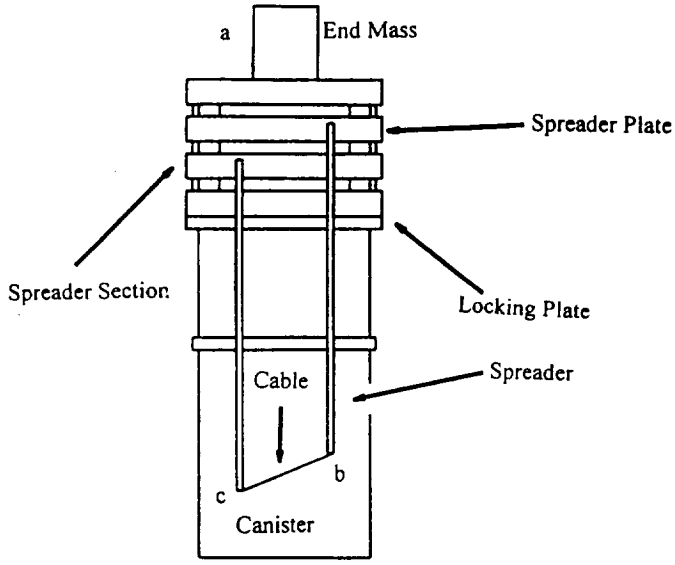

Figure 4.1 : Stiffened Boom in Stored Position

4.4 Analyses

4.4.1 Experimental Testing of the Laboratory Boom

After gathering information from the customer and on the NDB, the next task was determining the actual vibration levels of the deployed boom without stiffening mechanisms. The only boom available for testing was a lanyard deployed; however, as stated in the above, once deployed the nut deployed boom is assumed to be essentially equivalent to the lanyard deployed boom. First, a theoretical evaluation of the lanyard boom located in the Smart Structures Laboratory (SSL) was completed. The deployed boom is 16 feet long and was modeled as a simply supported cantilever beam. The following frequencies were obtained:

Bending Frequency:	2.5 Hz
Torsional Frequency:	21.3 Hz
Axial Frequency:	66.3 Hz

Once the theoretical calculations were produced, an actual experimental test of the lanyard deployed boom located in the SSL was conducted. The boom radius is 4.62 in., and the boom length was 16 ft. Two uniaxial accelerometers were placed at the boom tip in the configuration shown in Figure 4.2. Specifically, the two axes were defined in an effort to detect both bending and torsional frequencies since both were close to the customer requirement in the theoretical analysis. Axial vibration were not monitored.

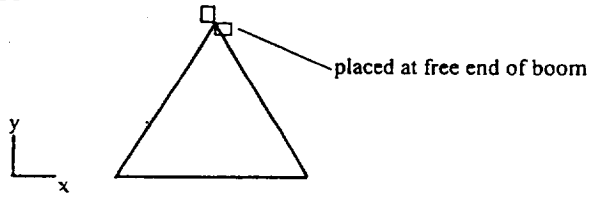

Figure 4.2 : Accelerometer Placement for Testing

Accelerometer data was fed directly into a Tektronic Fourier Analyzer, and the plots such as those found in Figures 4.3a and 4.3b were produced. The upper signal in each plot is the x-axis accelerometer, and the lower signal is the y-axis. The results show that bending modes are found around 2.85 Hz and that torsional modes are found around 13.85 Hz. These number are very similar to those found in the theoretical analysis. The overriding conclusion from this test is that the boom should be stiffened not only to push the bending vibrations past the 20 Hz mark but also torsionally to do the same.

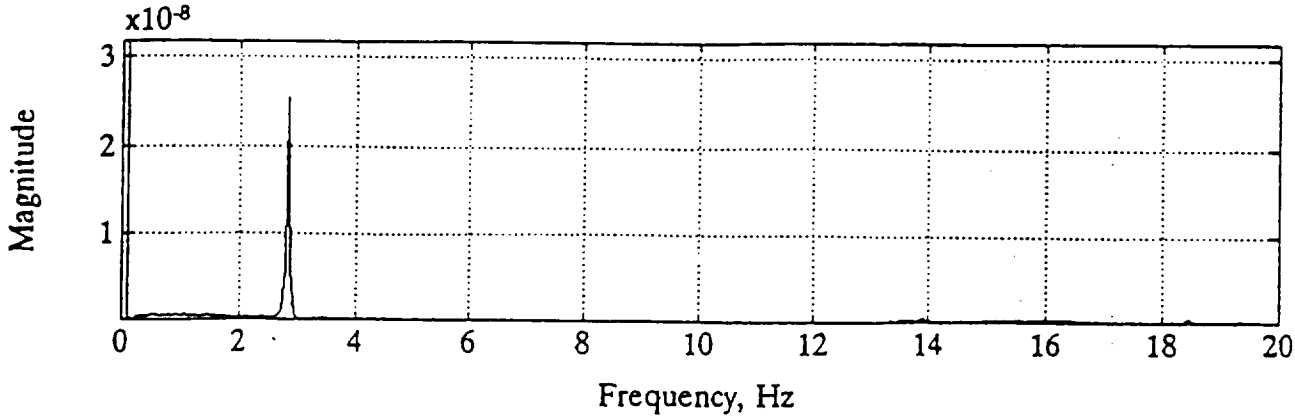

Figure 4.3a : Plot of Torsional Modes

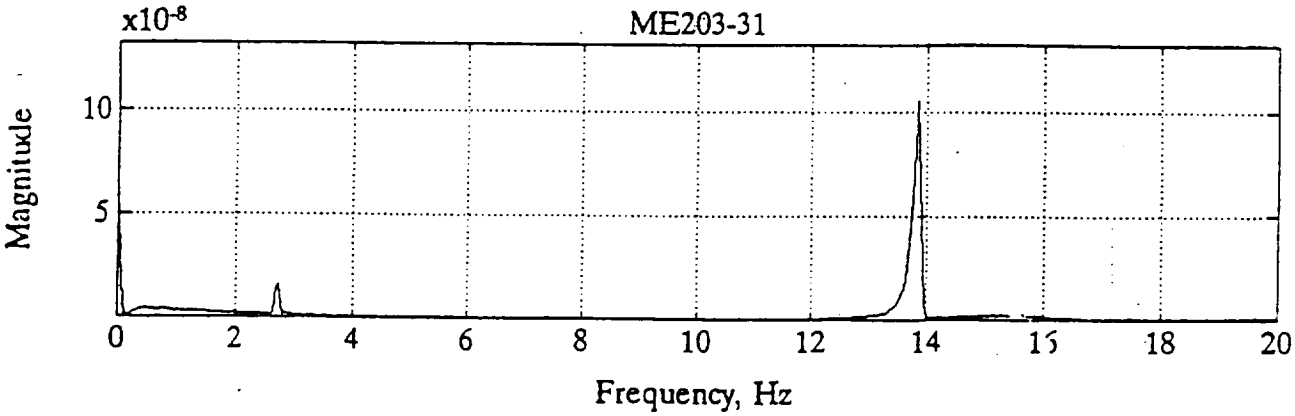

Figure 4.3b : Plot of Bending Modes

4.4.2 Mathematical Modeling for Boom Stiffening

The purpose of the modeling was to determine the optimum position of the spreader arms and the optimum spreader arm length to obtain the greatest rise in natural frequency. Since the natural frequency is the square root of the stiffness divided by the equivalent mass we needed the greatest amount of stiffness while minimizing any added mass. The stiffness must be increased one hundred times more than the mass to raise the natural frequency ten times.

Originally the boom was modeled as a simply supported beam with a center load since we were using a diamond bay configuration shown on Figure 4.4a. The modeling would only represent the stiffening of one diamond bay, not a beam with multiple bays. This is necessary for determining scalability. The greatest stiffness was found when there was only one bay, not multiple bays. To obtain the greatest stiffness for a sixteen foot boom an eight foot spreader arm in the middle is needed. This is not practical due to spacial constraints. Therefore the cable configuration on Figure 4.4b is used. This configuration is scalable and easier to deploy.

The boom is now modeled as a simply supported beam with two load points. The two load points represent the first and last spreader arms attached to the boom. The sixteen foot boom has only two

spreader arms, but a longer boom will have more than two spreader arms where only the first and last affect the boom stiffening.

The stiffening ratio was determined by comparing the deflection of the unstiffened boom with the deflection of a stiffened boom. The mathematical derivation of the mass and stiffness ratios are shown in Table 4.1 found in the appendix (section 4.10.2). The model uses an effective Young's Modulus*Moment of Inertia (EI) term given by NASA for the 16 foot boom. The model also is able to be changed for different cables and different cable sizes. The spreader length and the placement A were varied and the stiffness peaked along a 45 degree angle where the distance A equaled the spreader length Ls. Next the mass ratio was found by dividing the new mass equivalent by the original mass of the boom. The collars and the spreader arms along with the five pound end mass raise the mass equivalent greatly. Each collar mass is a 4.45 N (1 lb) and the spreader arms have a mass of 1.46 Newtons per meter (.1 lb per foot) (These are conservative estimates). Once the stiffness and mass ratios were found, the square root of the stiffness divided by the mass ratio gives the number of times the natural frequency is raised for each placement and spreader length. Using this information, the optimum spreader length can be determined.

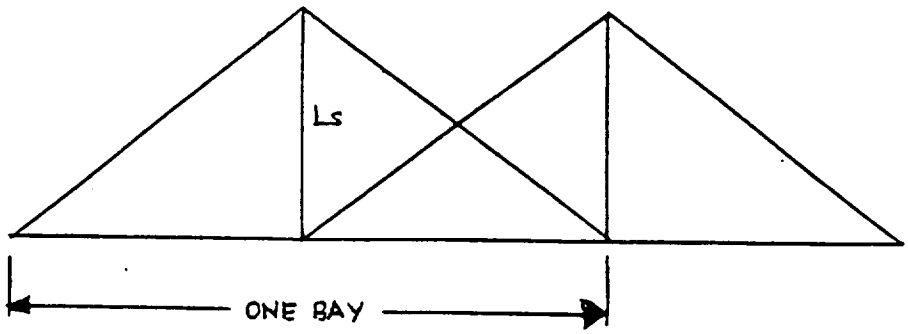

Figure 4.4a : Diamond Bay Configuration

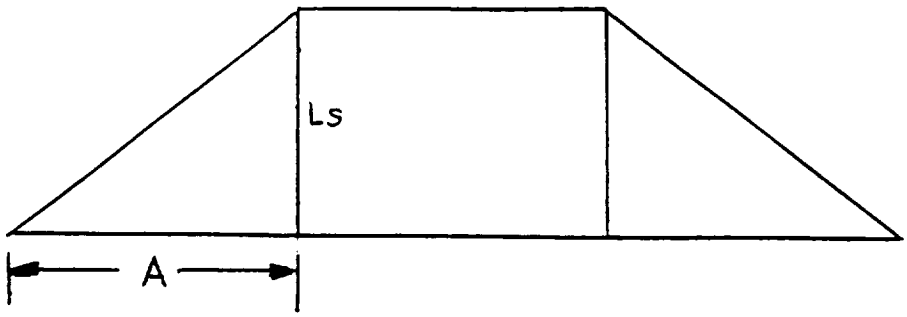

Figure 4.4b : Cable Design Configuration

4.5 Design Concept

The final design concept developed for stiffening the NDB utilizes the spreader and cabling system suggested by NASA engineers at MSFC. As stated in the NDB background information, the boom's canister is made up of three sections--the boom storage

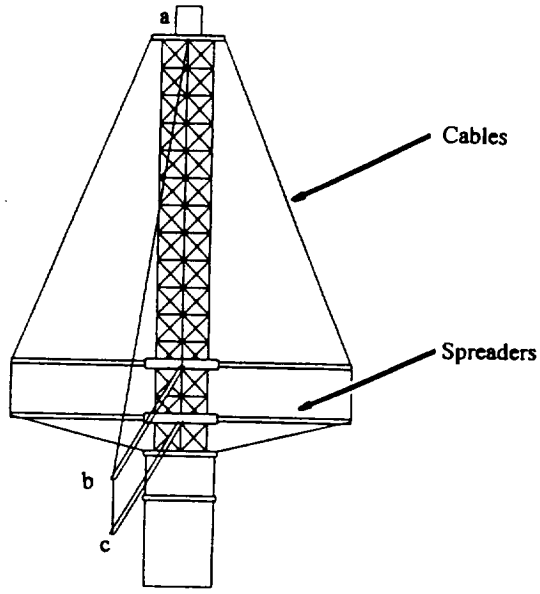

Figure 4.5 : Boom During Deployment

section, the transition section, and the nut section. The nut section contains the actual deployment mechanism which is highly complex. In order to avoid interference with this mechanism, it was decided that a mechanism picked up by the boom external to the canister would be best.

Therefore, another section was simply added to the top of the NDB canister. This section is called the spreader section and consists of three main parts: the top plate, spreader plates, and the locking plate. The top plate is the mechanism rigidly attached to the boom's tip that serves as a home to experiments. This device is shown in Fig. 4.1 with the end mass representing an experiment. The top plate also functions as a base to attach the cables to the booms tip. The spreader plates are the mechanisms to which the spreaders are attached and function to carry the spreaders up the boom at their proper position. Finally, the locking plate is the device that holds both the top plate and the spreader plates in position during launch and until deployment occurs. Figures 4.5 and 4.6 show the stiffened boom in various stages of deployment. It is important to note that the letters used to label Figs. 4.1, 4.5, and 4.6 are included to aid in simulating the actual deployment.

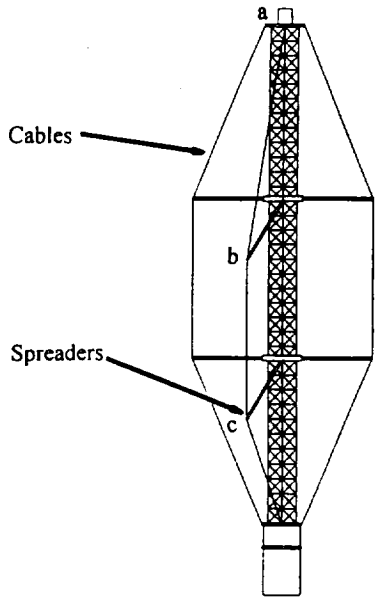

Figure 4.6 : Boom Fully Deployed

4.5.1 Locking and Spreader Plates

The detailed design of the locking and spreader mechanism is better shown in Figure 4.7a and Figure 4.7b. Specifically, the locking plate is rigidly attached to the canister top via screws, bolts, or clamps. Located on the locking plate are three locking pins which correspond to each corner of the boom's triangular cross-section. The locking pins extend upward through each of the spreader plates and end at the top plate. These pins are notched such that the pickup mechanism located on each corner of the spreader plate can hold the plates in place.

The spreader plate's detailed design is circular to allow for nesting of the spreaders along side the NDB canister. Actually, in an attempt to minimize the volume of the overall package, the spreaders were folded down along the sides of the NDB canister using spring hinges for attachment to the spreader plates and for future deployment. However, when this design option was put into place, it was found that each of the successive spreaders interfered with the one below it. Therefore, the spreader plates were made circular and were split into an inner and outer ring represented by the dotted line in Figure 4.7a. The inner ring is attached to the boom via the latch-and-lever pickup mechanism which corresponds to each corner of the boom's cross-section. The outer ring is spring loaded and can rotate relative to the inner ring. Figure 4.7a shows the overall spreader plates cross-section. Now, with this setup, the spreaders could be nested by simply rotating them a few degrees away from the spreader located above. Clamps are then used to hold the outer ring in the nested position. When the spreader plate above the current one is picked up to be carried up with the boom, it releases the clamps allowing the spreaders below to rotate and lock into their proper positions. This position is in-line with the continuous longeron corners of the NDB.

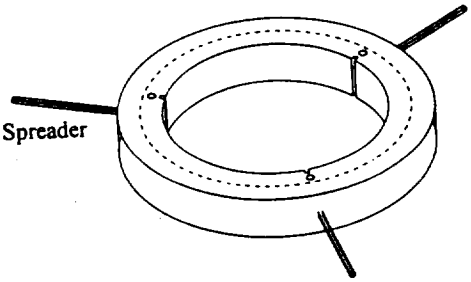

Figure 4.7a : Spreader Plate

The pickup mechanism is the most crucial part of each spreader plate because this is the mechanism which holds the spreaders in place on the locking pins and functions as the transition element in rigidly attaching the spreader plates to the NDB during deployment. A separate pickup mechanism is placed at positions on the inner ring corresponding to each corner of the NDB and is represented by the small slots shown on the inner ring in Figure 4.7b. The design for the pickup mechanism was spurred by a facsimile received from the Astro boom company. The mechanism makes use of a simple spring-loaded latch-and-lever system. When the spreader plates are locked to the locking pins, the latch is engaged. Then, when the boom, which has been prepackaged with pop out pins at each set of bay nodes where a spreader is required, is deployed, these pins pass through the slots shown on Fig. 4.7a. Upon passing through the slots, a lever is flipped which disengages the latch from the locking pins and rigidly attaches the spreader to the NDB. A small prototype of the pickup mechanism was constructed and is currently in the hands of the project manager, Dr. Tom Cruse.

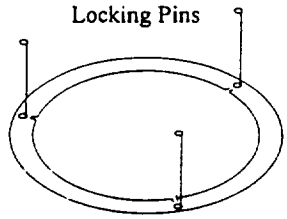

Figure 4.7b : Locking Plate

4.5.2 Cables

4.5.2.1 Attachment of Cables

The cables for the boom will be rigidly attached to the ends of the spreader arms. The lowest spreader arm on the boom will have spools attached on the upper and lower ends of the arm. The spool on the lower side of the arm will attach the cable from the spreader arm to the base of the boom. The upper side of the lowest spreader arm has a spool attaching that spreader arm to the spreader arm directly above it. That spreader arm has a spool attaching it to the top of the boom. The ends of the cables that do not have spools will be attached to eye hooks on the arm.

While the boom is deploying, the spools will be wound up with the cable. As the boom is deploying, the spools unwind the cable until the length of the cable is at its maximum; therefore, the length of the cable must be exactly the distance between either the base of the boom and the lowest spreader arm, one spreader arm to another spreader arm, or from the highest spreader arm to the top of the boom for the tensioning system to operate. While the boom is deployed, but before it is tensioned, the cables will have no slack in them, however, they will not be in tension.

4.5.2.2 Tensioning of Cables

The tension for the cables will be provided by the boom itself. The cables will function passively rather than actively. As the boom is deploying, the cables attaching the spreader arms will reach their maximum length just before the boom is fully deployed. When the boom length is increased, the cables will pull taut. After the cables are as tight as they can get and the boom length is still increased, the spreader arms will bend slightly which will cause an increase in tension in the system. The length of the boom should not have to be increased much for the system to raise its tension.

There are many advantages of this design. The first advantage is that a second motor is not needed to tension the system. There are no clamps on the ends of the spreader arms to keep the cables rigidly attached to the arms, which would probably need actuators to perform the clamping mechanism. The length of the boom does not have to change much to activate the tensioning.

4.5.2.3 Cable Material

The spreader arms had to be connected by some type of cable to perform the tensioning. The requirements to be satisfied by the cable were defined. These requirements are: high stiffness to mass ratio; high resistance to abrasion; ability to be coiled and uncoiled without deformation; satisfactory tensile breaking strength; minimal relaxation. Research was performed to identify materials which satisfy the above requirements. Sources of information were: Vanderbilt Science Library, the Thomas Register, and contacts made through telephone calls. As a result of this research, possible materials to be considered include: Kevlar, Steel, Carbon Fibers, and Fishing Line.

From the research that has been done, it appears that Kevlar is the best material. However, it has been difficult to find information regarding the use of carbon fibers and fishing lines as tensioning lines. Also, it has been difficult to obtain information regarding the abrasion, relaxation, and coiling capabilities of steel and Kevlar cables.

4.6 Stiffening Mechanism Deployment

4.6.1 Prototype

A prototype of the locking mechanism as discussed in section 4.5.1 was developed. The prototype was made of wood and accurately models the locking of the spreader collar to the top of the canister. The prototype was built to enhance understanding of the mechanism involved in unlocking the spreader plated from the canister and attaching them to the deploying boom.

4.7 Instrumentation

Included in NASA's requirements for this experiment is the ability to ascertain mode shapes once the boom has been deployed. NASA is specifically interested in the first ten mode shapes. In order to obtain these mode shapes, instrumentation is needed.

The Finite Element Model (FEM) was used to obtain relative displacements at boom nodal points (joints) over the entire length of the boom. Plots were then made of the first ten modes showing the displacement in the FEM direction of vibration. These plots are included as Figures 4.9. through 4.17. in the Appendix (section 4.10.1). It should be noted that these ten modes include four bending modes in the Y direction (parallel to one side of the boom), four bending modes in the Z direction (perpendicular to one side of the boom), one torsional mode about the boom's axis, and one axial mode. The reason for the difference in frequency for the Y and Z bending modes is geometry. Therefore, there are really only six independent modes. NASA has, however, stated that the number of mode shapes required to be measured is negotiable, and, due to limitations on the space bus, this is the best that can be done without research into methods of sending two signals in a single channel (multiplexing, for example).

Before instrumenting the boom, scalability must be taken into consideration. Although mode shapes on different boom will not be the same, an even spacing with some degree of redundancy of the instruments should map out the mode shapes in any size boom. In comparing the mode shapes predicted by the FEM for a 16 foot boom, a spacing of one device every five boom bays is found to be adequate. A plot of the highest bending mode to be measured with the output measured at every fifth bay overlaid is included as Figure 4.8.

The question now left is how to measure the deflections. Accelerometers are the best suited instruments for this job. Specifically chosen is a Kistler model 8694M1 Low Impedance PICOTRON

triaxial accelerometer due to its small size and weight and the need to measure displacement in all three directions. Seven of these are needed for the boom that was modeled, one on the end of the boom and one at every fifth boom node. These accelerometers will be placed along the inside of one of the longerons with one accelerometer pickup oriented in the vertical direction and the other two oriented such that the acceleration components in each direction (including torsion) can be derived.

Instrumentation is also needed to measure the tension in the cables. This will be done by placing strain gages on each of the three continuous longerons. Since strain is proportional to stress, the total compressive force on the boom can be obtained. This compressive force equals six times the tension in the cables in the vertical direction. It should be noted that the tension could be measured on a single longeron, but slight inequalities in tensioning could not be accounted for.

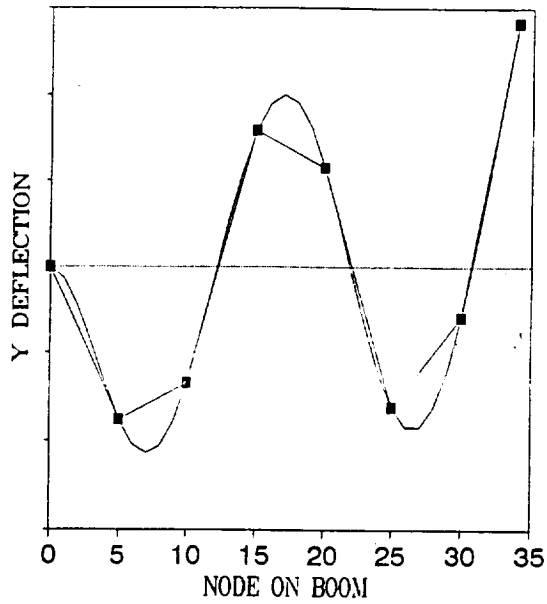

Figure 4.8 : Accelerometer Placement using Highest Bending Mode

4.8 Conclusions

The mathematical modeling results show that the aforementioned designs satisfy the design objective of this project. This model shows the importance of selecting materials that have a high stiffness to mass ratio. The placement and spreader length were varied along with spatial constraints to determine the use of 2.25 ft spreader arms placed 5 ft from the ends of the boom. The model shows that the natural frequency is raised 10 times. The model can easily be used for longer booms by changing the EI term and boom length in the model. Each length boom would have to be evaluated for optimal spacing and spreader length, taking spatial constraints into mind. The tension in the cable does not affect the stiffness of the boom, the cable need only to not have any slack to be effective. These results are somewhat validated by the Finite Element Analysis model created by the lanyard deployed boom design team, but are not validated by a working prototype of the design.

The overall designs use simple elements to avoid fouling potential once in orbit. Spreaders do not interfere with deployment mechanisms due to their location on top of the canister. The nesting of spreaders is used to minimize volume and to avoid interference with other spreaders. With the addition of extra spreader modules, scalability is achieved. Simply input the new overall boom length into the mathematical model and obtain the number of spreaders, their lengths, and locations.

4.9 Recommendation

Many results were obtained from this design project, but due to time constraints, there is a need for further recommendations to continue this project.

4.9.1 Overall Design Considerations

Research into the retraction methods should be completed since currently the stiffened boom will only deploy. A further search of materials for the stiffening mechanism so that the system components are lightweight, yet strong. A working prototype needs to be built to test the ability of the stiffened

mechanism to damp the vibrations and the kinematic function of the nut deployed boom. A better Finite Element Analysis Model should be developed to better predict stiffened beam frequencies. Finalizing the accelerometer placement using improved Finite Element Model methods.

4.9.2 Mathematical Modeling

For longer booms the optimal spacing of intermediate spreader arms to keep the cable tight and from vibrating below a desired natural frequency would have to be found. Furthermore, once the actual collars and spreader arms are made the actual masses should be found and put into the model to determine actual results. Also, the Young's Modulus of the cable was approximated in the model. The estimate was conservative, but for accurate results the actual value should be used.

4.9.3 Cabling Concerns

For attaching the cables, the exact length of the cable for the tensioning system to work and the size of the spool necessary to hold the cable must by addressed. To tension the cables a desired length, the necessary boom length should be researched. Although it has been decided to use Kevlar for the cable material, it is recommended that efforts be continued in the research of other materials with higher stiffness and a higher tensile strength at a lower mass than steel. This will insure a material being selected that best satisfies all of the requirements for a beneficial material for cabling.

4.10 Appendices

4.10.1 Figures

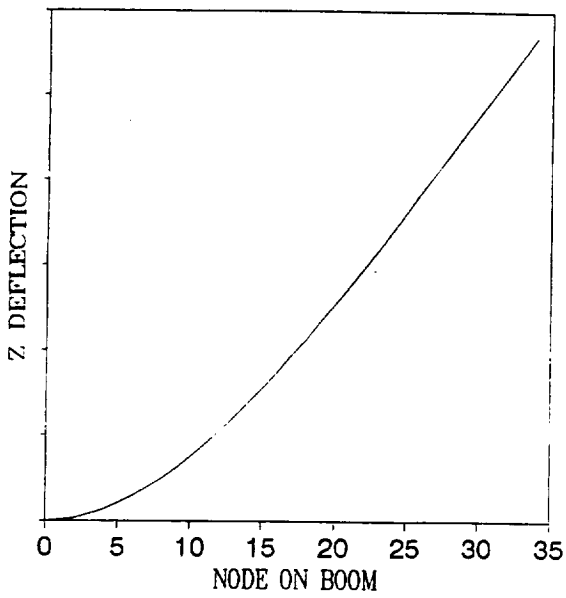

Figure 4.9 : First Mode from Modal Analysis

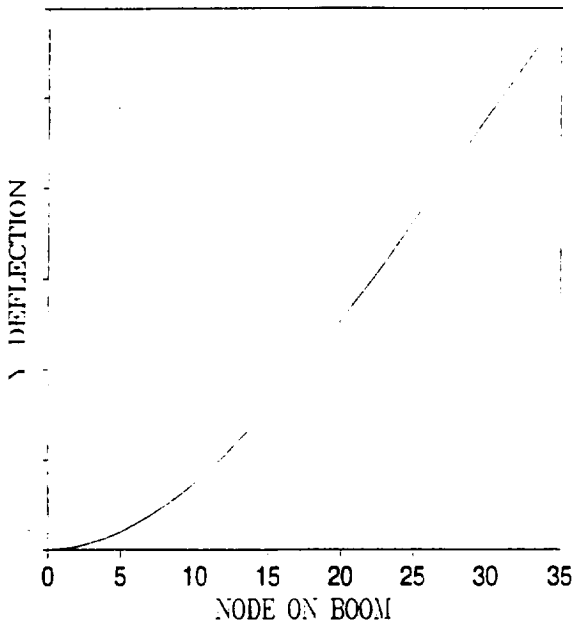

Figure 4.10 : Second Mode from Modal Analysis

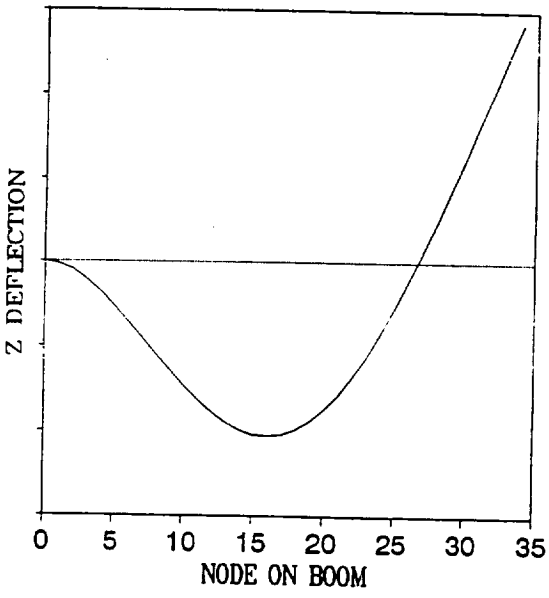

Figure 4.11 : Third Mode from Modal Analysis

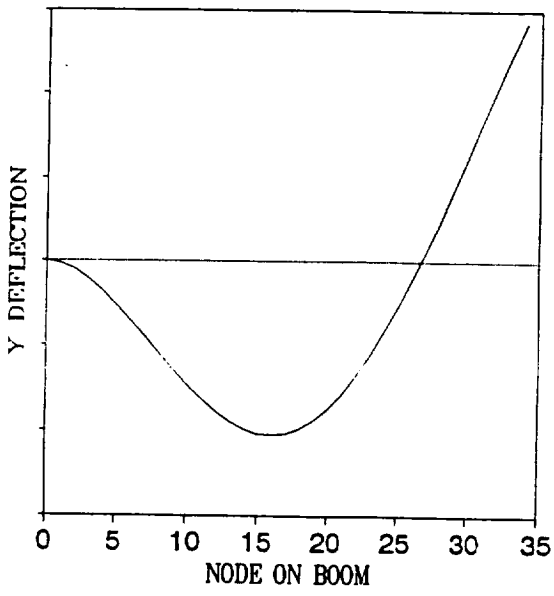

Figure 4.12 : Fourth Mode from Modal Analysis

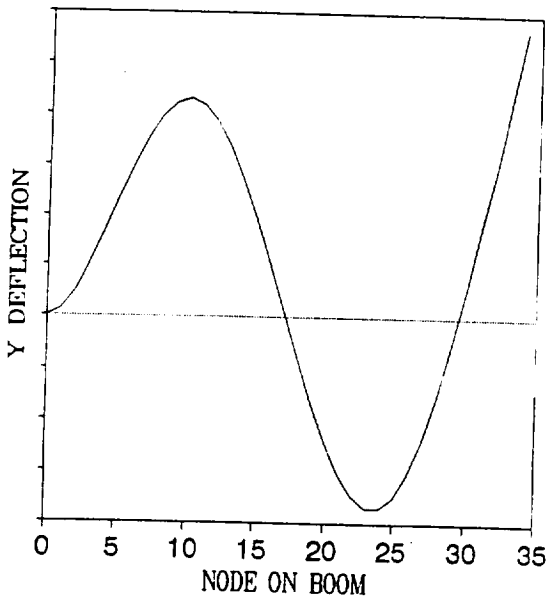

Figure 4.13 : Sixth Mode from Modal Analysis

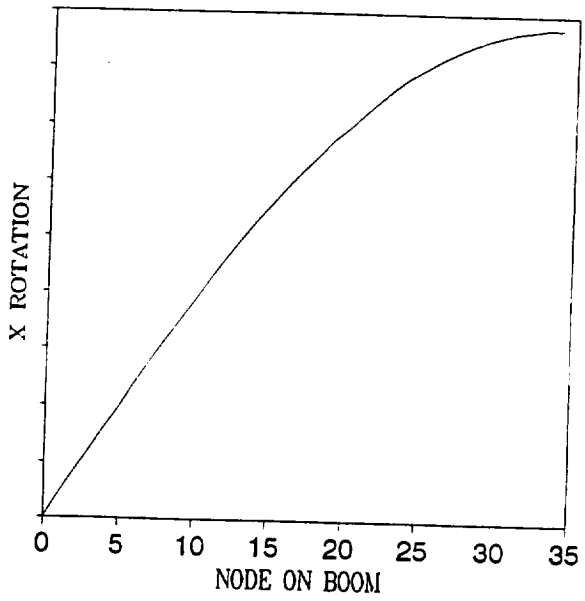

Figure 4.14 : Seventh Mode from Modal Analysis

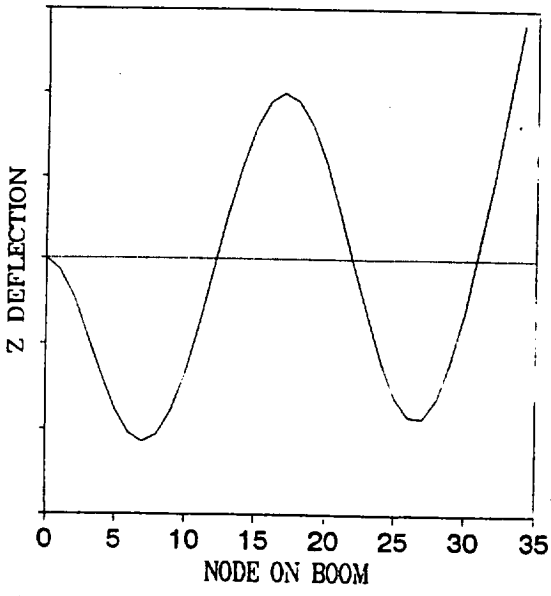

Figure 4.15 : Eighth Mode from Modal Analysis

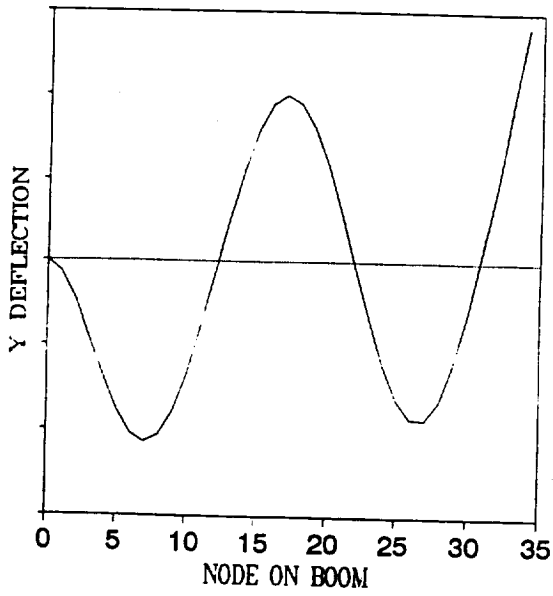

Figure 4.16 : Ninth Mode from Modal Analysis

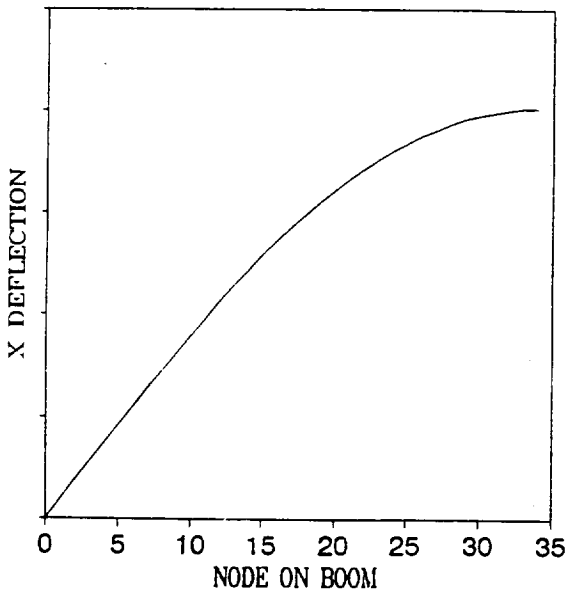

Figure 4.17 : Tenth Mode for Modal Analysis

4.11.2 Tables

Table 4.1 : Mathematical Model

Spreader Length	Stiffness Ratio	Mass Ratio 2 Collars	Frequency Ratio
0.2	145.9701	13.220	3.3229
0.4	289.5574	13.247	4.6753
0.6	430.4225	13.273	5.6945
0.8	567.3107	13.29982	6.531119
1.0	699.0868	13.32636	7.242854
1.2	824.7636	13.35291	7.859172
1.4	943.5208	13.37945	8.397626
1.5	1000.097	13.39273	8.641447
1.6	1054.716	13.40600	8.869888
1.7	1107.326	13.41927	9.083920
1.8	1157.886	13.43255	9.284398
2.0	1252.742	13.45909	9.647681
2.2	1339.156	13.48564	9.965058
2.25	1359.439	13.49227	10.03777
2.4	1417.145	13.51218	10.24105
2.5	1453.021	13.52545	10.36478
2.6	1486.852	13.53873	10.47961
2.8	1548.525	13.56527	10.68427
3.0	1602.493	13.59182	10.85824
3.2	1649.151	13.61836	11.00443
3.4	1688.934	13.64491	11.12554
3.6	1722.31	13.67145	11.22402
3.8	1749.757	13.69800	11.30213
4.0	1771.757	13.72455	11.36196
4.2	1788.783	13.75109	11.40539
4.4	1801.296	13.77764	11.43418
4.6	1809.734	13.80418	11.44991
4.8	1814.514	13.83073	11.45401
5.0	1816.026	13.85727	11.44780
5.2	1814.631	13.88382	11.43246
5.4	1810.664	13.91036	11.40905
5.6	1804.432	13.93691	11.37855
5.8	1796.216	13.96345	11.34182
6.0	1786.271	13.9900	11.29965

5 System Integration for Dynamic Stiffening of Deployable Space Booms

5.1 Summary

5.1.1 Design Objective

To provide a secure, vibration free, physical interface between the Eagle platform and a selected boom and a mechanism to provide a mechanism to excite the boom. The interface will deliver the required power to the specified data locations, be sturdy enough to withstand launch, and flexible enough to prevent interference with the boom excitation.

5.1.2 Abstract

The overall design objective of the class was to increase the stiffness of a deployable boom. In accordance with NASA suggestions, a spreader-arm and cable tensioning system was designed to accomplish this task. Two teams were assigned to develop these systems using different boom deployment mechanisms, lanyard deployment and nut deployment. A third team, our group, was organized to integrate either boom onto an Eagle Space bus. The main design objective was broken down into four major categories: physical interface, power distribution, data handling and telemetry, and testing.

The first objective involved the attachment of the space boom to the Eagle spacecraft. It is assumed that the other two teams will have already attached the boom inside a cylindrical container. Therefore, only the outer canister is left to attach. This canister will be rigidly attached to withstand any both launch and vibrational loads. A simple bolt hole pattern will be supplied.

Once the canister is attached, instrumentation and power must be supplied to the experimental boom. Electric power will be continuously supplied to the Eagle Space bus from solar panels arranged in a sun-synchronous array. This power must be directed to both the control of the satellite and its subsystems, as well as experimental devices.

When the boom is deployed, experiments will be conducted to test the vibrational response of the tensioned boom. This response will be measured by accelerometers and collected with a standardized computer data handling system available on the Eagle satellite. Once collected, the data must be transmitted back to Earth for analysis. An on board telemetry system must be defined to accomplish this task. This telemetry must be performed at regular intervals due to constraints on computer storage.

The final aspect of the design involves the creation of an excitation device. This device must excite the boom at variable frequencies in order to test the effectiveness of the stiffening device. A reaction mass actuator will be designed to excite the boom to at least ten modes of vibration. This actuator was selected due to its superior frequency range and its ability to impart variable forces onto the boom.

5.2 Glossary

ADACS - Attitude Determination and Control Subsystem
ARTS - Advanced Remote Tracking Stations
C&DHS - Control and Data Handling Subsystem
CSTC - Consolidated Satellite Test Center

DSN	- Deep Space Network
EPS	- Electrical Power Subsystem
HS	- High Speed
LASC	- Low-cost Active Structure Control
MRE-1	- Standard TRW Thruster
OSS	- Ground Operations Support Software
RMA	- Reaction Mass Actuator
STDN	- Space Tracking and Data Network
SSS	- Spacecraft Software Subsystem
STEP	- Space Test Experimenters Platform
TDRSS	- Tracking and Data Relay Satellite System
TRW	- Space Support Vendor, Consultant: Steve Thompson

5.3 Background

In the past, NASA has performed space experiments through the use of rigid bodies such as the Space Shuttle and the Titan rocket. Some types of experiments include terrestrial and solar observation, communication, and microgravity experimentation. But as the need grows for more compact and lightweight structures, NASA will need to utilize other means for experimentation. With the advent of Large Space Structures (LSS), many experiments can be performed over a large area simultaneously.

These structures are characterized by rigid central bodies that are surrounded by flexible trusses. These structures take up a large area once in place but are lightweight and compact when being taken into space. There are two predominant classes of trusses: erectable and deployable. The erectable truss involves a large amount of time for astronauts to assemble and requires extra-vehicular activities. The deployable truss requires no man-power; it is deployed by the flip of a switch. Both truss types are inherently unable to maintain complete stability due to their designs. This instability in the booms can cause the experiments to be disrupted or compromised. It is therefore necessary for the booms to be stiffened to increase their natural frequency so that experiments may be performed.

This mission, an operation under command of both NASA and Sandia Laboratories, is to test a method of stiffening a deployed boom. This technique involves the use of spreaders and cables attached to the boom. The subsequent attachment resembles the mast of a sailboat. Once this design is created, it will be attached to the Eagle spacecraft and launched into space by the Minuteman rocket. The pre-launch configuration of the Eagle system is presented as Figure 5.1. The boom will then be deployed and excited for testing. A schematic of the orbiting satellite including the deployed boom can be seen in Figure 5.2, although it is not to scale. Once stiffened, the computer on board must be able to monitor the first ten modes of vibration. Therefore the excitation device will be designed to create vibrations ranging from 0 to 1000 Hz. Observation of the reaction of the boom in various

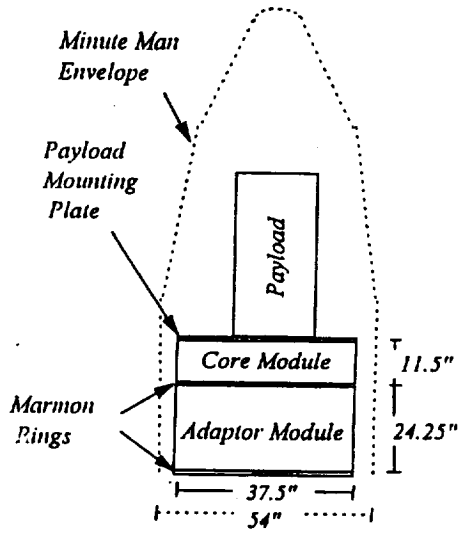

Figure 5.1 : Pre-Launch Configuration of Eagle Satellite Including Payload, Core and Adaptor Module

degrees of stiffness will occur. The information will then be relayed back to Marshall Space Flight Center to be analyzed and compared to an identical boom under the same stiffness in a 1 g environment. NASA requires that the stiffening device be able to increase the fundamental frequency of vibration by at least five times, and preferably ten.

The original design objective was to study the effects of zero gravity on the vibrational performance of space booms and compare these results to similar space booms in a one g environment. Therefore the space boom design was required to include a vibration generator to develop various modes of vibration in the boom. As an initial guideline, NASA requested that the boom be excited to the first ten modes of vibration. This was considered a suitable level of vibration to complete meaningful experiments on the boom and was set as the design goal. The excitation device must be capable of generating a wide range of frequencies because the vibrational response of the tensioned boom is unknown. This range of frequencies ensures that the ten mode shapes will be developed. From finite element analysis, the tenth mode shape of the lanyard deployed boom occurs at 106.5 Hertz. The vibration device must be capable of generating frequencies between 0 and 106.5 Hz, although a wider range would be preferred.

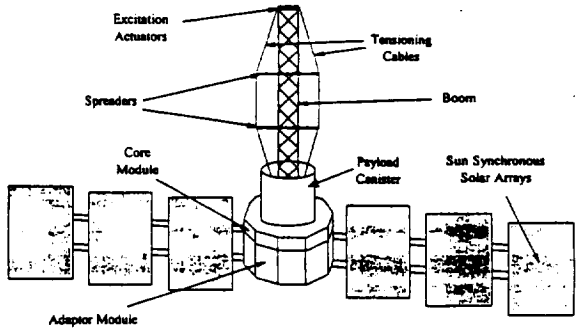

Figure 5.2 : Orbiting Configuration of Eagle Satellite

In addition, the instrument's mass must be limited so it will not interfere with boom dynamics. The initial design requirement from NASA was to include a five pound end mass. Therefore the vibration device selected must conform to this specification. However, the compromise between the mass of the excitor and the force that it is capable of generating must also be considered. Because the forces required to excite the boom are less than one lbf, the mass provided (5 lbm) should be more than sufficient to generate the required mode shapes. The final design requirements were that the excitation device be space qualified and easily mountable on the boom.

The vibrational properties of space booms are often their most limiting factor. Vibrations can be extremely harmful to the boom and its experiments and must therefore be controlled. Currently two types of trusses are employed for space structures: erectable and deployable booms. The erectable booms are preferable for their strength and rigid members, but they are difficult to assemble in space. Deployable booms are more desirable for their compact shipping size and self deployment that does not require any construction in space. The major problem with deployable booms is that they are much less stable, and more susceptible to harmful vibrations than erectable booms. While erectable booms are necessary in large applications, such as Space Station Freedom, self-deployable booms are a preferable choice for smaller applications, such as experiments which require an extended, remote platform. One of the goals of this design project is to test a deployable boom that has an improved natural frequency using a stiffening system. After a stiffened boom is designed, it will be important to test how effective this new system is in handling vibrations. This will be done by exciting the beam to its first ten mode shapes and analyzing its response.

The physical explanation of the phenomena of vibration concerns the interaction of potential and kinetic energy. A vibrating system must have a component which stores potential energy and releases it as kinetic energy in the form of motion of a mass. Vibration occurs in many directions and can be the result of the interaction of many objects. The deployable boom studied this semester has 41 nodes, each with three degrees of freedom, so it is easy to see that this boom will have complex vibrations. The other

groups tackled this problem by adding rigid spreader arms and tensioned cables. The stiffening system, as currently designed, increases the natural frequency of the boom from 2.65 Hz to 18.55 Hz.

5.4 The Design Concept

5.4.1 Boom to Space Bus Interface

5.4.1.1 Forces on Interface

The most important criteria when designing an interface between the boom and the Eagle space bus is to ensure that it will withstand all of the forces applied to it over the entirety of the mission. These forces include those at engine ignition (launch), engine shutdown, pyrotechnic separation of boosters and fairings, and those seen during the boom experimentation. After some calculations and consideration it was determined that the most severe loads would be seen during launch. Thus the interface was designed to meet these requirements.

5.4.1.2 Methods of Attachment

Several methods of attaching the boom to the Eagle were considered. Some of these methods were gluing, space velcro, and magnets. However, bolting was determined to be the best method because of its reliability. Knowing that shear would be the most destructive force on the interface, calculations were done to find the number of bolts needed and the width of each bolt (see appendices, section 5.8.1). It was determined that six carbon steel bolts with one centimeter diameter each would be sufficient.

In designing a way to attach the boom to the Eagle space bus it was first necessary to look at the way the boom is constructed and packaged. In both designs, lanyard and nut deployed, the retracted boom will be packaged in a storage canister that protects the boom during launch and shroud separation. This canister will be made out of 1/8 inch aluminum and will have a filleted flange on the bottom to reduce stress concentration (see Figure 5.3). The flange will be made so that it is 1.2 inch thick and the diameter of the flange will be 20% larger than the canister diameter. This will provide the necessary spacing between individual bolts and the outer edge to prevent tearing of the material due to shear. The finalized bolt pattern described in Figure 5.3, however, cannot be considered launch qualified. Because the vibrational and shock loads associated with a Minuteman launch were not clearly defined, no calculations for the effect of these loads on the bolts were completed.

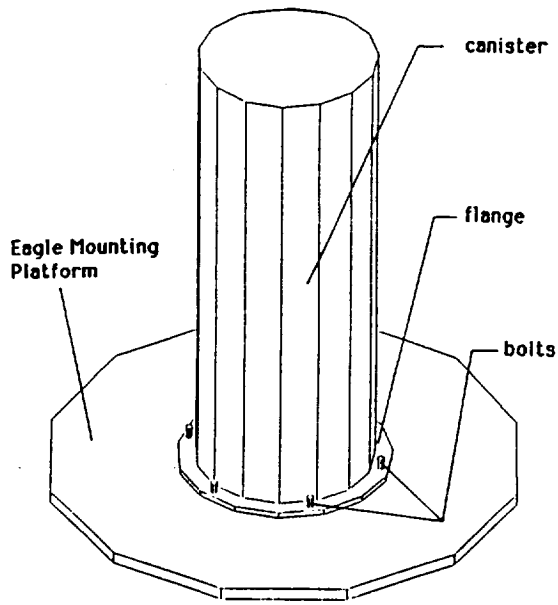

Figure 5.3 : Proposed Bold Hole Pattern

An additional feature of the interface between the core module and boom is an access hole in the center of the bottom of the canister. The hole is required to allow a passageway for the accelerometer and strain gage leads, as well as the electric supply cables for the tensioning motors and the excitation device.

5.4.2 Eagle Satellite Support Systems

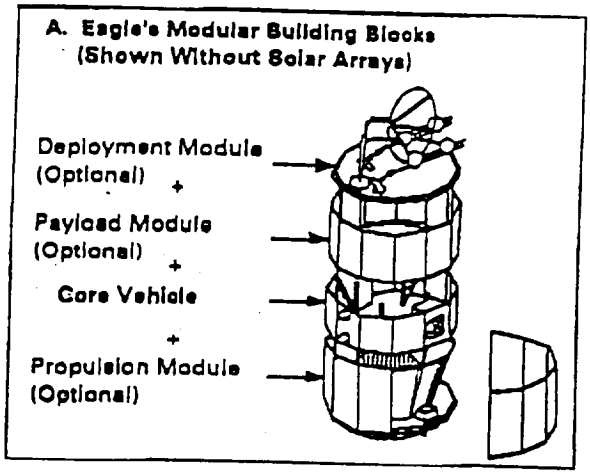

Figure 5.4 : Eagle Satellite's Modular Design

The Eagle satellite was selected as the support system for the stiffened space boom experiments. This satellite is an excellent choice because of its flexibility in design. The Eagle satellite is a Space Test Experimenters Platform (STEP) satellite designed for modularity and quick reusability. The STEP satellite concept is simple. Each STEP satellite is unique because it is designed around the specific requirements of a particular mission. The overall structure of any STEP satellite is modular, with different sections capable of different tasks. The Eagle's structure consists of a core module, various subassemblies, and solar arrays (see Figure 5.4).

The core module is the only required module in the Eagle assembly. The core module is driven by a software based system, which controls all communications, data handling, power, and experimental needs of the satellite. The core module acts as the intelligence of the Eagle design and is required for each mission.

Subassemblies can be included with the Core module as required by the experimenter. TRW has designed specific subassemblies to meet typical user needs. These subassemblies include a deployment module, a payload module, and a propulsion (or adaptor) module. The deployment module is a separable platform used to assemble and test payload deployables. The payload module is simply an enclosed volume dedicated for user payloads. The propulsion or adaptor module includes facilities for orbit maintenance, orbit raising, and maneuvers. If these modules are insufficient for the needs of the user, experimenters have the opportunity to include personally designed subassemblies as required.

The solar arrays of the Eagle satellite also exhibit great flexibility. At least five solar array configurations can be tailored for any mission. The capabilities of the configurations vary but in general they contain from six to twelve panels and can generate from 75 to 300 watts (average orbit) power.

The Eagle concept is truly only defined by the user. Beginning with the core module, the system is expanded by adding subassemblies and changing solar array configurations.

Mission Specific. For the stiffened space boom experiment, the Eagle satellite will require a core module, an adaptor (propulsion) module, and a sun-synchronous array configuration. Each of these components and their use as related to the stiffened boom experiments will be discussed in detail.

5.4.2.1 Core Module Systems

The core module on the Eagle Satellite can be divided into three basic sections: the electrical power subsystem, the control and data handling facilities, and the core module software.

5.4.2.1.1 Electrical Power Subsystems (EPS)

The Electrical Power Subsystem is responsible for generating, storing, regulating, and distributing power to the required drains. A simplified schematic of the EPS is included as Figure 5.5. The EPS

begins with the solar arrays which collect power from the sun. The sun synchronous solar array configuration provides an average of 200 watts power to the spacecraft. These solar panels dump the "raw", (28 volt, DC) power into the mains regulator, which sends the power to the drains if required. Otherwise, the power is sent on to the charge regulator.

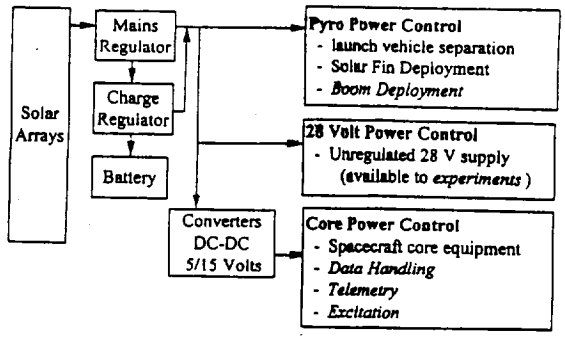

Figure 5.5 : Electrical Power Subsystem Block Diagram

The charge regulator monitors the battery storage capacity, and if there is a need for additional storage the charge regulator will send the power into storage. The charge regulator may also send power directly to the power drains for either of two reasons. First, if there is a power demand greater than the mains regulator can supply, the charge regulator will channel all available power to the drains until the need is satisfied. Secondly, if the solar arrays generate more power than the batteries can store and the drains require, the charge regulator will dump power directly to the 28 volt unregulated drain, thereby protecting the batteries (over charging batteries can result in permanent battery damage). Therefore, either the mains regulator or the charge regulator can send power onto the power drains.

There are three major power drains which feed power to each of the systems: pyro-power control, 28 volt power control, and core power control. The pyro-power control is a power drain with primarily preliminary functions.

Pyro-Power Control. The power from the pyro control (28 volts, 0.65 Amps, DC) is used for separation of the Eagle spacecraft from the launch vehicle. Additionally, the pyro-power control provides all the power for the deployment of the solar fins, and any payload deployables.

28 Volt Power Control. The 28 volt power control is an unregulated supply of power at approximately 0.63 Amps. The 28 volt power control only receives power after the pyro power control and core power control demands are met. Additionally, the 28 volt power control receives a power surge if there is no storage available and all electrical demands are met. For this reason, it is impossible to regulate this 28 volt supply. This power is available for payload users; however, since the current is unregulated, appropriate precautions must be taken before use.

Core Power Control. Power entering the core power control is carefully regulated so as to not overload any equipment. Power entering the core control first passes through electrical converters transforming the standard 28 volt DC power into 5 volt (3.4 A) and $\pm$15 volt (1.3 A) DC power. This power is then used to operate all of the core module equipment, including the telemetry transponder. It is also typical for users to draw the regulated power from the core power control drain.

Mission Specific. For the space boom mission, the solar arrays will be in a sun-synchronous configuration, thereby providing 200 watts total power to the spacecraft. Of those 200 watts, 106 are required to operate the core module base equipment; therefore, 94 watts are available to the payload. The stiffened boom payload has few power drains requiring much less than 94 watts. These power drains include power for the adaptor module (15 watts), telemetry transponder (5 watts), deployment motor (5 watts), tensioning motors (3 at 3 watts), and the excitation device (3 watts). The sum of these drains is at 37 watts, much less than 94 volts available.

The pyro-power control will be used to separate the Eagle spacecraft from the Minute Man Launch vehicle. It is also recommended to coordinate the boom deployment through the pyro power control. The boom deployment is very similar to solar fin deployment in that neither of these drains urgently require power upon demand. The remaining drains: the adaptor module drains, the telemetry transponder, the tensioning motors, and the excitation device are critical to the experiment, do require power upon demand, and should come from the core power control.

5.4.2.1.2 Control and Data Handling Subsystem (C&DHS)

The control and data handling subsystem is responsible for processing, storing, and handling all experimental data. This subsystem can be broken into three distinct parts: mass memory, command and data handling, and the attitude determination and control subsystem. These three areas interact closely with one another to make up the Control & Data Handling Subsystem (see Figure 5.6).

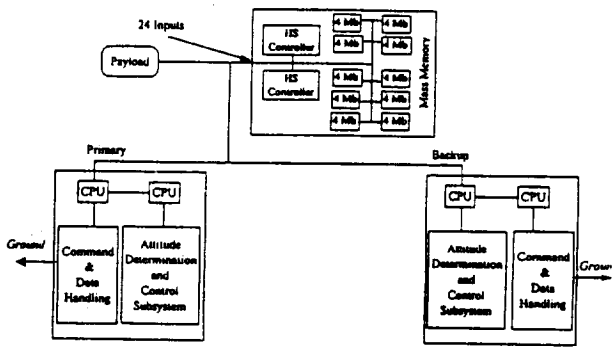

Figure 5.6 : Control and Data Handling System Block Diagram

Mass Memory. The mass memory component of the C&DHS interacts directly with the payload. Data is taken from the payload and enters through 24 input channels directly into the mass memory section. The memory section includes two high speed controllers (one primary and one backup) to manage the memory in the system. The memory consists of ten four megabyte storage areas. In these areas all the mission data is stored including the mission software. When it is required either for processing or downloading, payload data is sent from the mass memory into the main processor.

The C&DHS consists of two identical main processors (one primary and one backup). These processors are connected in parallel so that if there is a problem with the primary processor the backup processor can be quickly engaged. Within the main processors are the command and data handling area, and the attitude determination and control subsystem.

Command and Data Handling. The command and data handling part of the C&DHS is responsible for a variety of mission tasks. This section of the system is responsible for issuing and implementing any payload commands. The state of health of the payload and the satellite is also monitored in this area. Finally, command and data handling is responsible for any communication with Earth.

It is standard practice to download data from the satellite to the Earth using telemetry. The Eagle telemetry system can utilize many existing telemetry networks including:

AIR FORCE:

- Consolidated Satellite Test Center (CSTC)
- Advanced Remote Tracking Stations (ARTS)

NASA:

- Space Tracking and Data Network (STDN)
- Deep Space Network (DSN)

Tracking and Data Relay Satellite System (TDRSS)

The telemetry of the Eagle system is controlled completely by the Spacecraft Software Subsystem (See section 5.4.2.1.3). A small transponder is required to be used on the bus. Data can only be sent through a network when the satellite is in view of the receiving center, and it is not recommended to collect and transmit data simultaneously.

Within the Command and Data Handling section of the C&DHS, it is also possible to upload commands from earth. This is only done for corrections or changes in the original testing and mission plan (stored in the Spacecraft Software Subsystem). Therefore all communications with Earth occur through the telemetry network within the command and data handling part of the C&DHS.

Attitude Determination and Control Subsystem (ADACS). ADACS is the last component of the Control & Data Handling Subsystem. This subsystem is responsible for maintaining the satellite's position in orbit. ADACS collects data from the attitude sensors located in the core module (and adaptor module if included). This data is processed through the ADACS control system. The resulting control commands are then sent to the adaptor module for implementation (See section 5.4.2.2).

Mission Specific. The stiffened boom experiment mission will depend heavily upon the Control & Data Handling Subsystem (C&DHS). Data will be collected from seven tri-axial accelerometers and three strain gages mounted in the payload. The data from this instrumentation will travel into the mass memory through the 24 input channels in the system (21 accelerometer inputs and 3 strain gage inputs). This data will then be stored until it is required to be downloaded. The mass memory contains 40 megabytes of storage; however, because of the memory required for the mission and the memory required to operate the core module, only 28.5 megabytes is available to store experimental data. The data collected during a single excitation test was estimated using the following assumptions:

1. 4 data samples/instrument/cycle
2. 21 accelerometers providing data
3. A test lasts 10 minutes
4. 1 data sample requires 2 bytes memory storage

From these assumptions, it was possible to calculate the sampling rate required to monitor vibrations up to 100 Hz (first nine modes):

$$\frac{100\ cycles}{sec} \cdot \frac{4\ samples}{cycle} = \frac{400\ samples}{sec} \rightarrow \frac{2.5\ mS}{sample}$$

From this sampling rate, the storage required for a single test was determined according to:

$$\frac{400\ samples}{sec} \cdot \frac{21\ accel}{test} \cdot \frac{600\ sec}{test} \cdot \frac{2\ bytes}{sample} = \frac{10.08\ Mb}{test}$$

With only 28.5 Mb memory available, this result illustrates that only 2 complete tests can be stored in

memory before downloading must occur. The time required for downloading can also be estimated:

$$\frac{10.08\ Mb}{test} \cdot \frac{1\ \text{sec}}{3200\ bytes} = \frac{315\ \text{sec}}{test} \rightarrow \frac{5.25\ \text{sec}}{test}$$

From this data a potential test plan begins to take shape. Two back to back tests may be conducted, storing data in the mass memory. After the second test, the data is sent from mass memory through the command and data handling system and down the telemetry network to Earth for analysis. The recommended telemetry network for this experiment is the NASA TDRSS system. This network seems to be well suited for this application and its use is encouraged.

5.4.2.1.3 Core Module (STEP) Software

The STEP program uses software to control all spacecraft commands. This software control allows quick and easy changes thereby avoiding hardware capable of only specific functions. There are two different pieces of software required for each mission: the spacecraft software subsystem (SSS) and the ground operations support software (OSS)

Spacecraft Software Subsystem (SSS). This software is used to control all spacecraft, including payload actions, after launch. The software is coded in ANSI Standard Microsoft C. Once written the software resides in read only memory for quick access. The Software includes standard error detection and correction code, and allows uploads from the Earth. This software is mission specific and is created by the Eagle user for each mission.

The SSS must include code to control the three components of the C&DHS. The high speed (HS) controllers in mass memory rely upon the SSS to manage the memory, collect payload data, organize the data, and transmit data to the command and data handling for telemetry. The central processing unit in the command and data handling section, must coordinate with the EPS all the power requirements of the payload and bus, control satellite (and payload) deployment, distribute payload commands to the bus system, and distribute experimental commands to the payload. The central processing unit in the ADACS requires the software to obtain attitude sensor data, process the data, and implement and required control commands through the adaptor module.

Ground Operations Support Software (OSS). The ground operations software uses a UNIX operating platform to coordinate all ground support efforts. The OSS must also be capable of communicating with and (if needed) changing the SSS. This piece of software is very similar for each mission, and thus it is standard procedure for TRW to create the OSS.

Mission Specific. Although it is the responsibility of the experimenter to develop the SSS, it is likely that TRW has various consultants who have experience writing SSS software. For the boom application, a detailed experimental test plan is to be included in the software. Therefore, once this test plan has been established, it should be routine for a qualified vendor to create the SSS.

5.4.2.2 Adaptor Module

Due to concerns about base stability, the Reaction Control System (RCS) has been included in the design of the Eagle satellite. This system is responsible for the attitude determination and control of the space bus and will ensure that any vibration experiments performed on the boom will not adversely affect the trajectory of the satellite. An additional section, termed the Adaptor module, is required to house the RCS and can be seen in Figure 5.7 along with the core module. As seen, the adaptor module's cross section is that of a 12-sided polygon (0.9525 m (37.5 inches) in diameter) and stands 0.6414 m (25.25 inches) tall. This module is attached to both the core module and launch vehicle with a 0.9652 m (38 inch) Marmon ring. Because a Minuteman launch vehicle is required to lift the satellite to a sun-synchronous orbit, the available payload volume should easily accommodate the additional space required by the adaptor module.

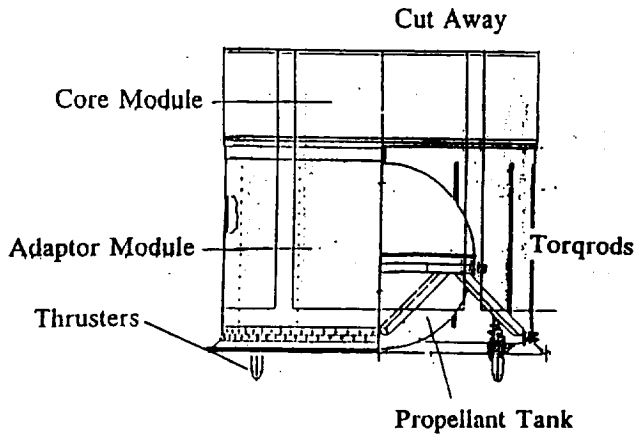

Figure 5.7 : Adaptor Module Layout

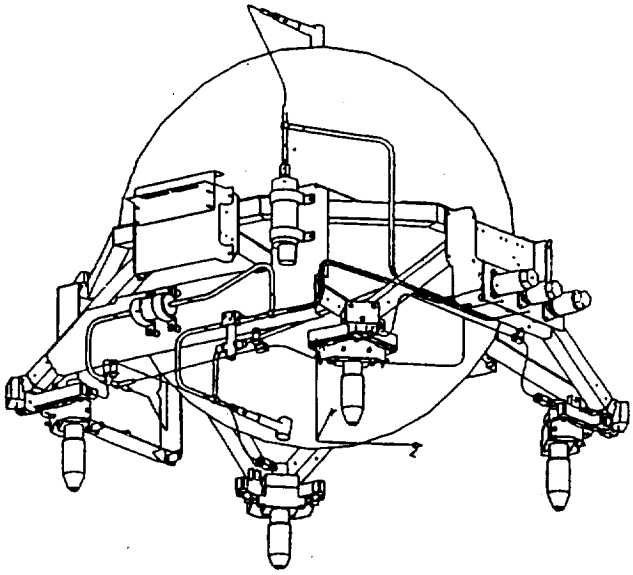

Figure 5.8 : Preliminary Reaction Control System Layout

The Reaction Control System consists of five basic elements: propulsion system, torqrods, reaction wheels, scan wheels, and a magnetometer. Figure 5.8 presents a preliminary layout of the Reaction Control System. The propulsion system is comprised of four 1 lb MRE-1 thrusters driven by a blowdown hydrazine process. The hydrazine fuel is enclosed in a 0.5588 m (22 inch) diameter sphere, which allows 0.091 m^3 (5555 $inches^3$) of storage space. The propellant capacity of this tank is 77.11 kg (170 lbs). The operating limits for each thruster range from a 0.025 second pulse up to a steady state mode. However, if operating in the pulse mode, the thruster firings should be limited to 20 pulses of 50 msec duration per perigee pass. The 0.4064 m (16 inch) moment arm associated with the thrusters allows each nozzle to react a moment of 1.803 N-m (1.33 ft-lb). Using the cantilever beam model equations, this moment can be converted to a force applied to the end of the boom. The resulting force at the excitation location which can be controlled by the thrusters is then calculated to be 0.32 N ($8.37*10^{-2}$ lbf). When compared to the forces required to generate vibrations, these relatively small numbers seem to be reasonable limits.

The Reaction Control System also includes four torqrods. These rods rotate around their bases

and are further measures to react any undesired moments placed on the satellite. A reaction wheel is also contained within the RCS and, like torqrods, spins to counteract any moments placed on the satellite due to the vibration experiments. The scan wheels and a magnetometer included in the RCS are also capable of reacting moments but are mainly used for attitude determination. The elements of the RCS described above are capable of maintaining the attitude of the space bus within ± 2 degrees. Additionally, the devices provided can sense the attitude of the vehicle within ± 0.5 degrees. This very tight attitude control should ensure a very stable boom base and therefore improve the cantilever beam model drastically.

The following mass summary presents the additional weight incurred by adding the adaptor module (STEP Mission 1).

Propulsion system	22.68 kg	(50 lbs)
Propulsion control	4.08 kg	(9 lbs)
Adaptor module structure	1.43 kg	(23 lbs)
Misc hardware	5.89 kg	(13 lbs)
Total	43.09 kg	(95 lbs)

As seen above, the adaptor module will increase the weight of the satellite tremendously. This added mass, coupled with the increased attitude control, at the boom base should improve the cantilever beam model further. However this design obviously did not take advantage of the total propellant capacity of 77.11 kg (170 lbs). Therefore for the current boom testing, it would be advantageous to include all 77.11 kg (170 lbs) of propellant, thereby further improving the cantilever beam model.

After speaking with Steve Thompson, a TRW STEP engineer, several concerns were mentioned dealing with vibration experimentation below one Hertz. When running experiments below this level, the ADACS system must be run in some off-nominal mode for a short period of time. Two modes were discussed that seemed capable of accounting for vibrations below the one Hertz level. The first is a modified delta V mode, in which only the thrusters are engaged. The second is termed a modified safe haven mode and requires that only torqrods operate.

The Reaction Control System described above will not act as an actuator, damping out the vibrations generated, but will rather ensure that the satellite remains on its given trajectory.

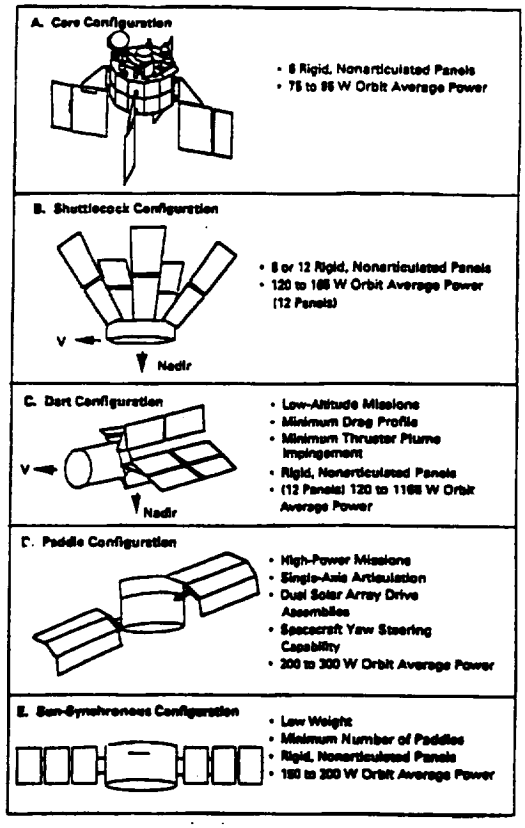

Figure 5.9 : Solar Array Patterns

5.4.2.3 Solar Arrays

Solar arrays are an essential part to the Eagle satellite. These arrays provide all the electrical power required by the spacecraft. The flexibility of the Eagle concept allows the solar arrays to take on any of five different configurations. These configurations are illustrated in Figure 5.9 and include: core, shuttlecock, dart, paddle, and sun synchronous configurations. Each of these configurations has particular advantages. The

core and shuttlecock configurations provide rigid panels with moderate power. The dart configuration is used for low altitude missions, exhibits minimum drag and moderate power. The paddle configuration utilizes solar arrays which rotate to face the sun as much as possible. This configuration provides high power, and enhances the spacecraft's steering capabilities. The sun-synchronous configuration is a low weight system providing moderate power. In this configuration three arrays extend out the diameter from both sides of the satellite. These arrays are immobile and provide between 150 and 200 watts orbit average power.

Mission Specific. For the stiffened boom mission, the sun-synchronous solar array configuration will be used. This configuration provides plenty of power, is low weight, and reliable. The solar arrays begin folded down along the circumference of the eagle (see Figure 5.10) to comfortably fit into the Minute Man launch vehicle. After satellite separation from the Minute Man, the SSS sends the command to the control and data handling system within the core module. This control system instructs the EPS to extend the solar arrays using the pyro-power control. Once the arrays are extended, power is generated and the Eagle comes to life.

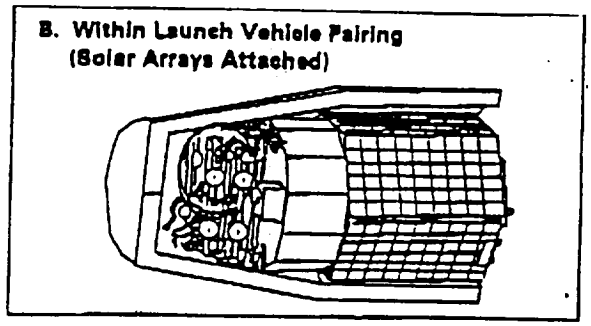

Figure 5.10 : Eagle Satellite in Stowed Position

5.4.3 Boom Excitation

5.4.3.1 Reaction Mass Actuators

A reaction mass actuator (RMA) has been selected to generate vibrations in the deployable booms. This is a relatively new type of vibration generator which has many useful qualities. A reaction mass actuator can be designed to be very lightweight and still generate a wide range of frequencies. Figure 5.11 presents a basic model of the RMA system. A RMA consists of four main parts: the reaction mass, a coil, linear bearings, and a Kaman sensor. The moving reaction mass contains a series of bar magnets arranged in a cylindrical pattern around a stationary coil of wire. This stationary coil of wire is used to create a magnetic field when a voltage is applied. A shaft is rigidly connected to the moving mass and passes through the center of the coil as well as through the center of a linear velocity transducer. This linear velocity transducer senses the velocity of the reaction mass relative to the velocity of the boom. The Kaman transducer is used to sense the distance between its plate and a sensor mounted at the end of the housing. This distance gives the relative position of the reaction mass. The shaft is also free to slide through a set of linear bearings located on the outward sides of the coil and reaction mass. This is clearly seen in Figure 5.12. A certain amount of uncontrollable rolling friction occurs due to the bearings and can be considered part of the damping

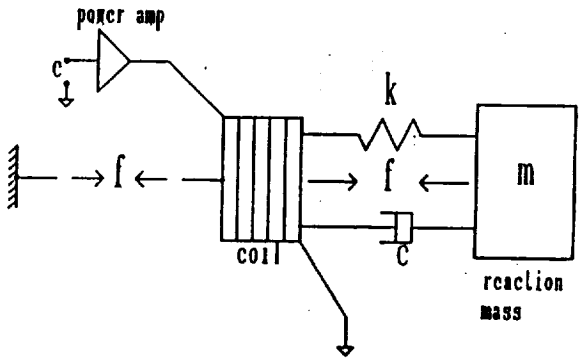

Figure 5.11 : Schematic of a Reaction Mass Actuator

term seen in Figure 5.11. However, the electromagnetic stiffness and viscous damping terms seen are primarily regulated by the two transducers described. By setting up a simple control loop and multiplying the analog signals by appropriate gain constants, both the stiffness and damping can be varied.[3] This in turn changes the natural frequency of the system and the electromagnetic force generated.

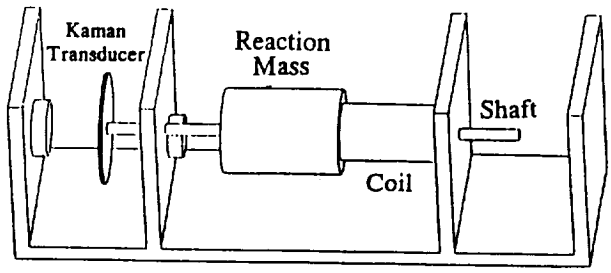

Figure 5.12 : Proposed Reaction Mass Actuator Design

The RMA creates vibrations when a voltage is applied to the coil. The voltage induces a current, which in turn induces a magnetic field that interacts with the reaction mass. The mass responds by translating back and forth. The force created by this motion is a crucial part of the analysis. An equal and opposite force reacts on the structure when the actuator pushes off its reaction mass. This interaction between the two allows the RMA to be space-realizable.[3] The force imparted to the boom can be regulated by the voltage input to the coil and the current driven through the coil. This is essential to the experiment because when the boom is in its original, unstiffened form, it will only require minimal stimulation to start vibrations. The stiffened boom, however, will require greater forces to generate mode shapes.

The force is a function of a force/voltage constant of the RMA and the voltage command signal. The theoretical transfer function which describes the open loop transfer between the force output and the voltage input is given by:[4]

$$\frac{F(s)}{E(s)} = \frac{Gs^2}{s^2+2\zeta\omega_n s+\omega_n}$$

Once this force is known, the acceleration can be found by the simple equation of Force=Mass*Acceleration. This is useful to know in the analysis of the force imparted to the boom.

The RMA is modeled as a simple single degree of freedom system with a spring and damper arrangement modelling a flexible suspension system. The system can be described mathematically as follows and illustrated in Figure 5.11:

$$m\ddot{x}+c\dot{x}+kx=F_o\cos(\omega_{driving}*t)$$

While the mass is a constant value, the spring and damper coefficients can be electrically tuned to their desired values. This then affects the frequency the mass vibrates at and the force imparted to the boom by the mass.[4]

From experimental testing by Troy Link, RMA's have been proven to cover a frequency range between zero and approximately 1000 Hertz. This range should be more than sufficient to generate the required 10 mode shapes. From experimental testing and FEA analysis, the tenth mode shape for the lanyard deployed boom has been found to occur at just over 100 Hz. Therefore the 1000 Hz frequency range available from the RMA surpasses this level ten fold.

The RMA used in our design must also be scaled to interact proportionally with the boom. It

must be designed to have an actuator mass to structural mass ratio of 0.03.[3] For the current boom weights, this ratio yields an RMA mass of approximately 0.68 kg (1.5 lb). This mass is required to ensure that the actuator will be capable of generating the force to excite vibrations in the space boom.

Additionally, the RMA must be easily mounted on the end of the space boom. The ideal mounting position has been provided on the top of the lanyard deployed boom. A flat circular plate, 0.254 m (10 inches) in diameter, is located on top of the lanyard boom. A RMA should be easily designed to fit in this 0.2026 m^2 (314 in^2) area.

Only one reaction mass actuator will be needed on the end of the boom. Earlier, it was thought that we would need to place actuators at strategic locations on the boom, but one RMA can generate all the desired mode shapes, bending and torsional, by itself. This again has been proven experimentally on a space truss constructed at Vanderbilt.

The reaction mass actuator can be used in our design because it is able to fulfill all of the design criteria and customer requirements. The main drawback of an RMA is that it is not commercially available. One will have to be designed and built according to the specifications of this project.

5.5 Conclusions

5.5.1 Physical Interface

The attachment of the boom to the Eagle space bus is most easily and safely done using steel bolts and compatible nuts. This method of attachment is space qualified and highly reliable. Using this method of attachment, a factor of safety of 48 was calculated. (see appendices) This large margin of safety is needed to ensure miscellaneous shocks and forces do not cause an interface failure. Although shear calculations have been performed, this interface is most certainly not launch qualified.

5.5.2 Support Systems

The primary conclusion from the support systems examination, is that the Eagle satellite is capable of supporting the stiffened boom experiments. The Eagle will for this mission will consist of a core module, adaptor module, and a sun-synchronous pattern of solar arrays. Of the 94 watts power available to the user, approximately 37 watts power will be required to power the payload during experimentation. Data will be taken through 24 data channels from 7 tri-axial accelerometers (21 inputs) and 3 strain gages. With only 28.5 Mbytes storage available to the user, it was estimated that only 2 complete tests sampling 100 Hz frequencies at a 5.25 mS sampling rate, can be stored before downloading must occur. The Ground Operations Support Software (OSS) will be complete by TRW, while it is the experimenter responsibility to create Spacecraft Software Subsystem. The adaptor module plays the most critical role in ensuring a reasonable cantilever beam model is achieved on the Eagle satellite. The additional mass of this system, coupled with the tight attitude control, should prove reasonable the assumption of a cantilever beam.

5.5.3 Boom Excitation

The Reaction Mass Actuator is capable of generating the forces necessary to excite vibrations for testing. This type of actuator has been used in the past in space applications, and is the most suitable choice for the current design specifications. The RMA is also capable of generating frequencies up to 1000 Hz. The customer requirements, therefore, can be fulfilled and the specification of generating 10 mode shapes will be met.

5.6 Recommendation

5.6.1 Physical Interface

Our recommendation is to use six steel bolts arranged in a circular pattern, each 60 degrees apart. The bolts will attach the flange of the canister to the Eagle.

It is recommended that further study of the shock and loads produced by pyrotechnic separation of the boosters and fairings, and how these forces affect the payload, be conducted. An understanding of these forces is critical to ensure that the boom-Eagle attachment does not fail. A standard NASA procedure for mounting would obviously be preferred due to past experience with mounting interfaces and the launch loads experienced.

5.6.2 Support Systems

It is recommended that the data not be collected and transmitted simultaneously. Once collected, the NASA TDRSS telemetry network should be employed. This network will quickly and efficiently handle the downloading needs of this mission. The potential of adding additional memory should also be examined. With the standard memory in the Eagle satellite, only two tests can be conducted before data downloading must occur. The addition of memory will increase the possible number of consecutive tests. Finally, it is recommended that after a NASA completion of the test plan, a TRW recommended consultant should be identified to complete the Spacecraft Software Subsystem. The entire STEP structure has been designed and tested for a Pegasus launch vehicle. Therefore, if the launch loads associated with a Minuteman rocket are substantially different, the structure will require retesting or at worst a slight redesign. Secondly, the moments generated by the vibration testing should be experimentally determined and compared the moments that the adaptor module is capable of controlling. Finally, the total propellant capacity of 77.11 kg (170 lb) should be utilized in order to improve the cantilever beam model.

5.6.3 Boom Excitation

Although the Reaction Mass Actuator has been designed from other experiments used to generate vibrations, one needs to be designed specifically for this boom application. Further study must also be performed to determine the force required to generate vibrations in this boom. The RMA must also be scaled properly for this application, and all components in the RMA design should be fully space qualified and tested.

5.7 References

1. All information concerning Eagle satellite systems was obtained from the TRW Eagle User's guide.

2. Background information on vibrations was obtained from ME 259 Class Pak #1, Spring 1992.

3. Garcia, E., Webb, S., & Duke, J., "Passive and Active Control of a Complex Flexible Structure Using Reaction Mass Actuators".

4. Hallauer, W. & Lamberson, S., "Experimental Active Vibration Damping of a Plane Truss Using Hybrid Actuation", AIAA Paper #89-1169-CP.

5.8 Appendices

5.8.1 Calculations

Calculations for Boom to Space Bus Interface
Total weight of Canister (M) = 28.11 kg (62 lb)
Bolts

Grade:	ISO 9.8
Endurance Limit:	140 MPa
Diameter:	0.01 m
# of Bolts:	6

Shear Stress Calculations
tau = F/A
F = (5g's)*M = 5 * 9.81 m/s^2 * 28.11 = 1380 N
A = cross sectional area of all bolts
A = (6 bolts) (pi/4) $(0.01)^2$ = 0.000471 m^2
tau = 1380 N / 0.0004712 m^2 = 2.9 MPa

Factor of Safety
nu = endurance limit / max load
nu = 140 MPa / 2.9 MPa = 48

6 Automated Protein Crystal Growth

6.1 Abstract

The scientific value of experimental protein crystal growth has been well established in recent years. For full three dimensional growth of crystals, the zero gravity environment of space has been found to be an attractive alternative to normal laboratory environments. The Automated Protein Crystal Growth Facility was designed to provided a facility that is fully compatible with the Space Station Freedom (SSF).

In keeping with this objective, a protein crystal growth chamber was designed to eliminate waste, use space efficiently, and facilitate monitoring and control of the crystal growth. The precipitant, protein, and quenching solutions are pre-mixed, pre-loaded, and contained in the chamber. Growth is induced and terminated through the use of an automated robot. The rack was designed to optimize the space available in the ISPR (International Standard Payload Rack) by using an octagonal shape with a combination of storage and active growth sites. There are 132 active growth sites and 756 storage sites. This allocation of sites maximizes the number of experiments during a 90 day untended period on SSF.

The automation of this experiment requires the use of both a robotic arm and an end-effector that is designed to interface with the crystal growth chambers. The Zymate II robotic system fills the role of the robotic arm since it has well defined parameters and meets all physical reach requirements. The end-effector was designed to move chambers to and from active and storage sites as well as operating the protein solution, the precipitant, quenchant, and plungers of each chamber. The end-effector operates plungers and grasps chambers through the use attachments mounted on a rotating wheel at the end-effector tip. Systems for alignment and tolerance are passive to reduce design complexity. The only active dynamic system on the end-effector is the rotating part which functions to orient different attachments.

The experiment is supported by an integrated environmental control and data management system. The basis for the environmental control is to create a completely sealed, cooled environment with specific site heating in order to achieve accurate thermal control of individual crystal growth chambers. The data management system offers continuous ground based control of the experiment through the use of a standard IBM compatible computer with optical sensors (fiber optics and photo transistors), heat sensors (thermocouples), and heat generators (electrical resistance heating coils). The optical system monitors the nucleation and growth rate of the crystals with a sampling rate of up to three times per second. The heat generators and sensors provide thermal control of the crystal growth over a range of 4 to 22 degrees C within 0.5 degrees C. The report gives detailed explanations of the entire iterative design process and a description of the final Automated Protein Crystal Growth Facility design.

6.2 Introduction

Since completion of the first crystallographic study of a protein crystal structure (myoglobin) in 1960, crystallography has become a valuable tool for revealing the structure and functional relationships that are of major importance in understanding how macromolecules operate in biological systems. More recently, pharmaceutical, biotechnological, and chemical industries have become interested in crystallographic studies of proteins because of their promise in protein engineering, drug design, and other applications to biological systems.

Crystallographic structural information reveals important features of a protein that provide insight concerning amino acids which are important for the biological function of the protein. This information

can be used in several ways. It allows the molecular biologist to quickly recognize important areas of the tertiary structure of the protein so that changes in the DNA can be made in an effort to create proteins with altered biological activity. Knowledge of the three-dimensional conformations of the active site of an enzyme provides protein chemists with the atomic framework from which pharmaceutical compounds can be designed that interact in a highly specific manner with selected areas of the protein.[1]

Gaining the three dimensional structure of the protein can be done in a variety of ways. Due to the effects of gravity on the growth of the crystal on earth, it is difficult to grow a crystal which has not been affected. Thus the growth of crystal in reduce gravity would ease the study of the crystals.

6.3 Background

The Preliminary Design Branch at Marshall Space Flight Center has been investigating the possibility of developing a fully automated protein crystal growth facility. Currently, the space program on the shuttle supports a partially automated facility. The shuttle system requires human intervention in the beginning of the growth process, the monitoring of the crystal growth and the halting of the growth before the shuttle returns to earth. The idea which Melody Herrmann suggested was to develop a facility which would require no human interaction and therefore could be placed in the Space Station Freedom during the tended period.

Melody Herrmann, Frederick Herrmann, Elaine Hinman-Sweeny and others had developed an automated system using a Zymark Zymate II robot.[2][3] The system was designed to utilize the robot for manipulation of the chambers which would hold the crystals during transport and growth. This design was the basis for the design of the students.

6.4 Assumptions and Requirements/Customer Requirements

The goal was the develop an automated protein crystal growth facility for use on space station. During a meeting on January 21, 1993 at Marshall Space Flight center with Melody Herrman and Elaine Hinman-Sweeny, the specifications of the project were determined.

1. The experimental facility must fit within an ISPR payload rack.
2. A minimum of 500 protein crystals must be grown during the 90 day un-tended period between shuttle flights.
3. Each protein must be individually controlled with respect to temperature and time of growth.
4. The control and monitoring of the growth process may be done from a remote location.
5. The final crystal must be encase such that it can be returned to earth successfully.
6. Viewing of each crystal is required.
7. The facility must be completely safe and comply to space station requirements for astronaut interaction.
8. All experimental equipment place within the rack must be space qualified and meet launch requirements.
9. The experiment must not interfere with any other experiments on board.

These specifications were used to guide the students to a successful design of an automated protein crystal growth facility.

6.5 References

(1) DeLucas, Lawrence J., Bugg, Charles E., "Protein Crystal Growth in Space". Advances in Space Biology and Medicine, Volume 1, pp 249-278, JAI Press Inc., 1991

(2) Herrmann, F. T., "Advanced Protein Crystal Growth Flight Hardware for the Space Station", AIAA 26th Aerospace Sciences Meeting, Jan 11-14, 1988, Reno, NV.

(3) Quinn, A. W., Herrmann, M. C., Nelson P. J., "Space Manufacturing in an Automated Crystal Growth Facility", Society of Manufacturing Engineers, 1989.

7 Protein Crystal Growth Experimental Facility

7.1 Summary

7.1.1 Design Objective

The overall design objective is to create an environment capable of sustaining superior protein crystal growth under dynamic conditions present in a space station in orbit. The system will be able to perform at least 500 simultaneous crystal growth experiments in a fully automated manner.

7.1.2 Abstract

Upon researching protein crystal growth and the requirements for growing crystals, the design objective was simplified to two basic parts: the chamber design and the experimental facility design. The chamber design was necessary to create the proper environment for growing the protein crystals. The design considerations for the experimental facility encompassed the removal of the chambers, the automated robot used for maintaining the protein experiments, data acquisition equipment for recording growth of the crystals, and the environmental control systems used to facilitate protein crystal growth. These two designs are rather intricate, but serve to simplify the functions of the robot and minimize astronaut intervention.

The experimental facility geometry chosen, based on mobility constraints of the Zymate robot and the optimization of usable space, is an eight-sided polygon with a window for viewing the inside of the experimental facility. Four sides of the polygon are designated as active experimental sites (holding 132 chambers). The horizontal and vertical sides of the rack are designated for storage sites (holding 630 chambers). The active chambers will be changed 9 times in a 90 day untended period and placed in the storage sites upon crystal growth completion. A total of 630 experiments will be completed in the 90 day period.

For human interface purposes, the chambers will be stored in removable shelves that are built into the storage site drawers. These cylindrical drawers can then be removed to obtain the chambers. The chambers will be secured in the shelves by a keyway lock and spring mechanism.

The chamber design created is a self-contained unit which eliminates waste removal. The chamber holds precipitant, protein, and quenchant solutions, which are all preloaded. The protein and precipitant solutions are mixed to initiate protein crystal growth. These solutions are extruded by annular pistons into a conical cavity, which the fluids enter obliquely with turbulent flow. This motion causes adequate mixing of the two solutions so the crystals can be properly grown.

A fiber optic tube is installed in the center of the pedestal so that an unobstructed pathway from the robot end effector to the crystal is created. The end effector will carry a fiber optic light source that will shine through the tube and optical sensors, located at the bottom of the chamber, will absorb the refracted rays from the crystals and record the growth of the crystal. Once the recorded data indicates the crystal is fully grown, quenching solution is extruded into the mixing area where the crystal is growing to halt further growth. To facilitate protein growth, the chamber will be heated by heating coils that wrap around the conical section of the chamber.

7.2 Glossary

Experimental facility - the space allotted in the rack for the actual crystal growth experiment.

Extrusion	- the pushing in of the pistons to mix the protein and precipitant solutions.
Chamber	- the cylindrical container where mixing and protein crystal growth occurs.
Drawer	- the tube which holds the storage shelves and is accessible by the astronauts.
Precipitant solution	- the solution that is mixed with the protein solution to instigate crystal growth.
Protein solution	- the solution consisting of the desired protein to be grown.
PROCRYG	- Protein Crystal Growth Facility
Quenchant solution	- diluted precipitant solution used to halt further crystal growth.
Rack	- the entire unit containing the experimental facility. It is the standard unit used on Space Station Freedom.
Shelf	- the rectangular areas cut out of the drawers that contain the individual chambers (for active sites and storage sites).

7.3 Background

7.3.1 Importance of Proteins

Currently, the properties and functions of protein molecules are not fully understood. Complete understanding of the mysteries of proteins will provide scientists with insight into areas that they previously had been unable to research. Proteins are an integral part of life. They are used by plants, animals, and humans to grow, reproduce and resist disease. The study of proteins provides the foundations of molecular biology and biochemistry. They play crucial roles in the areas of drug design, agriculture, and medicine. More complete knowledge of proteins makes breakthroughs in medical procedures such as cancer treatments and tissue transplants more promising.

7.3.2 Protein Crystals

Unfortunately, individual protein molecules are too small to be analyzed. For this reason, protein crystals are grown. A protein crystal is simply a regular, repeated chain of protein molecules. The crystal provides a large enough specimen for examination. This crystalline structure can be analyzed using x-ray diffraction techniques. The data from the x-ray diffraction can then be used to create computer simulated models of the protein molecules. These models provide the scientists with the structure of proteins that will help them comprehend their functions.

Protein crystals require very specific growing conditions. The temperature surrounding a growing crystal must be monitored closely to ensure a successful result. Typically, crystals are grown in a temperature range of 4 to 25 degrees celcius. The concentration and content of the solutions involved in crystal growth are also very specific. Different protein crystal types require different solutions. The composition of these solutions requires the knowledge of a protein crystal expert. The length of time for a crystal to grow to its full size is also variable. It can range from hours to weeks, again depending on the protein type.

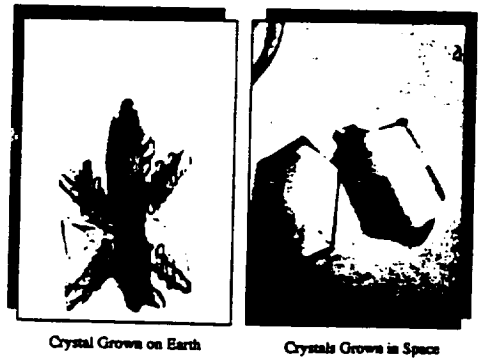

Figure 7.1 : Comparison of Crystals Grown on Earth and in Space

7.3.3 Microgravity and Protein Crystals

When grown on Earth, convective effects tend to alter the growth of protein crystals. Density gradients cause buoyancy induced flows within the fluids present for growth. The result is a crystal that is rather two dimensional. This does not represent the optimal structure for clear diffraction analysis. In micro gravity, convective effects are, for the most part, not present. Therefore, thermal stratification within the crystal has a negligible effect on its growth. For this reason, crystals grown in space are more three dimensional and develop a better internal order. This allows for diffraction analysis data that is of a higher resolution. The result is superior computer model simulations. Figure 7.1 compares crystals grown in space with those grown on Earth.

7.3.4 Vapor Diffusion Method

A common and rather simple method of growing protein crystals is the vapor diffusion method. This is the method that will be employed in the Space Station Freedom facility. In this method, a drop of solvent combined with crystalline material and precipitating salts is suspended by surface tension over a reservoir of the same precipitating salts with a higher concentration. This concentration gradient produces a low vapor pressure in the gas tight chamber. The result is evaporation of the solvent from the suspended drop. As the volume of the drop decreases, the protein concentration in the drop approaches the saturation point and crystal nucleation occurs. As dehydration of the drop continues, more crystalline material collects around the newly formed nuclei and a crystal is formed. The growth process continues until a quenchant solution is introduced into the chamber. Figure 7.2 shows a schematic diagram of the vapor diffusion setup used on Earth. Obviously, this will need to be altered slightly in space since the fluids will not be contained by gravity.

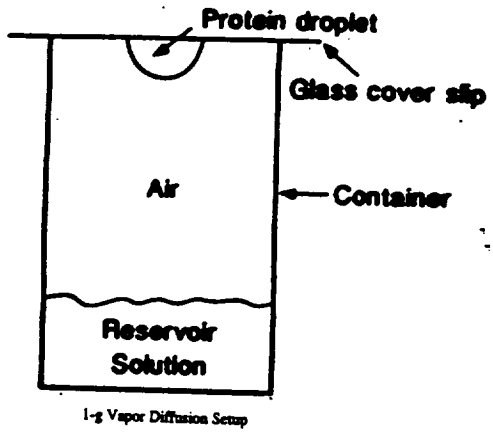

Figure 7.2 : Vapor Diffusion Method

7.3.5 Old Chamber Design

NASA currently has a chamber design developed for its previous protein crystal programs. While this design was changed considerably for this facility, several of its design features were retained. The overall chamber geometry, as far as the cylindrical shape, is the same. The method of containing the precipitant by surface tension to chromex, a plastic wool material, has not been changed. The new design, like the old, incorporates a pedestal on which the protein drop adheres. An optimal range of diffusion area and chamber volume was determined by NASA, and this design utilizes their research. Finally, the fiber optic monitoring of the crystal previously used will again be used in the new system.

7.4 The Design Concept

7.4.1 Protein Crystal Chamber

The advantages of growing crystals in space prove the need of designing a protein crystal growth

chamber capable of producing crystals in micro gravity without any human interaction. The design of the chamber incorporates several key design specifications as discussed in section 6.4. These specifications are the driving force behind the chamber design. Key specifications include preparing the chamber for growing the crystal, minimizing waste from the chamber, and controlling and monitoring the crystal growth. Since the experimental facility will be automated, minimizing robot interaction with the chamber is also a key specification.

The initial protein crystal growth chamber was developed by NASA. Figure 7.3 shows the chamber design proposed by NASA. The new protein crystal growth chamber incorporates a few of the ideas expressed in NASA's preliminary design. Figure 7.4 shows a solid rendering of the new chamber design. The proposed chamber is a cylinder with an outside diameter of 0.83 in, and a length of 1.78 in. Because thin chamber walls are designed to minimize space requirements, PET polymer is chosen as the chamber material. This polymer's high yield strength and modulus of elasticity make it amenable for containment of the protein crystal. PET is chosen over high molecular weight polyethylene because it is a more commonly produced polymer. The cost is roughly the same for the two choices. At this point the decision of whether the chamber will be machined by cast molding or extrusion remains undecided.

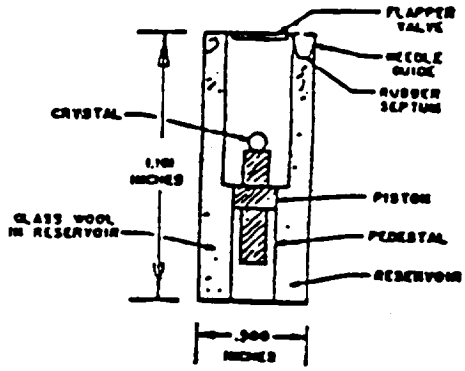

Figure 7.3 : Old Chamber Design

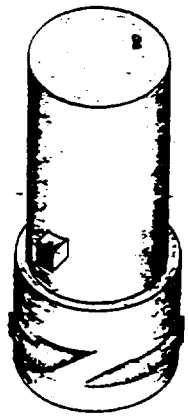

Figure 7.4 : Chamber Rendering

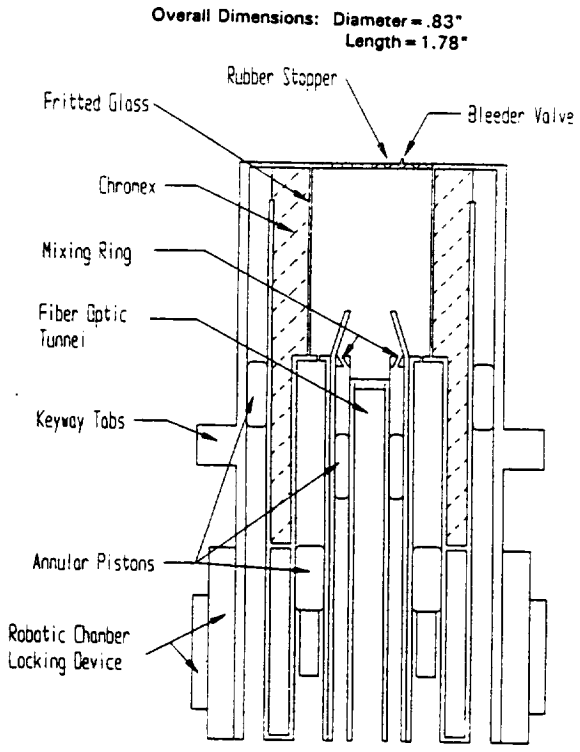

Figure 7.5 : Chamber Before Extrusion

There is a robotic chamber locking device located on the bottom of the chamber where the robotic end-effector will attach to the chamber for movement and storage. The keyway tabs on the side of the chamber secures the chamber within the slot. Figure 7.5 shows a sectional view of the proposed chamber. The chamber is entirely self-contained. This eliminates the need for any type of waste accumulation system once the experiment is terminated. The chamber has pre-loaded protein/precipitant, precipitant, and quenching solutions. These solutions are separated from each other and are contained in the chamber before usage.

The protein/precipitant solution is contained in the inner annular region of the chamber. The protein and precipitant solutions are separated by a partition within the mixing chamber. They are

dispensed onto the pedestal by the end-effector pushing the annular plunger into the chamber. As the end-effector drives the annular plunger in, the solutions are extruded through six 1/64 in diameter holes which are obliquely machined within the mixing ring. The small holes cause the fluid to move through the mixing ring with turbulent flow. The angled holes cause the fluid swirl in a vortical motion as it moves through the mixing ring. This, incorporated with the turbulent flow, assure adequate mixing of the protein and precipitant within the solution. Because of this mixing scheme, settling of the two substances prior to takeoff will have no effect of the development of a homogeneous protein/precipitant crystal droplet on the pedestal. A benefit of a single extrusion method is the decreased demand on the end-effector to perform the necessary operations. As the end-effector extrudes the solution, 40 μl will be administered to the pedestal, while 40 μl will be left within the conical cavity. Obviously, due to the geometry of the protein/precipitant solution extrusion assembly, any drop size is possible by varying the initial amount of fluid within the inner annulus. Since 40μl of fluid is left within the conical annulus after extrusion, any amount of fluid exceeding 40 μl within the inner annulus will produce the appropriate drop size. The drop pedestal is actually an optic light tunnel which becomes flush with the tapering conical cavity as the solution in extruded. Therefore, the light tunnel is fixed to the inner annular piston. As the inner piston is moved by the robot, the light tunnel moves with it.

While the protein/precipitant solution is extruded into the chamber, the precipitant solution is thrusted into the chamber. This simultaneous solution extrusion is performed by the unique geometry of the end-effector's extrusion device. The end effector uses two concentric cylinders to perform the double extrusion. The reader is advised to read the section of the report covering the end effector design to get a full understanding of the geometry used. The outer annular region of the chamber contains the precipitant solution. This solution is initially restrained from entering into the chamber by a small membrane between the precipitant and the chromex which is a fibrous high molecular weight polyethylene material. As soon as the precipitant solution is moved by the end-effector, the membrane is broken, and the precipitant moves in toward the center of the chamber. As the precipitant enters the chamber, it comes into contact with the chromex and clings to the fibers via surface tension. Fritted glass becomes an impermeable barrier between the chromex and the interior of the chamber. This keeps the precipitant from floating around the interior of the crystal chamber and disrupting the protein crystal growth. The fritted glass is a porous media so that the vapor diffusion method is still the driving force behind the growth of the protein crystal.

Crystal growth is monitored through the use of light diffraction. As previously mentioned, the crystal rests on top of the drop pedestal. The drop pedestal is actually a light tunnel which acts as a fiber optic. The end-effector will produce another fiber optic which will be flush with the light tunnel. The inner diameter of the light tunnel is 0.095 in, while the smallest outer diameter of a fiber optic is 0.09 in. This fiber optic will have to be custom fabricated. With the two dimensions given, there is adequate room for both the fiber optic to enter into the light tunnel, and for the fit between the fiber optic and light tunnel to be a tight one so that minimal light escapes out of the back of the chamber. The light will propagate down the light tunnel until it comes in contact with the crystal. Since the crystal will rest on top of the light tunnel, there will be no air gap between the light source and the protein drop. This is essential for accurate monitoring of crystal growth. As the light passes through the crystal it diffracts. A sensor on the top side of the chamber will receive the diffracted light and then relay the data to the rack database and to a scientist on Earth. In this way careful monitoring of the crystals can be performed. It should be noted that since the robot will supply the initial light source, only one protein can be monitored at a time. This means that if there are over one hundred active sites, individual chamber crystal development can only occur once every hour or so. This is not considered to be a major problem since the average growth of crystals is about fourteen days. There will be ample time to monitor the development of most types of protein crystals during each experiment.

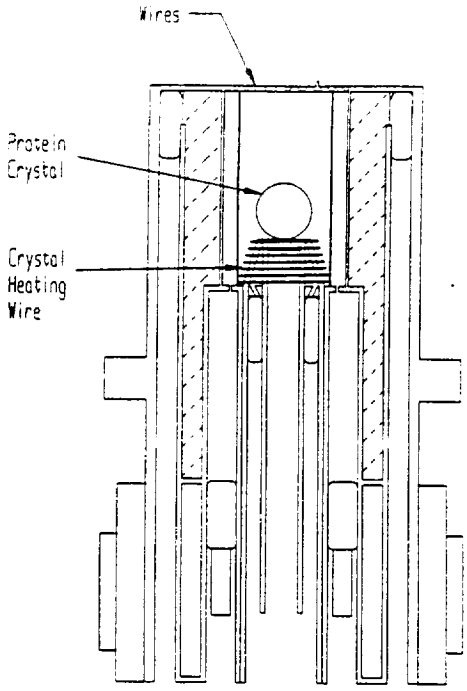

Figure 7.6 : Chamber After Extrusion, Heating Wires Shown

Each chamber also has the ability to be individually thermally controlled. Temperature is the major variable which effects the rate of vapor diffusion of the crystal. Therefore, individual chamber temperature control gives the user the ability to develop a range of growth rates. This presents the idea of producing many different types of loading conditions to determine what the best environment for growing any particular protein crystal. Figure 7.6 shows a cross-section of the chamber with the heating wire placed on the conical section. The thermal control is implemented by the use of an electrical resistance heated wire wrapped around the conical section of the chamber and extended to the top of the chamber. Adjusting the current through the wire will vary the heat transfer to the crystal drop. This in turn will give the temperature control needed. A thermocouple is placed on the conical section above the heating wire. It should be noted that Figure 7.6 shows the heating wire covering the entire conical section of the protein/precipitant extrusion mechanism. This is not completely accurate, since the thermocouple is placed above of the heating wire. The thermocouple is just below the protein crystal, and does not touch the heating wire. The thermocouple will provide the user with an accurate temperature reading of the crystal.

Once the user decides to terminate the crystal development and store the crystal for analysis, the quenchant solution is extruded by the end-effector. The quenchant solution is usually a lower concentration of the precipitant solution. Since the precipitant solution aids in the growth of the crystal, a lower concentration of the precipitant solution will simply cause the vapor diffusion to cease. This will halt the growth of the crystal. Extrusion of the quenchant solution is accomplished by pressing the middle annular piston in toward the chamber interior. The quenchant solution is injected into the chamber through six needles evenly spaced around the middle annular dispensing ring. The quenchant solution in administered until the chamber interior is entirely engulfed by the fluid. The chamber is then removed from the active site and put into chamber storage. Filling the chamber interior with the quenchant solution will provide the crystal with the "packaging" it needs to arrive safely back to earth to be analyzed. The liquid will act as a buffer to keep the crystal from "smashing" into the chamber walls. Once the crystals are ready to be analyzed, the rubber stopper on the top of the chamber is removed. The fluid is then drawn out of the chamber. The crystals will be drawn out with the fluid, and can be analyzed.

7.4.2 Experimental Facility

7.4.2.1 Geometry of Experimental Facility

The experimental facility had to adhere to the constraints of the robot end effector while maximizing the space allotted and promote and store protein crystals. Space within the experimental facility was allotted for data acquisition devices, HVAC units, as well as other environmental or data

control hardware. For the dimensions of the experimental facility were as follows: 41.5" in length by 53" in height by 21.3" in depth. From these dimensions additional considerations were taken to ensure room for any wiring and an opening for an emergency door on the front of the facility. Seven inches on the top, bottom, and sides were allotted for the wiring and three inches of depth for the door.

Robot accessibility was a high priority in designing the facility geometry. By mounting the robot on the back wall, it could reach all the chambers because it has the ability to extend approximately 22.8". The placement of the robot restricted the orientation of the chamber sites. The slots for each chamber are angled toward the robot making accessibility easier and lessens the wear on the robot.

As stated by NASA, a goal of the design is to complete 500 protein crystal growth experiments during the unmanned 90 day period on the SSF. Maximization of number of locations for growth was a consideration when choosing a experimental geometry. So the heating and air conditioning and data acquisition systems may interface with the chambers, space considerations for these systems were made. An acceptable geometry will have space for all of these systems to interact. Another concern when choosing a geometry is the access that the astronaut will have when he/she removes or replaces the chambers. Ideally the astronaut can open the hatch a see all the chambers, if necessary, or can see and access them without even opening the door. A final criteria for an acceptable geometry is the ability of removing the chambers when they are finished growing to keep them secure, but also maximize the space and decrease to work of the robot and astronaut. Based on all of these criteria an experimental facility in the shape of an octagon with cylindrical removable storage shelves was design. The final overall design is shown in Figure 7.7.

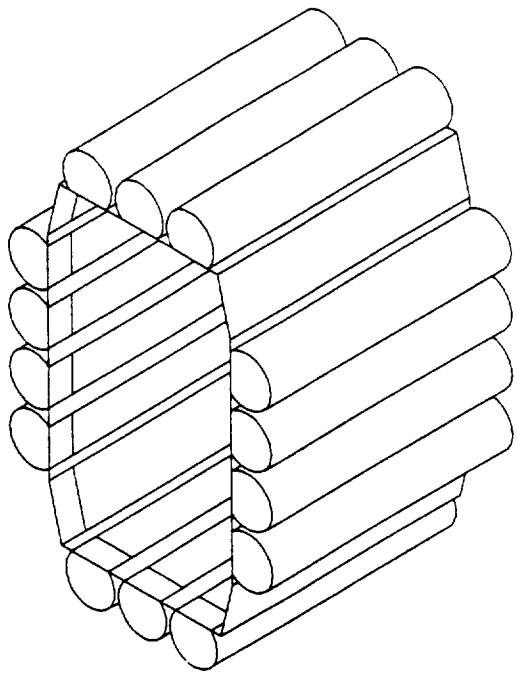

Figure 7.7 : Experimental Facility

The design chosen has four active growing region while it also has fourteen cylindrical shelves where chambers are stored before or after growth. The cylindrical shelves met the criteria of accessibility for the astronaut. The shelves are turned 90 degrees and pulled out of the facility. A vacuum will ensure that the air between the experimental facility and cabin do not mix. Due to the orientation, the robot will be secured to the back wall and be able to extend to reach the whole depth of the facility. The octagonal shape allows a maximum number of usable space for growth or storage sites.

7.4.2.2 Active versus. Storage Sites

The goal of the project is to conduct the maximum number of experiments over a ninety day period. It was determined that the number of experiments conducted over a ninety day period could be maximized by storing inactive chambers while others were growing crystals. These chambers could be exchanged with inactive chambers by the robot when experiments are concluded. The number of storage and active sites were determined from the assumption that experiments last approximately 15 days. For the final design, the total number of possible experiments is 630. The ratio of storage sites to active sites is approximately five to one.

7.4.2.3 Active Sites

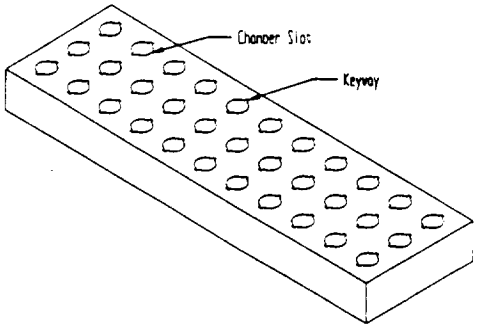

Figure 7.8 : Active Site Shelf

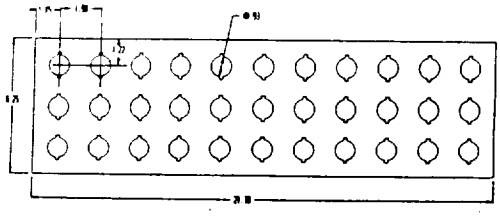

Figure 7.9 : Active Site Shelf, Top View

There are four locations for the active sites. The angled corners of the experiment facility house the active sites. These corners are referred to as the active shelves. Each of the four shelves contain 33 experiment sites; thus, there are a total of 132 active sites. The active shelves are insulated with aluminum silica because of its high thermal resistivity properties; thus, the environment of each chamber is isolated and can be easily controlled. The rest of the shelf is made of acrylonitrile-butadiene-styrene (ABS). This material was chosen because it is dimensionally stable and frigid with good strength and toughness. The shelves are made by an injection molding process. The process was allows good dimensional control and can mold parts with multiple cavities. A view of the active shelf is shown in Figure 7.8.

The slots for the active chambers are 0.93 inches in diameter and 2.03 inches in depth. They are spaced 1.9 inches apart, horizontally and vertically, Figure 7.9. Each slot has two keyways and four springs used for holding the chambers in place, Figure 7.10 and 7.11. The chambers are inserted by the robot by matching the keys and keyways, depressing the springs 0.25 inches, rotating the chamber 20°, and releasing the chamber. The springs are also used as an electrical conductor for the heating elements of the chamber.

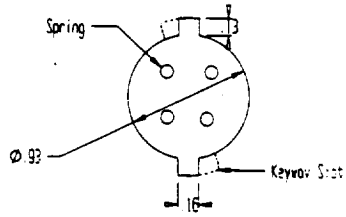

Figure 7.10 : Chamber Slot

7.4.2.4 Storage Sites

There are fourteen locations for storage sites in the automated protein growth facility. The storage sites are located along the top, bottom, and sides of the facility. The storage sites reside in removable trays housed in drawers, shown in Figure 7.12. These trays, like the active sites shelves, are also made of acrylonitrile-butadiene-styrene (ABS) by an injection molding process.

Once a tray is full of chambers, the drawer can be

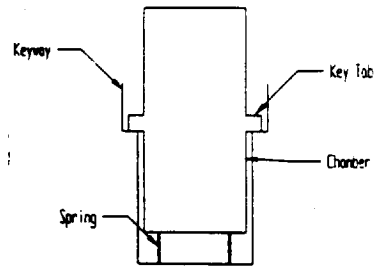

Figure 7.11 : Chamber and Slot

retracted, and the tray replaced by another with new chambers. Each tray can hold 45 chambers for storage. There are three sites for chambers storage across the width of the tray and 15 along the depth of the tray. The chambers are spaced with 1.36 inches between their centers. A top view of the storage tray in shown in Figure 7.13. The total number of storage sites for the entire facility is 630. Each site in the storage tray is identical to the slots in the active sites with the exception of the data acquisition provisions. The chambers are locked in place by keyways and springs as with the active sites.

Transporting the trays between earth and space will require equipment that damps vibrations experienced during lift-off and re-entry. An idea for this equipment includes a transportation box that would hold the fourteen trays and isolate them from vibrations. Other ideas may need to be developed and lift-off vibrations analyzed.

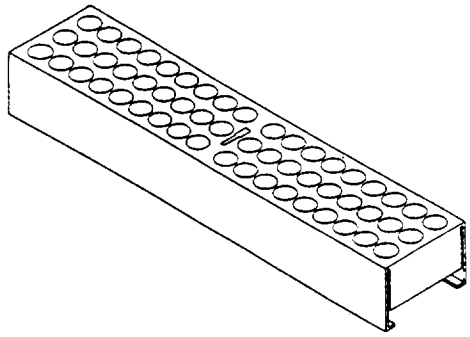

Figure 7.12 : Storage Tray

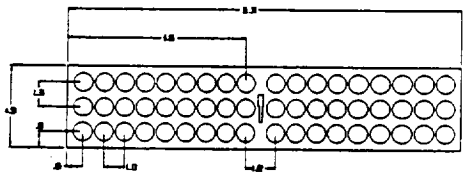

Figure 7.13 : Storage Tray, Top View

7.5 Conclusion

7.5.1 Overall Progress

The objective of this design effort was to create a suitable chamber design that could sustain crystal growth in a controlled environment. It was also to establish a rack design that could encompass the stipulations set by protein crystal growth experiments, and integrate these factors with the chosen Zymate robot and the new chamber design. The chamber and rack designs, according to the design objective, meet all of the required specifications.

7.5.2 Chamber Design

The chamber design, much like the rack, meets all of its design criterion. It is well integrated with the rack design and is easily accessible by the Zymate robot. The cylindrical chamber design simplifies the robot's manipulation of the chamber. The single extrusion method for the solutions also decreases robot interaction with the chamber. The solutions necessary for protein crystal growth are self-contained as well, and, as a result, eliminate possible waste products. The fiber optic tunnel used the crystals to be easily monitored. The thermocouple and heating wires located within the chamber allow the temperature of the crystals to be properly controlled. These features of individual thermal control, fiber optic crystal monitoring, and minimal robot and astronaut interaction make the proposed chamber design, as well as the rack design which strongly integrates these features, optimal for use aboard Space Station Freedom.

7.5.2 Experimental Facility Design

The first requirement set by NASA was for the rack design to be able to produce at least 500

protein crystal experiments. The design created has made it possible for up to 630 experiments to be completed by maximizing space used for the active and storage sites. By dividing the rack into thirds, and further maximizing space, the design is spacious enough to encompass the actual protein crystal experiment site, as well as the environmental control systems needed to sustain the experiments. The rack is also easily accessible by the astronauts for retrieving the completed chambers and for maintenance purposes.

7.6 Recommendations

Though the design objectives of this protein crystal growth facility were completely achieved, there are some details that could be explored in furthering this design effort. First, the sensor used for detecting the growth of the crystal is for the most part unidentified. This sensor design needs to be finalized and integrated into the chamber and rack designs. Also, the protein crystal chamber itself needs to be analyzed on a manufacturing standpoint. Due to the thinness of the chamber walls, the chamber may be hard to manufacture using machining or molding methods. This analysis may lead to a materials search to find a material that can be used to manufacture the chamber with its current dimensions. Finally, a much more in-depth analysis of the vibrations and shocks occurring during takeoff needs to be completed. This analysis will test to see if the chamber and rack designs can withstand the severe gravitational forces experienced during takeoff. If the designs fail, modifications to the proposed designs should be introduced encompassing vibration issues. Upon completion of these analyses, full prototypes of the rack and chamber designs can be made. Eventually, these designs will be capable of being aboard Space Station Freedom and hopefully will help to benefit the scientific world in the area of protein crystal growth.

8 Robot End Effector for the Automated Protein Crystal Growth Facility

8.1 Summary

8.1.1 Design Objective

To design a fully-automated system that can facilitate the growth of protein crystals in microgravity while conforming to the constraints of a space station environment.

8.1.2 Abstract

The design objective for the group was to design a fully automated system that can facilitate the growth of protein crystals in micro-gravity while conforming to the constraints of a space station environment. The Zymate II was chosen to provide the motion inside the rack. The existing end effector for the Zymate is insufficient for a micro-gravity environment so that a new end effector had to be designed to operate the new growth facility. The end effector has to perform the functions of : 1) Gripping chambers for transport. 2) Extruding the solutions required for protein crystal growth. 3) Illuminating the crystals for observation. The gripping motion is achieved by a screw top mechanism similar to a bottle cap, and the extruding is accomplished by annular cylinders used to depress pistons in the chambers. Each tool is isolated on a side of a rotatable tetrahedron which is oriented such that the active tool is along the centerline of the robot arm and normal to the surface of the chamber. The alignment of the tetrahedron is controlled by a timing and locking mechanism which provides and maintains the appropriate orientation for the active tool. The robot arm then provides whatever motion is necessary.

8.2 Glossary

Chamber	- Self-contained capsule holding all solutions necessary to grow protein crystals as well as the site of individual crystal growth.
Experimental Facility	- The part of the rack that contains the robot, end effector, and all of the chambers, and where all crystal growth processes take place.
Pistons	- Annular rings in the chamber that are depressed to extrude needed solutions into the growth site area of the chamber.
Plunger	- The cylindrical tool used by the end effector to depress annular pistons in the chambers.
Protein Crystal	- A chain of protein molecules arranged in a repeating pattern and used by scientists to study protein structure.
Rack	- The modular containment vessel for use on the Space Station Freedom in which the Experimental Facility and all its controlling equipment are stowed.
Repeatability	- The tolerance in which the robot can return to the same position time and again.
Screw-Top	- The gripping apparatus mounted on the tetrahedron of the end effector and used to grasp individual chambers.
Spider Gear	- A gear used to translate motion on a 90 degree angle.
Tetrahedron	- A four-sided figure. On the end effector one side is mounted to a drive shaft

that provides rotational motion while the other three sides hold the two plungers and the screw-top respectively.

8.3 Background for REE

Currently, protein crystal growth in space has been performed by manual astronaut manipulation. Hand manipulation has been adequate so far, but with the advent of the Space Station Freedom there is need for an automated facility. The reasons for automation are that the facility will be unmanned for extended periods of time and to reduce the work load of the astronauts. These reasons have lead NASA to research and develop a fully automated protein crystal growth facility. The ground test facility for protein crystal growth is equipped with a Zymate Z-110 robot to manipulate the crystal growth solutions and the growth compartments. The robot is manufactured by the Zymark corporation. The robot is a bench type with a height of 27.5 in., a 12.3 in. square base, and an arm that extends 25.6 in. It has six degrees of freedom which enables the robot to efficiently manipulate the solutions and growth compartments. The Zymate is equipped with a end effector which has a pipette and a clamping device. The pipette is used to measure and deploy the solutions required for the growth of protein crystals. The clamping device is use to manipulate the crystal growth compartments within the confines of the test facility. This existing end effector, however, is designed for use in a 1 g environment, and is therefore not suitable for use in a micro gravity situation. If protein crystal growth is to be achieved on the Space Station Freedom, a space-qualified automation system must first be designed.

8.4 The Design Concept

The Zymate II is a laboratory robot that has been used in medical experiments in the past and therefore has proved its reliability in that area. The Zymate's small size allows for efficient use of space in the experimental facility, but its reach is still sufficient to access all areas of the rack. Furthermore the Zymate II has acceptable repeatability. At a 27 inch radius its rotary repeatability is 0.04 inches maximum, while vertical and reach repeatabilities are 0.02 inches. The Zymate II has two degrees of freedom in the end effector. These two degrees of freedom are adequate for the requirements of the protein crystal growth procedure. A color rendering of the Zymate II with end effector is shown in Appendix 8.8.1 Figure 8.7.

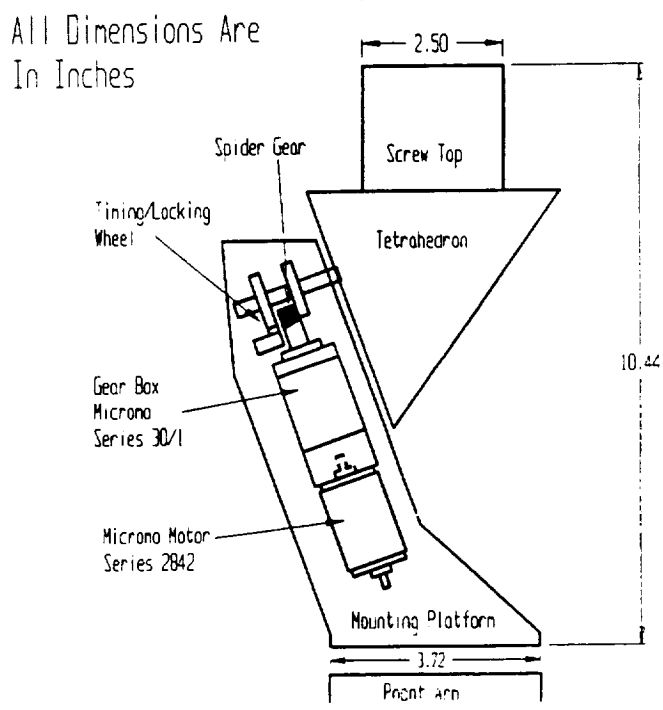

Figure 8.1 : Schematic of End Effector

8.4.1 Overall End Effector Design

The most prominent feature of the end effector is its tetrahedron-shaped tool head which rotates to orient different tools similar to the way that a compound microscope switches lenses. One of the four faces of the tetrahedron is

connected via spider gear to a MicroMo motor and gearbox which provides rotational motion. The various tools required for protein crystal growth are mounted on the other three faces of the tetrahedron. These tools include two plungers and a screw top gripping apparatus. The active tool on the tetrahedron is located along the centerline of the robot arm, and the inactive tools are oriented back and away from the active tool. Thus, the two tools which are not in use will not interfere with the operation of the active tool and will not collide with the rack wall when the active tetrahedron face rests flatly against it. There is a timing and locking system that allows the active tool to be properly oriented to perform the necessary functions and maintains that orientation while these functions are being performed. The tools themselves are stationary in that they do not provide any motion on their own. Any required motion is provided by the robot itself. The Zymate II has precise enough repeatability that it can accomplish such tasks, and the absence of active mechanisms in the end effector itself reduces the number of moving parts, reduces power consumption, extends end effector life, and improves reliability. The end of the end effector is also equipped with a light source for use in retrieving data from the crystals. An overall two-dimensional picture of the end effector is provided in Figure 8.1, and a three-dimensional rendering is shown in Figure 8.6 in the appendix (8.8.1).

8.4.2 Screw Top Gripping Concept

In order to grasp the crystal growth chambers, the end effector utilizes a locking thread that screws onto a collar at the end of the chamber. The thread configuration used is the same one utilized on Heinz 57 Catsup bottles, Gatorade bottles, and some juice bottles, and it suits the purpose well for several reasons. Once locked in place, the screw-top provides a solid grip on the chamber, and the threads require only 1/8th to 1/16th of a rotation and 5 foot pounds of torque to lock in. The required rotation is a range because when one screws a cap onto a bottle, there is no way to know what the initial alignment will be, but in the experimental facility, a very specific chamber orientation will be maintained so that the optimal 1/16th of a rotation is all that will be required. This minimal requirement is advantageous in that it cuts down on wear to the robot as well as the time required to grip each chamber.

In considering the actual movements of the robot during the gripping procedure, it is important to remember that repeatability and manufacturing tolerances will keep the positioning of the end effector from being exact. Thus, the chambers must be protected from breakage by either over extension or over torquing. In order the address the problem of over extension, the screw-top gripper has built in springs in the axial directions (2, 3,& 4 on Figure 8.2) that are capable of absorbing the maximum total of repeatability and manufacturing errors. There is also a set of springs that allow the "cap" part of the screw-top mechanism to float from side to side (7, 8,& 9 on Figure 8.2). The purpose of these springs is to make up for any error on the robot's part that may result in misalignment to one side or the other of

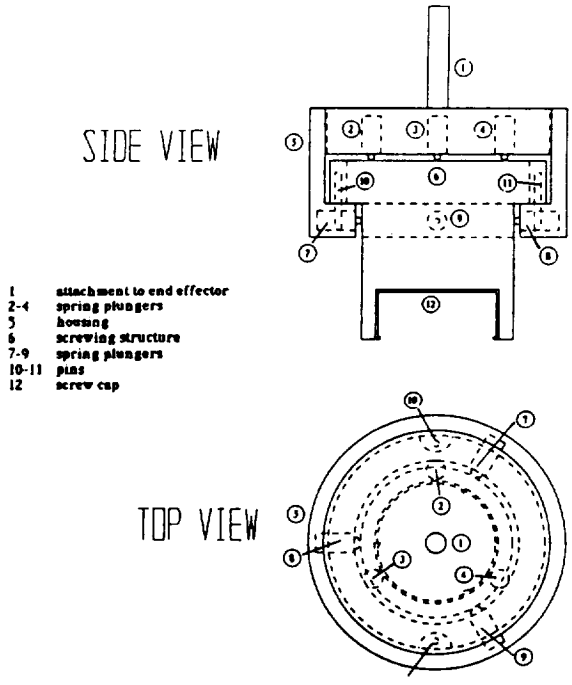

Figure 8.2 : Chamber Gripping Device

the chamber. As for the question of over torquing, analysis showed that the maximum torque of the robot's wrist is not enough to cause chamber damage. Therefore, no spring system is required to protect the chambers from that particular type of error, but the mechanism rather utilizes rigid pins (10 & 11 on Figure 8.2) that rest in recesses on either side of the "cap." These pins, while allowing the cap to float, provide the resistance required to torque the cap onto the chamber threads. Some recommendations for materials for the screw-top mechanism are springs from Carr Lane Manufacturing Co., steel torque pins for strength, and an aluminum housing for light weight.

8.4.3 Plunger Design

The primary functions of extruding the protein solution and quenchant for crystal growth are accomplished through the use of a two plunger system. The plungers will accomplish the task of extruding the solutions by depressing annular pistons. They are cylindrical in shape and are stationary. Therefore the robot provides the plunging motion that depresses the pistons. First, a double plunger was designed to extrude the precipitant and protein solutions simultaneously. By using a double plunger the number of sides for the end effector was reduced. The second plunger is a single plunger that will extrude the quenchant used to halt the growth of the protein crystal. For safety precautions, due to manufacturing tolerances and repeatability of the robot, a passive spring system was chosen to prevent breakage of the chambers. The spring coefficient must be greater than the resistance incurred while plunging the pistons, but low enough to prevent breakage of the chamber when the pistons are fully depressed. Detail drawings of the plungers are shown in the appendix (8.8.1) Figures 8.4 and 8.5 along with solid renderings of the overall end effector that contain the two separate plungers in the appendix (8.8.1) , Figures 8.6 and 8.7.

8.4.4 Gearbox and Motor

A D.C. MicroMotor Series 2842 was used to provide rotation to the tetrahedron. This motor produces 2883 revolutions per minute and 0.0156 foot pounds of torque. A MicroMo Gearhead Series 30-1 was used that will lower the revolutions per minute to 4.869 and produce a torque of 5.08 foot pounds. There is a spider gear that transmits the rotation to the tetrahedron from the gearbox. To avoid transmitting any vibrations or movement to the space station the rotation of the tetrahedron was limited to 5 revolutions per minute.

8.4.5 The Timing and Locking Mechanism

As previously stated, the purpose of the timing and locking mechanism serves the dual purpose of providing correct orientation for the active tool as well as locking the tetrahedron in place to maintain proper orientation during use. The mechanism accomplishes these tasks through the use of a timing wheel. The timing wheel is merely a wheel with three notches, one for each tool, that are equally spaced about the circumference of the wheel. The wheel is then rigidly mounted on the same shaft that drives the tetrahedron so that when it is locked in place, so is the tetrahedron. As the wheel turns, there is a wedge shaped follower that is held against it by a spring, and when the follower reaches a notch the wedge drops into it. The physical presence of the follower in the notch locks the tetrahedron in place and assures that the needed tool is properly oriented. Furthermore, attached to the follower is a contact switch that completes a kill switch circuit when the follower drops into the notch. The purpose of this kill switch is to deactivate the motor and prevent it from straining against the follower. Once the tetrahedron is thus oriented and locked, the desired tool may be used. When the operation at hand is

complete, the robot then activates an electromagnet that pulls the follower out of the timing notch, disengaging the kill switch, and allowing the motor to rotate the tetrahedron around until the next notch is reached and the next tool is aligned. The beauty of this system is twofold. First, the two tasks of aligning the tool correctly and then locking it in place have been accomplished by the same system. Thus, the system uses less power and is more reliable. Second, the end effector as a whole only requires one degree of freedom. The only action required of the robot is to activate the electromagnet for a short period to disengage the follower, and the next tool will automatically align itself and the motor shut off. A of the timing and locking mechanism is shown in Figure 8.3.

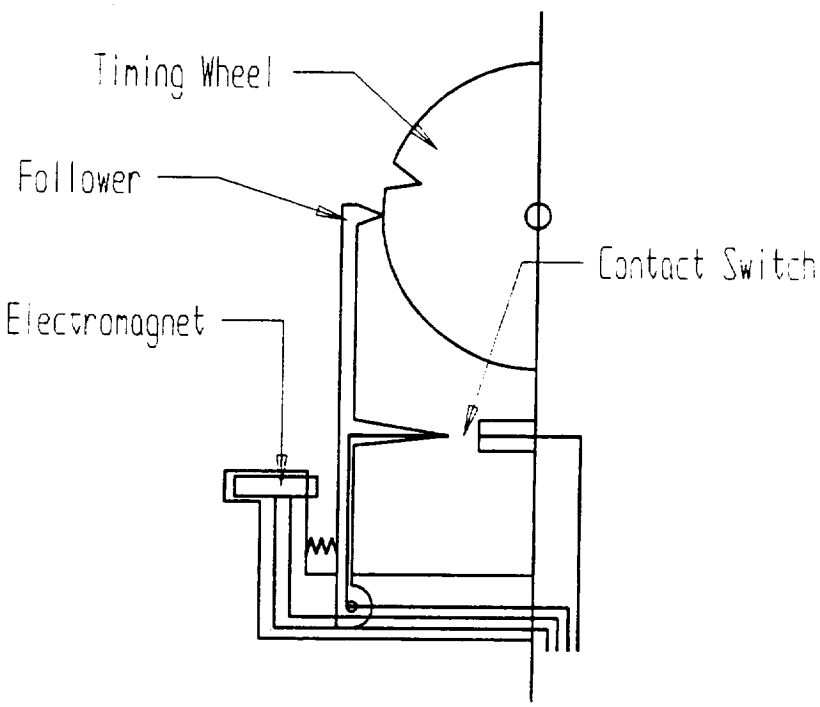

Figure 8.3 : Timing and Locking Mechanism Rendering

8.5 Prototypes and Visualization

8.5.1 End Effector Prototype

A prototype of the end effector was developed for visualization purposes by members of the team. The prototype was made of cardboard assembled in the tetrahedron and plunger configuration. The prototype aided in the proof of concept and spacing needed for the robot interaction with the chambers.

8.5.2 Screw Top Mechanism Prototype

A high density foam prototype of the screw top mechanism was built. The foam was formed around the top of a Heinz 57 bottle top and a mold of the bottle was made. The mold of the bottle was formed into a high density foam model of the top. The model screws together and simulates the end effector mechanism which will grasp the crystal growth chamber.

8.5.3 Robosim Robotic Movement Visualization

A robotic simulation of the movements of the robot was completed using the ROBOSIM robotic simulation package. The simulation shows the Zymark Zymate II robot rotating into position and grasping a chamber. The chamber is then moved from the storage position into the active site and twisted to secure it. The simulation was completed for visualization purposes.

8.6 Conclusions

The Robotics Group has successfully developed an end-effector for the existing Zymate II robotic system that allows for the development of an integrated, fully autonomous protein crystal growth facility. The Zymate II was chosen because its accuracy and tolerances fell within the minimums specified by the functions the robot would be required to perform. The final end-effector design is a tetrahedron. One side connects the end-effector to the drive shaft, allowing rotational movement. The other three faces of the tetrahedron hold the "tools" which perform actions on the protein chambers. There is a screw-top attachment, which allows the robot to securely pick up and manipulate the protein chambers. The second tool is a double plunger, which extrudes the protein solution and the precipitant solution at the same time. The final tool is a single plunger which extrudes the quenching solution. The tetrahedron head rotates, allowing the proper tool to be selected, in much the same way a microscope lens is selected. At the base of each tool is a spring system which accommodates manufacturing differences and prevents damage to the protein chambers. There are several benefits to this design. First, by combining functions and limiting the number of tools to three, the need for separate end-effectors for each function is eliminated. Second, the size of the end-effector is minimized. Finally, the tetrahedron shape insures that the tools not in use at the time do not interfere with the operations of the robot. This design is fully automated and can be controlled by computer from either on board Space Station Freedom or by ground uplink. An overall view of the rack with its components is shown in the appendix (8.8.1), Figure 8.8.

8.7 Recommendations

There are several areas that need further research and development. The robot and end-effector need to be re-qualified for use in space. The design of the springs and development of the spring constants for the passive breakage protection systems incorporated in each tool needs to be accurately defined. The fatigue lifetime and specific dimensions for the timing and locking mechanism must be determined, as well as the overall reliability of the system. Furthermore, the exact placement and configuration of the data retrieval system has yet to be determined. Possibilities for this system could be either a fiber optic mounted on the semi-stationary part of the end effector or perhaps a light source that utilizes convex lenses to create a focal point that rests in the center of the fiber optic tunnel of an active chamber. This latter concept is in many ways the more favorable of the two because it does not involve physical appendages to the end effector that might get in the way of plunging or gripping operations. There exists an additional possibility for expansion in the area of robotics. This end effector design is not limited to the Zymate II robotic system but can be adapted to take advantage of any advances in robotic technology that may take place in the future. The subject of alignment tolerances due to repeatability in the robot and manufacturing of specific chambers has still not been addressed. Possible solutions to the problem include chamfering the edges of the plungers, chambers, or both, or perhaps producing plunger cylinders whose thicknesses are .04 inches smaller than the piston thickness. This difference would allow for the +/-.02 inches of repeatability tolerance the robot experiences when extended to its maximum reach of 27 inches.

8.8 Appendices

8.8.1 Figures

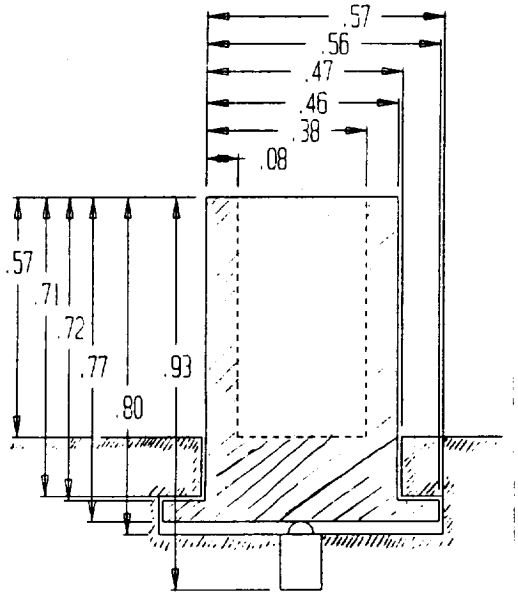

Figure 8.4 : Single Plunger End Effector Tool

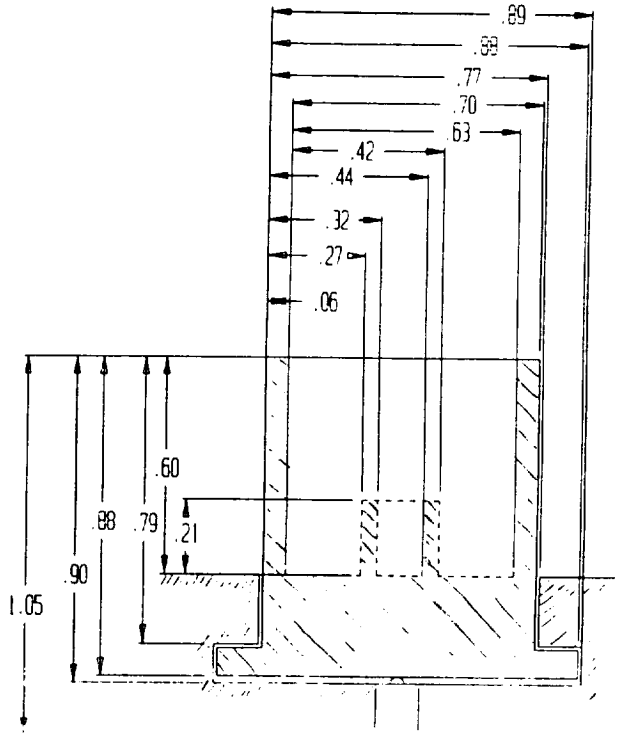

Figure 8.5 : Double Plunger End Effector Tool

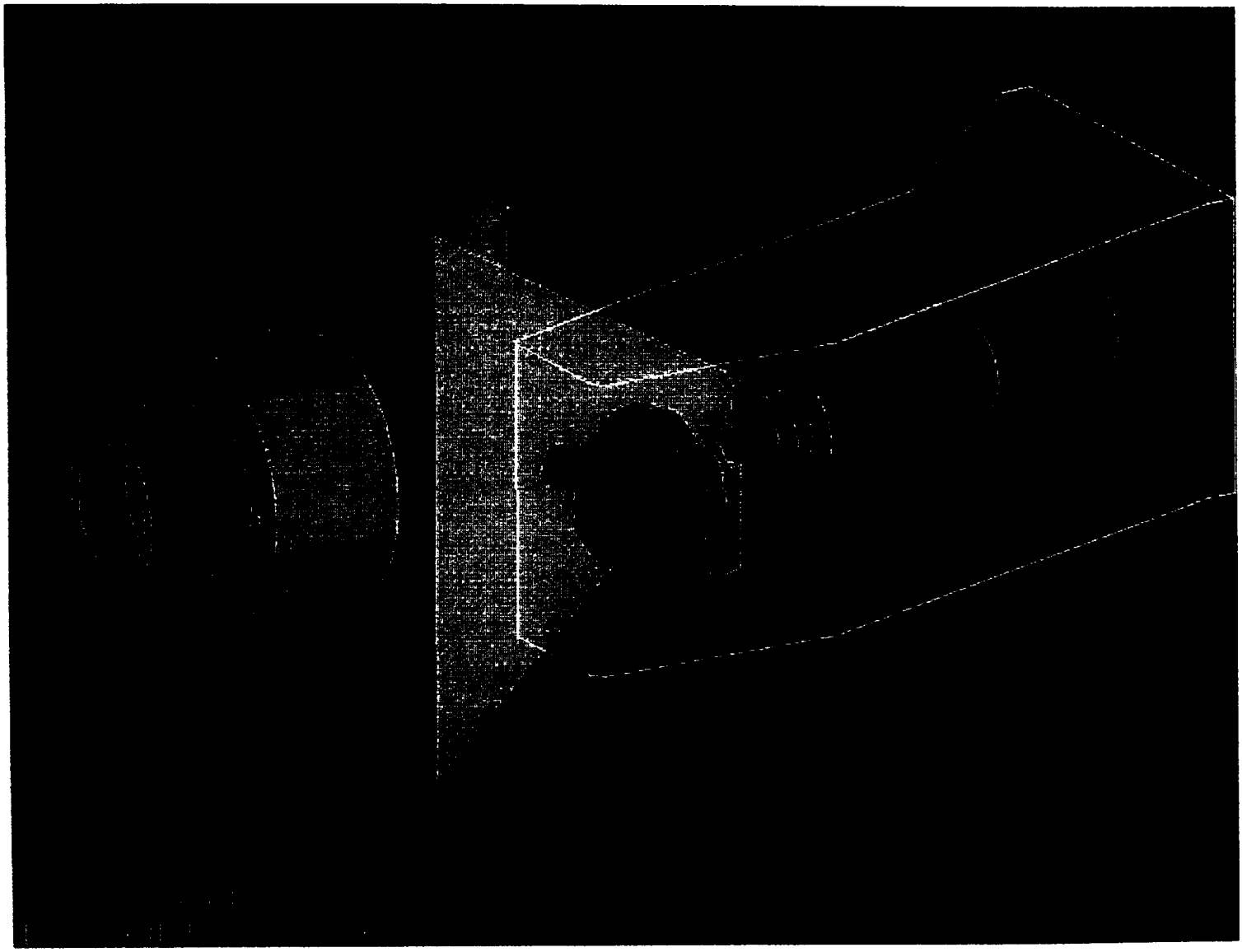

Figure 8.6 : End Effector Rendering

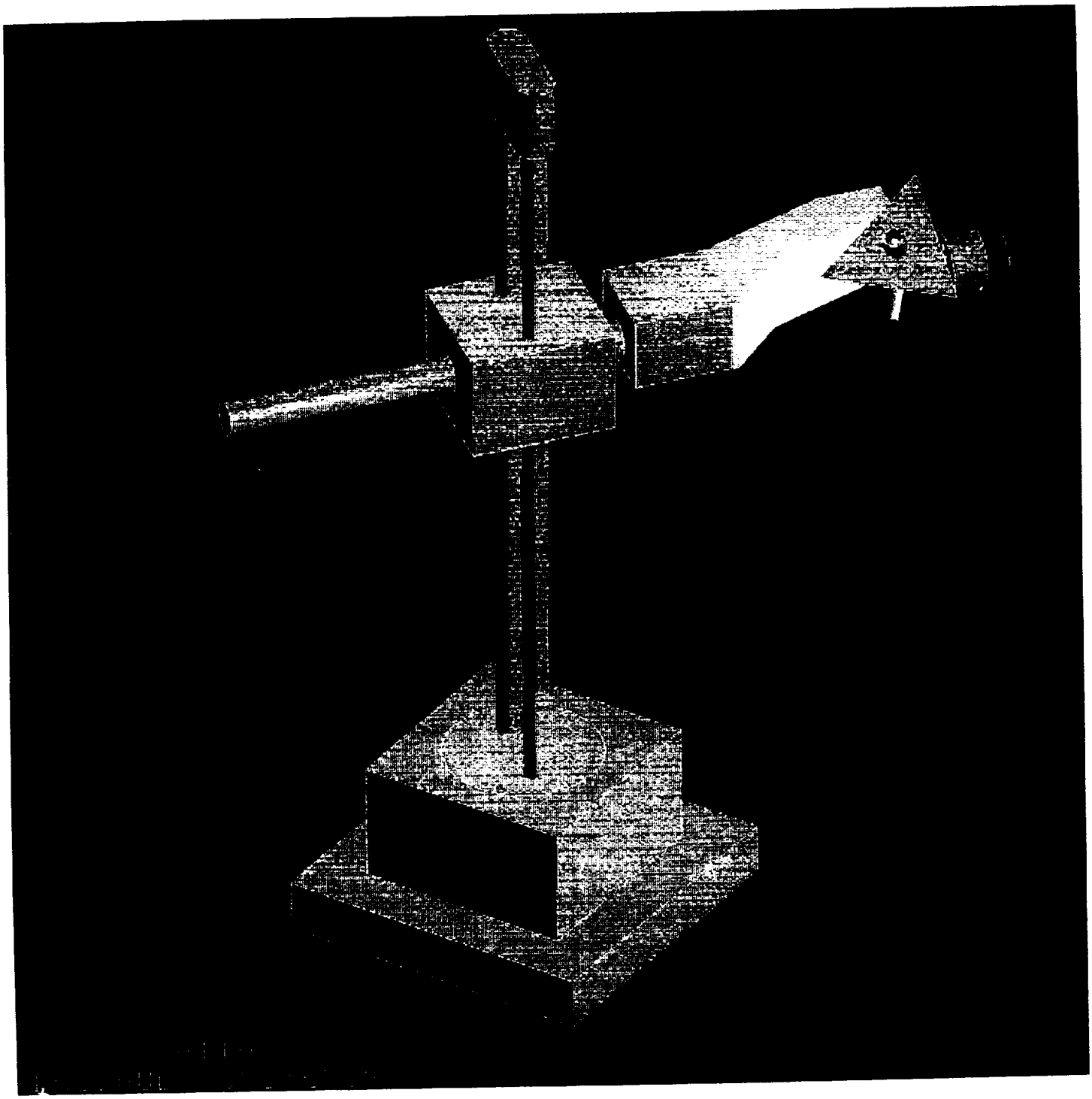

Figure 8.7 : Zymate II Robot Rendering

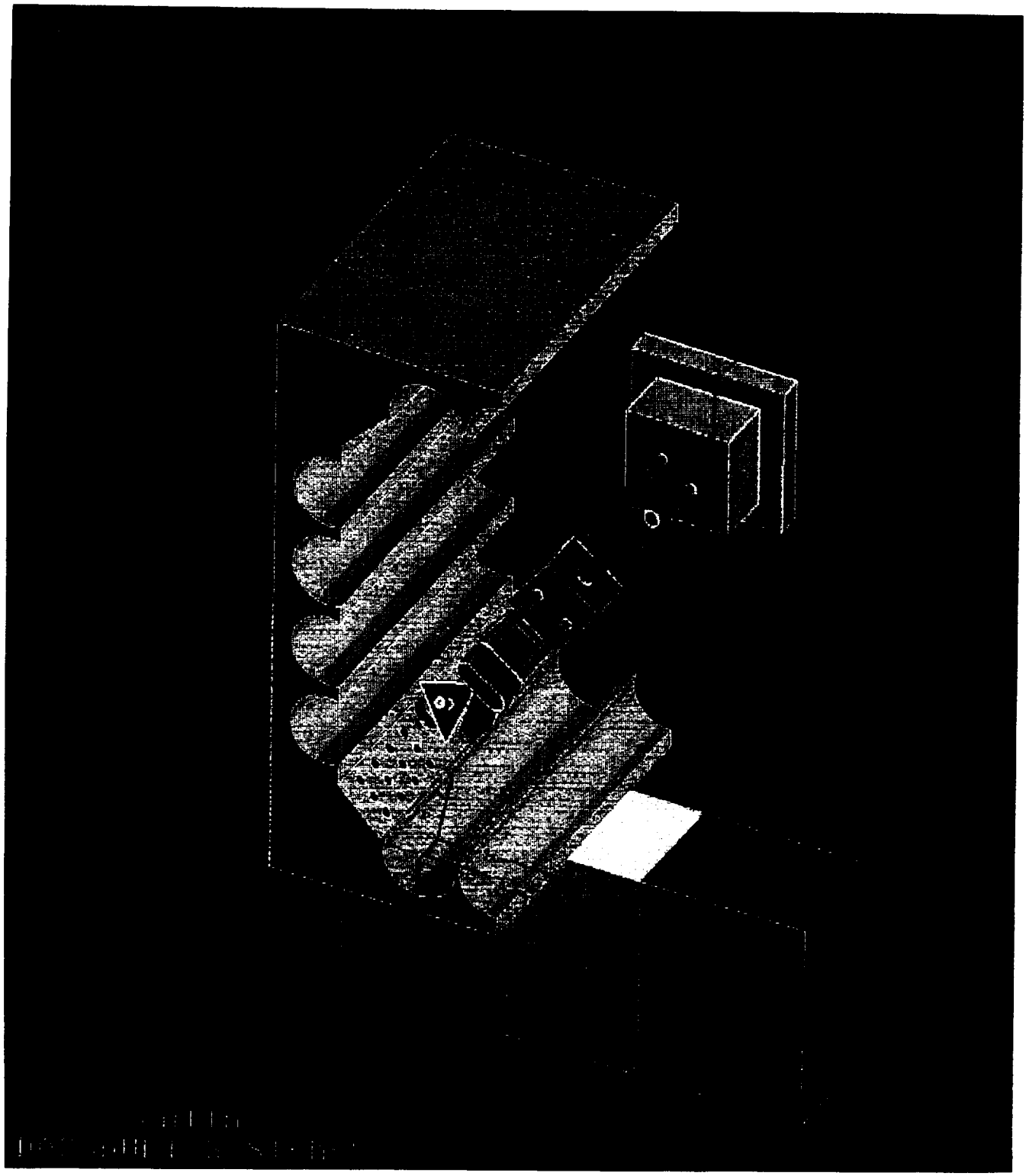

Figure 8.8 : ISPR Rendering

9 System Integration for Automated Protein Crystal Growth Facility

9.1 Summary

9.1.1 Design Objective

To integrate into SSF an automated protein crystal growth facility that meets user and program requirements, has complete interfaces with SSF, without harming SSF or its operators.

9.1.2 Abstract

A protein crystal growth chamber was designed to eliminate waste, use space efficiently, and facilitate monitoring and control of the crystal growth. The precipitant protein and quenching solutions are premixed pre-loaded and contained in the chamber. Growth is induced and terminated through the use of an automated robot. The rack was designed to optimized the space available in the ISPR (International Standard Payload Rack) by using an octagonal shape with a combination of storage and active growth sites. There are 132 active growth sites and 756 storage sites. This allocation of sites maximizes the number of experiments during a 90 day untended period on SSF.

The experiment is supported by an integrated environmental control and data management system. The basis for the environmental control is to create a completely sealed cooled environment with specific site heating in order to achieve accurate thermal control of individual sites. The data management system offers continuous ground based control of the experiment through the use of a standard IBM compatible computer with optical sensors (fiber optics and photo transistors), heat sensors (thermocouples), and heat generators (electrical resistance heating coils). The optical system monitors the nucleation and growth rate of the crystals with a sampling rate of up to three times per second. The heat generators and sensors provide thermal control of the crystal growth over a range of 4 to 22 degrees C within 0. 5 degrees C. The report gives detailed explanations of the entire iterative design process and a description of the final Automated Protein Crystal Growth Facility design.

9.2 Glossary

APCGF	- Automated Protein Crystal Growth Facility
ISPR	- International Standard Payload Rack
NASA	- National Aeronautics and Space Administration
SSF	- Space Station Freedom
UV	- ultraviolet light

9.3 Background

The scientific value of experimental protein crystal growth has been well established in recent years. For full three dimensional growth of crystals, the zero gravity environment of space has been found to be an attractive alternative to normal laboratory environments. The Automated Protein Crystal Growth Facility was designed to provided a fully automated protein crystal growth facility that is fully compatible with Space Station Freedom.

All experiments that are resident on Space Station Freedom must be placed in International Standard Payload Racks. These racks offer approximately 55 cubic feet of usable volume. The rack is a four-post structure with mounting holes on the posts in the interior. All experimental equipment placed within this rack structure must be space qualified. In order to satisfy this requirement, the equipment included in the ISPR must be able to withstand shuttle launch conditions, which can involve forces of up to 7 G's. This calls for a very robust design.

Once the experiment is on SSF, it must be fully automated due to the fact that SSF will be non-tended for 90 day periods. During the brief periods of time when astronauts are tending SSF, the system will receive limited maintenance. The presence of astronauts on SSF results in a set of special requirements for payloads. Waste disposal is very carefully monitored and no experiment may release gases that could be harmful into the space station environment. A fatal requirement precludes the experiments from interfering with any other experiments.

9.4 The Design Concept

9.4.1 Spacial Considerations

One of the first major concerns in the development of the APCGF is the maximization of the experimental volume. The two major constraints for the experimental volume are the AAA environmental control device and the Zymate II robotic components. With these limitations considered, the maximum experimental volume was determined. This volume is a three dimensional rectangular structure 37 inches wide, 21.3 inches deep, and 53 inches high. See Figures 9.1, 9.2 and Figures 9.11 and 9.12 in the appendix (section 9.8.1). Three dimensional views of the experimental area and rack are provided in Figures 9.13-9.15 in the appendix (section 9.8.1). Within this volume is the entire experimental facility, which consists of an octagonal shaped area, oriented in the same manner as a common clothes dryer (Figure 9.14). The active and storage sites (which are located outside of the octagon) are also placed within the experimental volume.

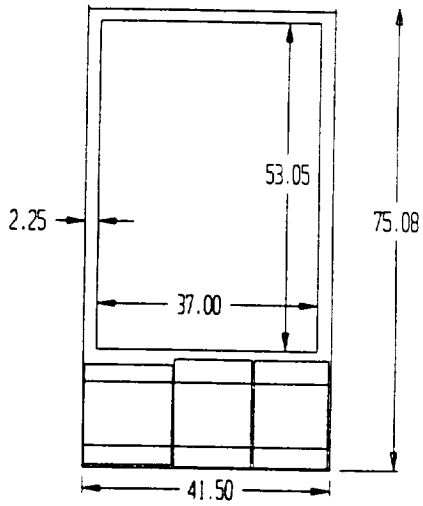

Figure 9.1 : Schematic of ISPR - Front View

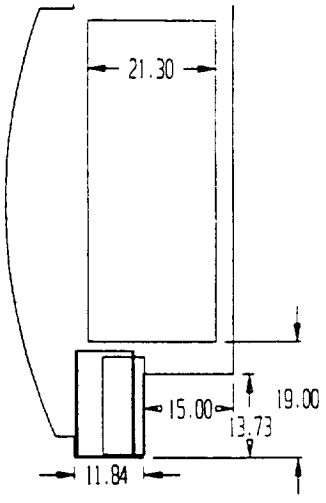

Figure 9.2 : Schematic of ISPR, Side View

With the experimental volume determined, the next consideration is the placement of the experimental volume within the ISPR. (Figure 9.15) The major consideration for experiment placement within the rack is astronaut interface. When the astronauts interface with the facility, the access panels should be oriented much like they would be if on Earth (with a definite top and bottom). On this basis, the experimental facility was placed in the top portion of the ISPR. This placement allows for the rack to be oriented as it would be on Earth, and serves to improve interface conditions with astronauts. Launch conditions were also considered in the placement of the experimental volume. The "back" side of the ISPR can be placed down for launch in the Space Shuttle, so

the configuration that best serves astronaut interface is also a "launchable" configuration. This configuration, as can be seen in the side view shown in Figure 9.12 in section 9.8.1, also provides ample room for equipment that will interface the APCGF with SSF.

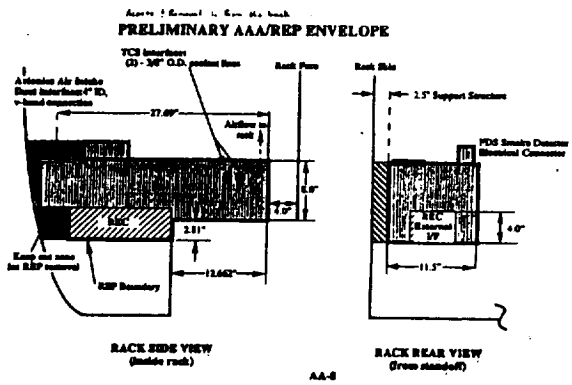

Figure 9.3 : Internals of ISPR

Another consideration in the placement of the experimental volume is the physical accessibility of the experimental facility to the other "support" components in the ISPR. Along the back of the experimental volume, ample room is provided for HVAC ventilation components, as well as cables from the computer monitoring system. In the event of failure, all of the components of the APCGF can be accessed by astronauts from the front of the ISPR. (see Figure 9.15, section 9.8.1)

The failure considerations are the final concerns dealing with the placement of the experimental facility. The next spatial considerations are the placement of the exterior "support" components within the rack. These components are the HVAC/Environmental Control System and the Data Management/ Computer Control System. The major component of the Environmental Control system is the AAA, which was considered when determining the placement of the experimental volume. The AAA will be placed as shown in Figure 9.3. The only other major component of the environmental control system is a dehumidifier, which will be placed directly under the AAA (this will give plenty of room for a standard sized dehumidifier). The computer for the Data Management system will be located in the lower left hand corner of the ISPR. See Figures 9.4 and 9.5. The space between the computer, located on the bottom lower left of the ISPR, and the AAA device, located on the lower right of the ISPR, will be used for the Workhorses (to be described in the Section 9.4.2). With the placement of the final Data Management components, the general layout of the ISPR is complete, and the next major consideration is the accessibility of the APCGF to astronauts.

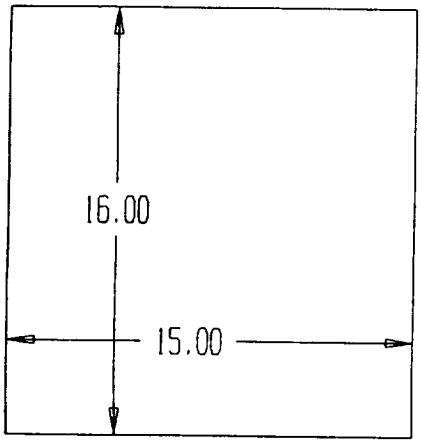

Figure 9.4 : Computer - Front View

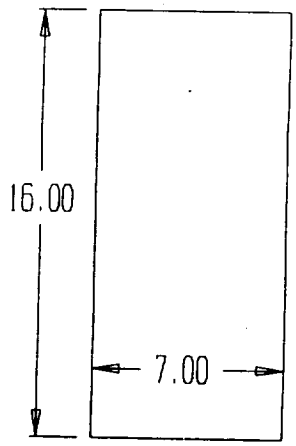

Figure 9.5 : Computer- Side View

9.4.2 Human Interface

The APCGF is designed to provide enough space to grow a minimum of 500 protein crystals during the 90 day untended period. The need for a system to store the quenched crystals originated because some crystals grow in less than a week. The problem was first defined by exploring the requirements of a system that could allow for the removal of the crystals. The design team decided that more than 500 crystals could be grown using a rotation of active growth and storage sites. The storage

sites needed to be easily removable for astronauts to collect and return to earth for structural analysis of the crystals. The idea of a system of drawers was decided upon and a brainstorming session was held to develop possible concepts. It was then announced that the rack environment could not mix with the SSF environment. The idea of a cylindrical drawer was then developed. This drawer could be made with an o-ring seal to separate the two environments and still be easily removable by an astronaut See Figure 9.16 section 9.8.1. A sleeve was created to seal the inside of the experimental facility from the SSF environment during the removal of the storage trays. Several requirements were generated for a locking mechanism to prevent the drawer from floating out of its sleeve while in micro gravity. These requirements included long life, the ability to withstand vibrations during shuttle launch, ease of operation, and a minimum of moving parts. Several concepts were generated that could satisfy these requirements. These included a spring loaded trigger release, a torsionally spring loaded lock, and a key way. The key way concept proved to be the most feasible. The drawers are 6 inches in diameter and 27 inches long. These dimensions are compatible with the previously determined experimental volume and rack layout. Fourteen drawers are placed concentrically around the experimental area. The drawers and sleeves (Figure 9.17, section 9.8.1) must be lightweight to reduce cost, yet strong enough to withstand shuttle launch conditions. On this basis, Aluminum, which has performed well on many shuttle missions, will be the material for the drawers. The sleeve is a cylindrical tube that holds the drawer and keeps the seal. This component has a slightly larger diameter than that of the drawer, and a cutout section 5.25 inches wide and 21.3 inches long to provide access to the interior of the experimental facility. The opening of the drawer faces the interior of the experimental facility, and can be rotated 29.3 degrees for the vacuum (Figure 9.6) and another 29.3 degrees to fit the key way that allows for drawer removal. The drawer can then be reloaded with new chambers, inserted back through the key way, and rotated to its original position for more experiments.

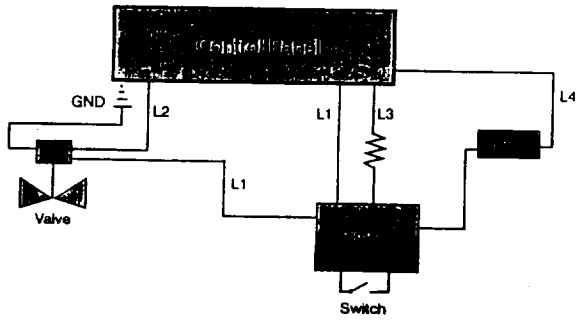

Figure 9.6 : Vacuum Electrical Schematic

The environments of the space station and rack must be separated because of the possibility of contamination of SSF by broken chambers. A Teflon o-ring was chosen as the drawer seal. Greg Lucas of Parker Packing, Inc. was consulted as to the use of Teflon seals, and a PTFE Flexisteal spring loaded seal was chosen as the best option for o-rings (Table 9.1, section 9.8.2). The space station provides a vacuum system which will be connected to the storage drawers in order to remove any excess gasses from the interior of the experimental facility. This system is connected to the drawers by way of a manifold and fourteen hoses. An electronic valve will open the vacuum.

The emergency access drawers are the final human interface concern. These doors provide the astronauts with access to the interior of the experimental facility. The requirements for the door are: must maintain an airtight seal, be light weight, withstand vibrations due to shuttle launch, have long life with little maintenance, allow easy access to the facility, consume very little space, be transparent, not protrude into the space station corridor, and allow for the use of space gloves. A regular door with an o-ring was chosen to fit these design requirements (Figure 9.18, section 9.8.1). Two separate doors are used in order to avoid any intrusion upon the space used for the robot running bars. Human anthropometric were also considered in the development of the door. The door design includes a half inch thick aluminum frame that is 21.5 X 15.75 X 3 inches on the outer edge. The door size is 16.5 X 10.75 X 0.5 inches. The four Davis Horizontal Handle Toggle Action Clamps, can be used to generate

150 pounds of force for a sealing pressure of 182.0 psi. The teflon o-ring to be used will have a diameter of .139 inches and be set in a groove with a depth of .124 inches and a width of .187 inches.

9.4.3 Data Management

The APCGF has a computer system which controls the Zymate II robot, the data collection system, and the heating of the facility. The computer commands the robot to retrieve an inactive crystal chamber and activate it. After activation, the computer checks the growth of the crystal and ultimately commands the robot to quench the crystal and replace the finished crystal in storage.

Previous attempts to create an automated protein crystal growth facility resulted in the use of an optical device to determine the nucleation and growth rate of protein crystals. This system allowed NASA scientists to control the quenching of the protein growth. The APCGF uses an updated design of the previous system, a 280 nm UV light source to monitor the nucleation and growth rate of the protein crystals. The previous system used a photo transistor that monitored the absorption spectrum of the growing protein crystal.

The APCGF uses an adaptation of the previous system and offers an option for automatic or ground-based quenching. The APCGF contains a UV light source that transfers the light down a bundled fiber optic cable along the robot arm to the end effector. The IBM 386/486 directs the robot to illuminate a specific crystal site to check the growth rate of the crystal. The transmitted light is absorbed with a photo transistor and converted into an analog signal to be stored and analyzed in the IBM 386/486.

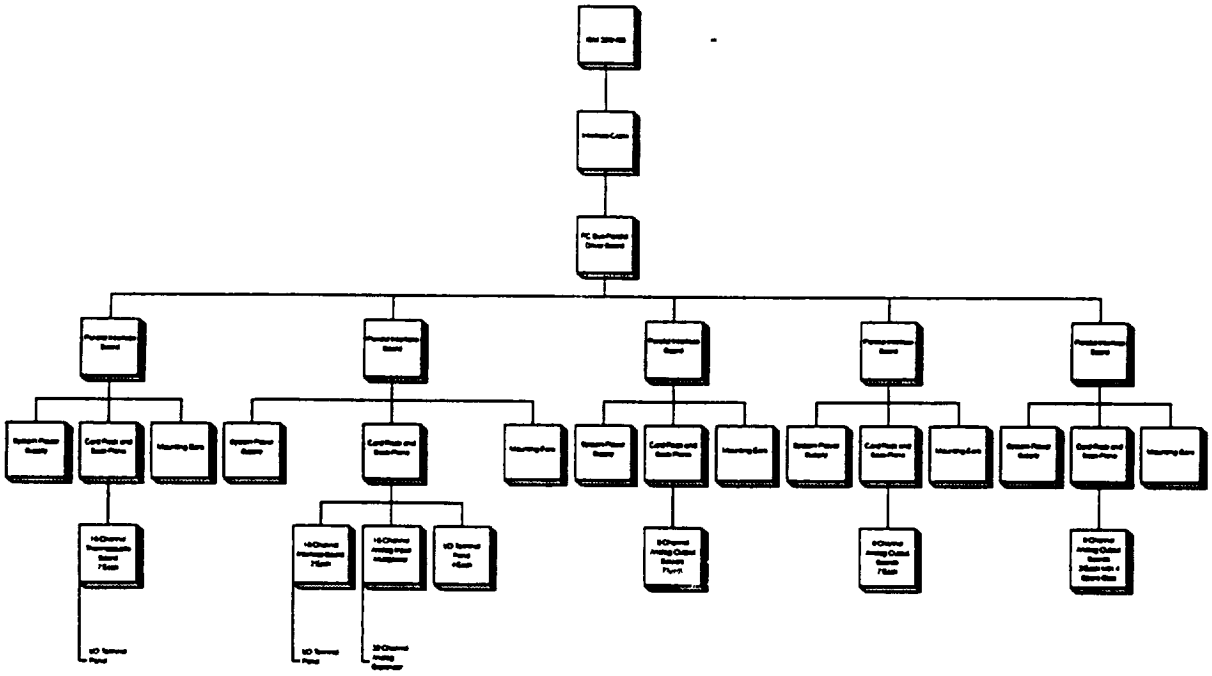

Figure 9.7 : Electrical Block Diagram

The IBM 386/486 receives digital data from a source, located in the base of every active crystal chamber, and sends the data to the Workhorse system that converts analog to digital data. The Workhorse system consists of five (5) interconnected Workhorses (Figure 9.7). Each Workhorse contains 132 separate analog input connections that receive thermocouple and photo transistor data, as well as 132

output connections that supply power to resistance heating coils in order to individually control the temperature of each crystal site. The optics system monitors the rate of each crystal's absorption of UV light allowing for the automatic control of nucleation and growth. A bill of materials can be found in section 9.8.2, Table 9.2.

The timing of the data retrieval is determined by the rate set from prior experiments and updated by the computer. The computer system stores the data of the crystal growth rate for monitoring from the ground. The system is connected to SSF's mainframe and allows the transmittal of data to scientists on the ground.

The management of data and the control of the overall APCGF is done by an IBM 386/486 in coordination with the SSF mainframe. The analog data collected by the thermocouples and photo transistors is converted into digital data to be stored in the IBM 386/486 for eventual down link to NASA's mission control. The entire facility is automatic and needs only to be reloaded every ninety (90) days by an astronaut. There are options for direct control by mission control of the experiments, but the system has the ability to decide the duration of each experiment automatically. The only part of the APCGF, that is not under direct control of the facility, is the cooling system; however, the rack computer has the ability to shut down any system at any time, specifically during emergencies. A complete system diagram is provided in Figure 9.8.

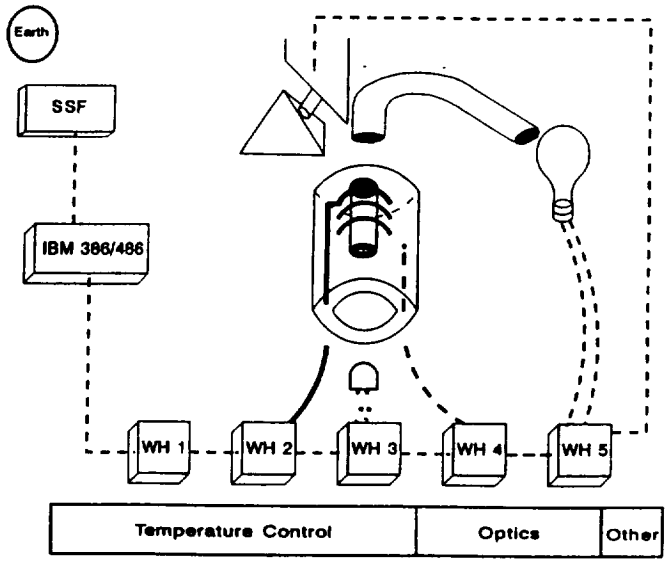

Figure 9.8 : Diagram of Data Management System

9.4.4 Environmental Control

A major systems integration issue is environmental control. This consists of providing the proper lighting, temperature, humidity, and pressure to support the experimental project. In the case of the automated protein crystal growth facility, systems integration was responsible to design a system that would individually control the temperature of the growing crystal at each of 132 active experimental sites. The growing crystals must be kept within .5C of the desired temperature. The system must be able to detect the temperature of the growing crystal, and respond automatically to maintain the preset temperature if the detected temperature is not satisfactory. As mentioned before, the chambers are sealed and coated, which not only prohibits mass transfer into and out of the chamber, but also prevents radiation heat transfer from taking place. Thus, with respect to the chambers, the objective of the environmental control system is to regulate temperature only.

With respect to the automated protein growth facility, Space Station Freedom in general, and its operators, however, other issues must be addressed. Of utmost concern is the protection of the men and women who will be interfacing with the facility. The environmental control system must be designed and integrated in such a manner as to ensure the safety of these astronauts. Thus, proven techniques for providing the proper environment must be employed, so that expensive testing may be held to a minimum. Secondly, the environmental control system must meet SSF standards for vibration, heat

release, power consumption, fire protection, and launch procedures. Without meeting these requirements, any facility design is of no use. Finally, the environmental control system must not be harmful to the other components of the facility, such as the computer equipment and robot.

When developing the concepts for meeting these requirements, it became clear almost immediately that the system must combine a heating and a cooling system to maintain each individual site temperature. This could be accomplished by heating the facility to a temperature above 25 C (the maximum temperature at which the crystals is grown), and then cooling each site separately according to the individual site requirements. Conversely, these requirements may also be met by providing general cooling of the facility (below 4 C) and providing individual site heating.

For many reasons, the latter concept best meets the design requirements. First, the general cooling of an experimental facility has been done in space many times. In fact, NASA and Boeing have developed hardware that serves this very purpose. On the basis of this information, the general cooling system concept has merit. It is safe for the astronauts and for SSF, as well as the facility itself. However, due to the low temperature of the facility air, a dehumidification unit must be added to the base system, so that the relative humidity is maintained lower than 100% (condensation may damage the electronics). In addition, the air must be recirculated continuously to reduce the load on the equipment, especially the dehumidifier.

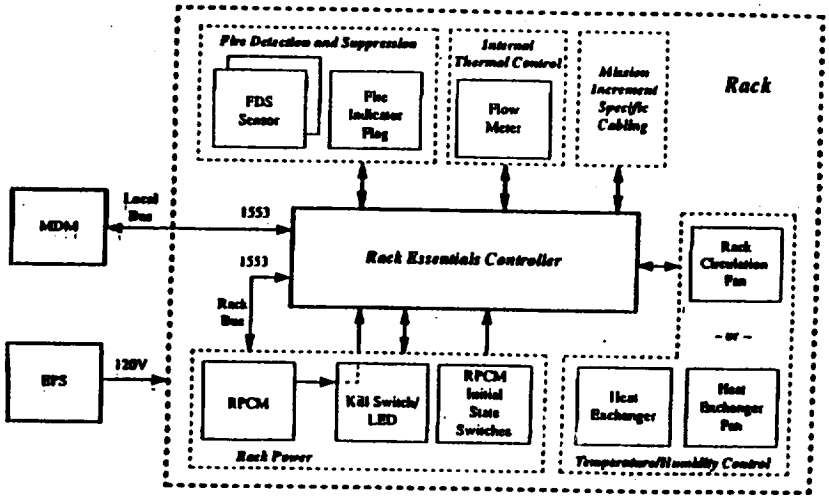

Figure 9.9 : Rack Essentials Controller

The base hardware offered by NASA and Boeing is called the Avionics Air Assembly (AAA). This hardware may be connected to the Space Station's low-temperature loop, which will enable the facility to reach the desired ambient temperature. The air flow rate will be roughly .057 m^3/s, and will flow from the wall on which the robot is mounted to the front of the facility, and back to the robot around the perimeter of the facility. The Rack Essentials Package (REP) is a mandatory package that provides fire detection and suppression (Figure 9.9). Unfortunately, the dehumidification technology does not exist at this time. Thus, the design of the environmental control system is not yet complete. The recommendations section of this report discusses this issue, along with other future design work possibilities

Likewise, the concept of electrical resistance heating for experimental sites is a common approach. It is a safe method of heating, and there are many existing materials that are capable of providing such heating. In addition, electrical resistance heating is 100% efficient, and is more easily controlled by an electronic system. In an effort to reduce temperature gradients within the chamber, and to lower the necessary power consumption of the system, the heating wire, with a diameter of .00002 m, a length of 2.93 m, and composed of 72.5% Fe, 22% Cr, and 5.5% Al, is placed inside the chamber and wrapped around the pedestal. This alloy was selected because of its low thermal expansion coefficient, low variation in resistance with temperature, high strength, and high resistivity (the highest of all the

common heating materials) [1]. Additionally, a Copper-Constantan thermocouple is placed on the pedestal, as close as possible to the growing crystal. These thermocouple materials were chosen because of their high voltaic sensitivity, low cost, small error, and the availability of these wires in small diameters [2]. Electrical connection of the heating wire and the thermocouple is made via the metal spring connection outside the chamber. Refer to Table 9.3, section 9.8.2 for the bill of materials.

The general cooling and dehumidification system is controlled by the data management system. If a thermocouple placed in the facility detects that the ambient air temperature is above the preset temperature, the control system will engage the cooling system. The dehumidification unit will activate if the relative humidity exceeds the preset value. If the temperature or humidity drop below their preset values, the systems will disengage automatically. Likewise, the growth temperature for each active experiment is stored in the data management system. A similar thermostatic process is used to control the temperature of the growing crystal. The range of crystal temperatures is 0.5 C.

A physical model of heat transfer was employed to determine the characteristics of the design. The model is based on forced convection of air (from the cooling unit) across the exposed ends of the cylindrical chambers. If the heating wire and cooling unit were perfectly sized so that they could stay on continuously and maintain steady-state conditions, the heating wire at the specified size must have a resistivity of .00006 ohm*m to maintain a crystal at 298 K with 277 K ambient air. However, the physical model used to derive these numbers is by no means exact. In order to be conservative, the common heating material with the next lowest resistivity to the theoretically correct material was chosen (the previously mentioned Fe-Cr-Al alloy). This material has a resistivity of .000001455 ohm*m, an order of magnitude lower than necessary [1]. Consequently, the heating wire produces excess heat, and must be turned off and on by the thermostatic control to maintain a preset crystal temperature. The temperature of the heating coil, during actual operation, is 350 K (77 C), which is not high enough to melt the polyethylene around which it is wrapped. Incidentally, the heating wire is expected to only be in operation 2.5% of the time. If a coefficient of performance of 2.5 is assumed for the cooling unit, thermal waste heat from the equipment is assumed to be 100 W, and if it is assumed that the walls of the facility are composed of 2" polystyrene boards (except for the access wall), the total cooling load is 1056 W, and the total power requirement is 525 W [4]. For a full explanation of heat transfer modeling, including assumptions, equations, and intermediate values, consult the appendix, section 9.8.3.

9.5 Conclusions

The experimental volume in the ISPR was maximized using the dimensions of the Zymate II robot and support equipment as constraints. The environment of the experimental area is completely sealed from the SSF environment through the use of cylindrical storage drawers which function as airlocks. The maintenance demand of the system is low, as these storage drawers can be changed out in approximately 30 minutes. In the event of additional maintenance requirements due to a failure in any part of the facility, front access panels offer the astronauts access to the robot as well as the active and storage sites.

The APCGF contains an IBM 386/486 control system that provides direct system analysis for all systems. The IBM 386/486 allows for automated production of protein crystals using a UV light source and nucleation detection system. This apparatus allows the computer to directly monitor and control the protein crystals throughout the entire growth process.

The environmental control system will maintain an ambient facility temperature of 4 C by using the standard AAA/REP package, equipped with a dehumidification device, connected to the low temperature loop on the Space Station. The cooling unit will be controlled by a thermostat. The temperature of the individual experimental sites will be regulated by a heating wire that is placed inside the chamber, wrapped around the pedestal. It, too, will be thermostatically controlled. Electrical

connections will be made through the bottom of the chamber, via a spring conductor on the outside of the chamber. The heating wire is 2.93 m long, with a diameter of .00002 m. It is constructed of an alloy containing 72.5% Fe, 22% Cr, and 5.5% Al by mass. All thermocouples used in environmental control are constructed of copper and constantan. The heating wire reaches a maximum temperature of 350 K during operation. The total power requirement for this system is 525 W.

9.6 Recommendations

All of the designs presented should be further developed. The concepts are well developed, but must be refined on a detailed level. One particular item that demands further research and design work is the sizing of the electronic data gathering components (Workhorses). A custom system of Workhorse components must be developed for this system. The current Workhorse components simply will not fit into the bottom of the ISPR, but the components could easily made smaller with customization.

Another issue that calls for further design is the vacuum system safety valve. A mechanism to lock the storage drawers in place during activation of the vacuum system must be designed. Additionally, the emergency access doors could possibly be combined into a single drawer that does not interfere with the space used by the robot. This possibility has not been fully investigated.

As mentioned before, the general cooling/dehumidification has yet to be fully developed. It is a possibility that the dehumidification unit may be combined with the existing AAA system. If this is not possible, then perhaps the design objective for this system will include a total redesign of the space-ready environmental control equipment. Whatever the case, the REP must be a component of the final design, as it is necessary in order to meet SSF standards.

In addition to the redesign of the ambient air control system, the physical model employed in calculating critical property values, energy requirements, and temperatures must be tested. Since natural convection is not a factor in the heat transfer dynamics, the system will be capable of being tested on Earth. Some of the important considerations include: frequency of heating wire activation and deactivation, total power load, temperature of heating wire, proper thermal monitoring of crystals, and competency of heating wire.

9.7 References

(1) Boyer, Howard and Timothy Gall. Metals Handbook. Metals Park, OH: American Society for Metals, 1985.

(2) Dike, Paul H. Thermoelectric Thermometry. Philadelphia: Leeds and Northrup Company, 1954.

(3) Incropera, Frank P. and DeWitt, David P., Introduction to Heat Transfer. New York: McGraw-Hill, 1981.

(4) McQuiston, Faye C., and Parker, Jerald D., Heating, Ventilating, and Air Conditioning. New York: John Wiley & Sons, 1988

9.8 Appendices

9.8.1 Figures

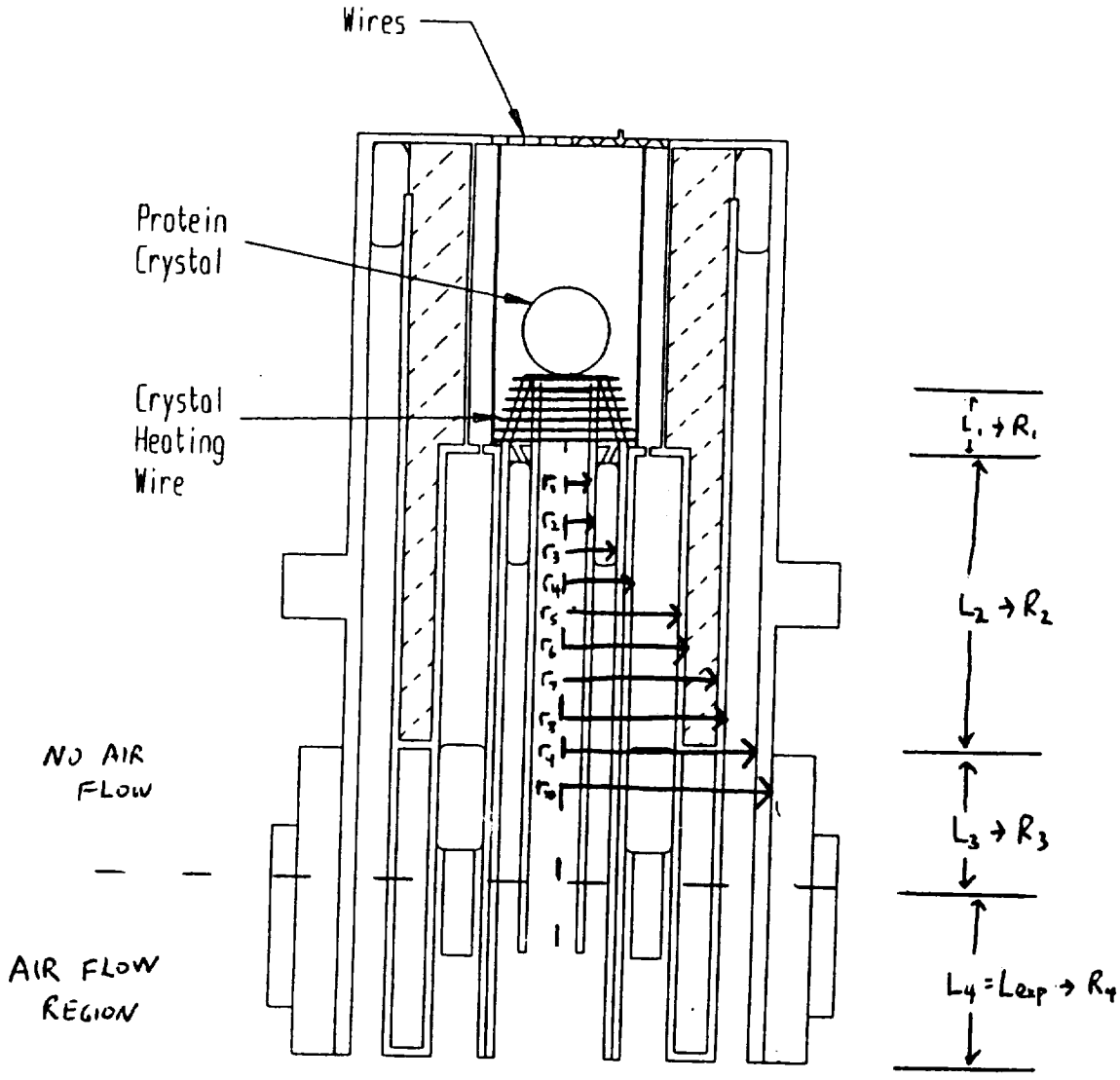

Figure 9.10 : Chamber for PCG

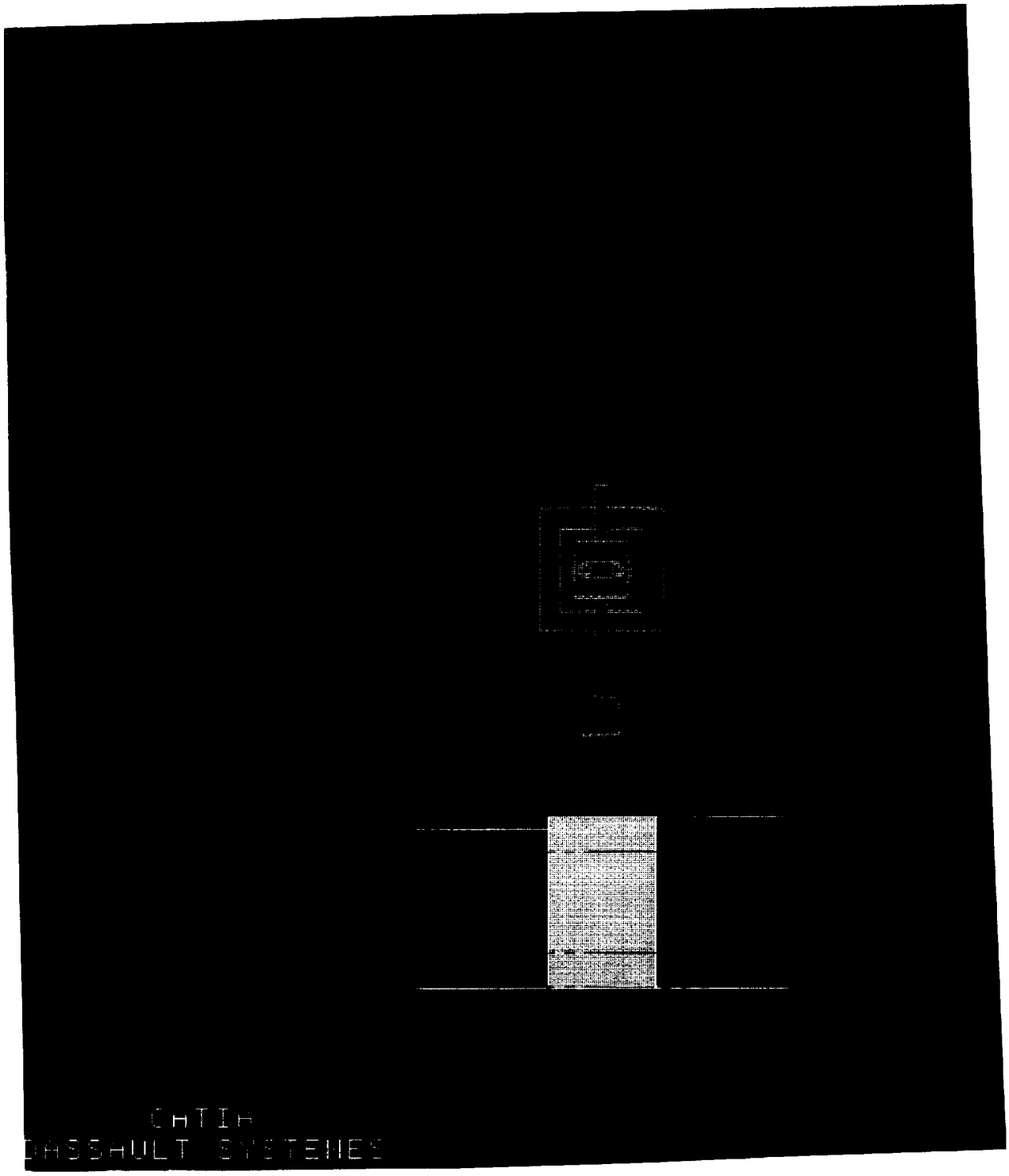

Figure 9.11 : ISPR - Front View

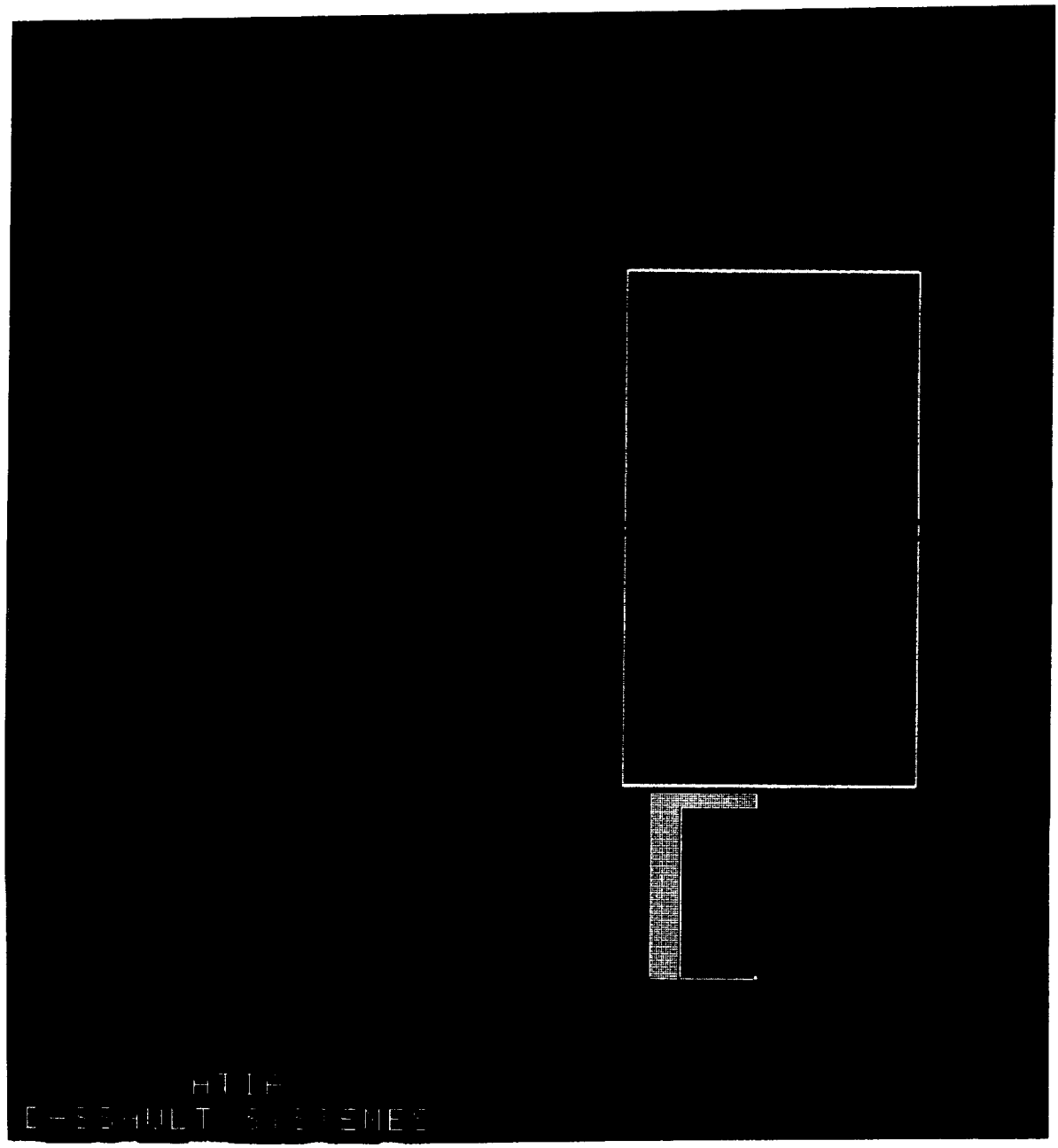

Figure 9.12 : ISPR - Side View

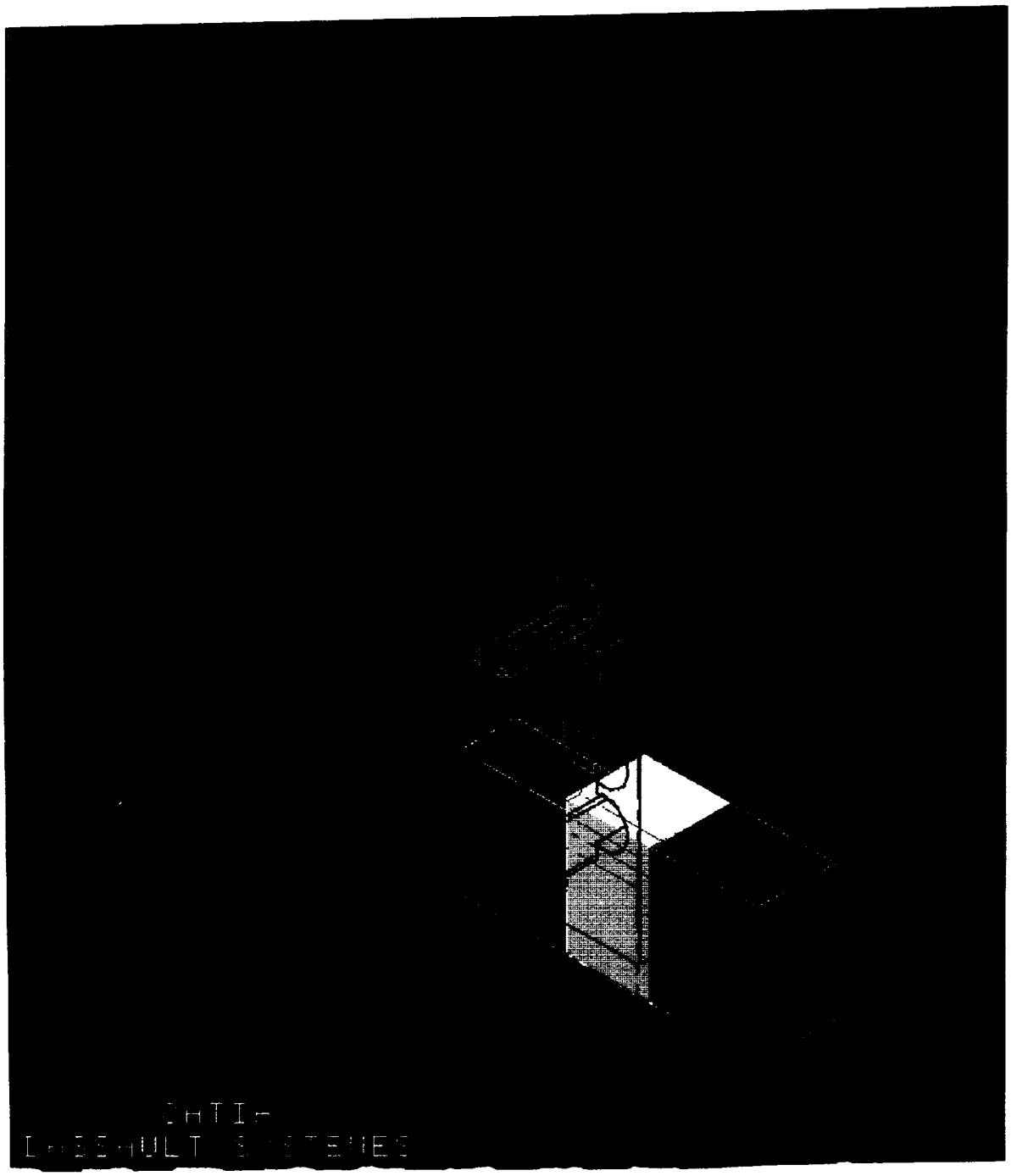

Figure 9.13 : ISPR Rendering with PCRF

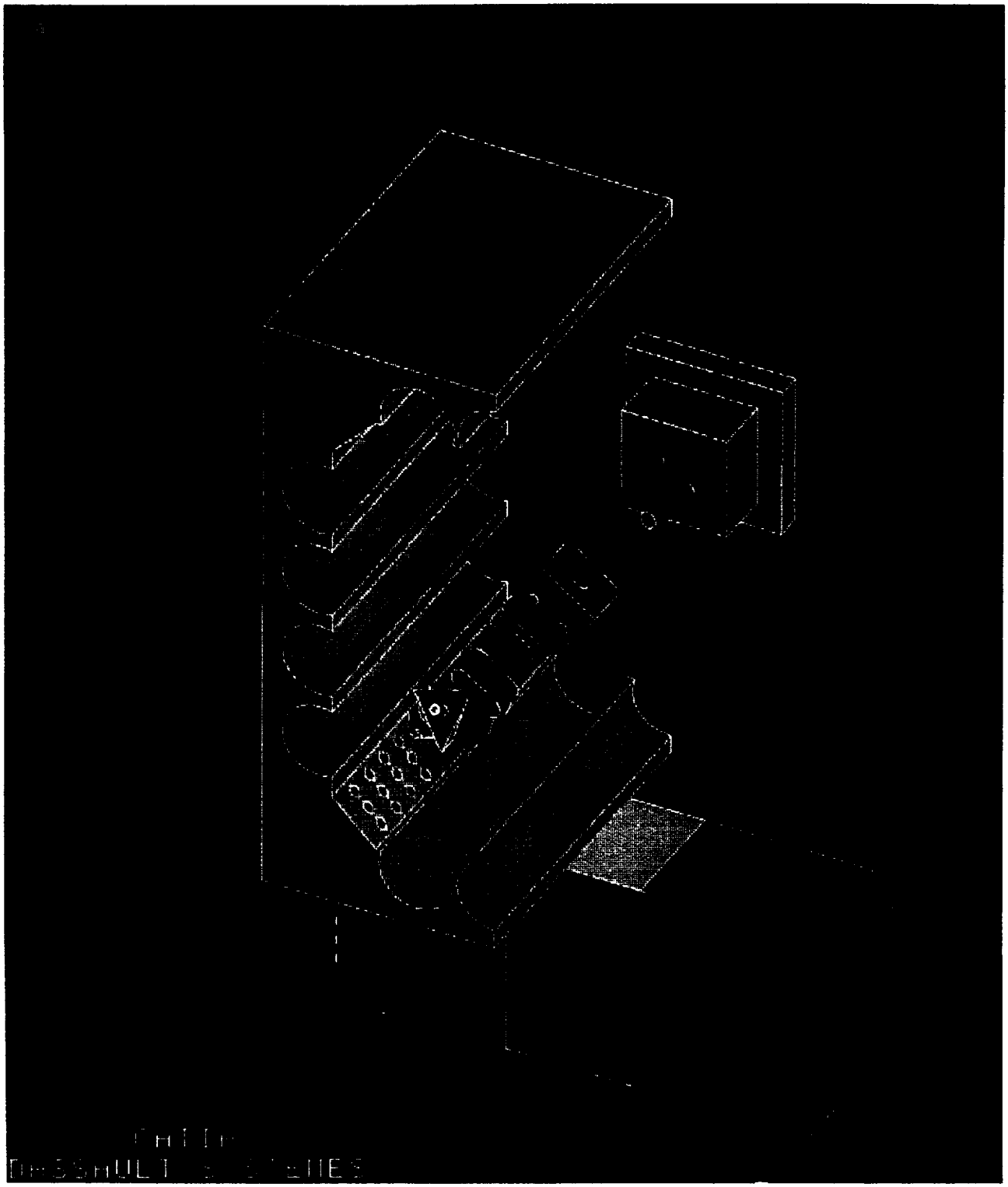

Figure 9.14 : ISPR Internal Rendering

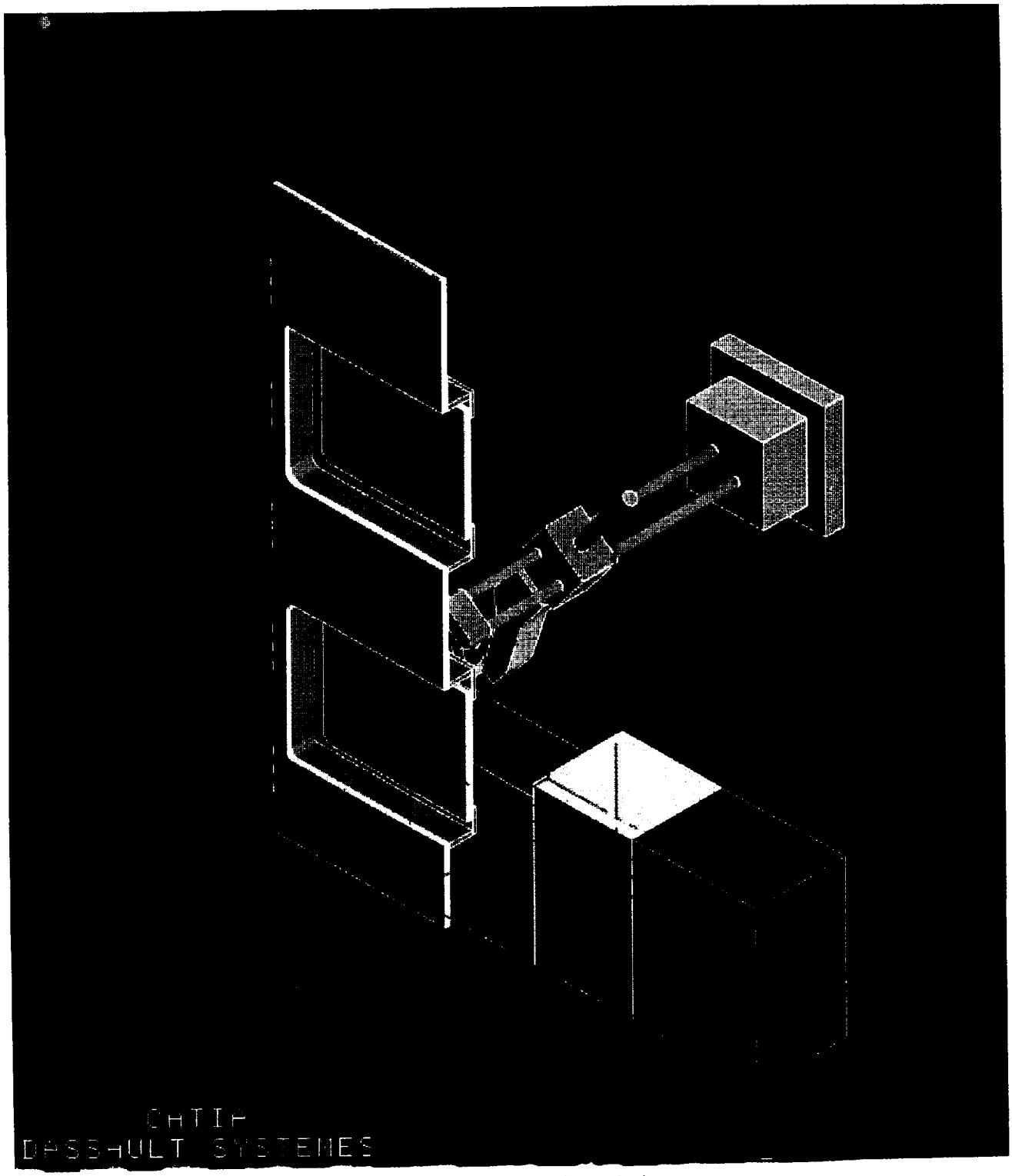

Figure 9.15 : ISPR Internal Rendering

ORIGINAL PAGE
COLOR ~~PHOTOGRAPH~~
ILLUSTRATION

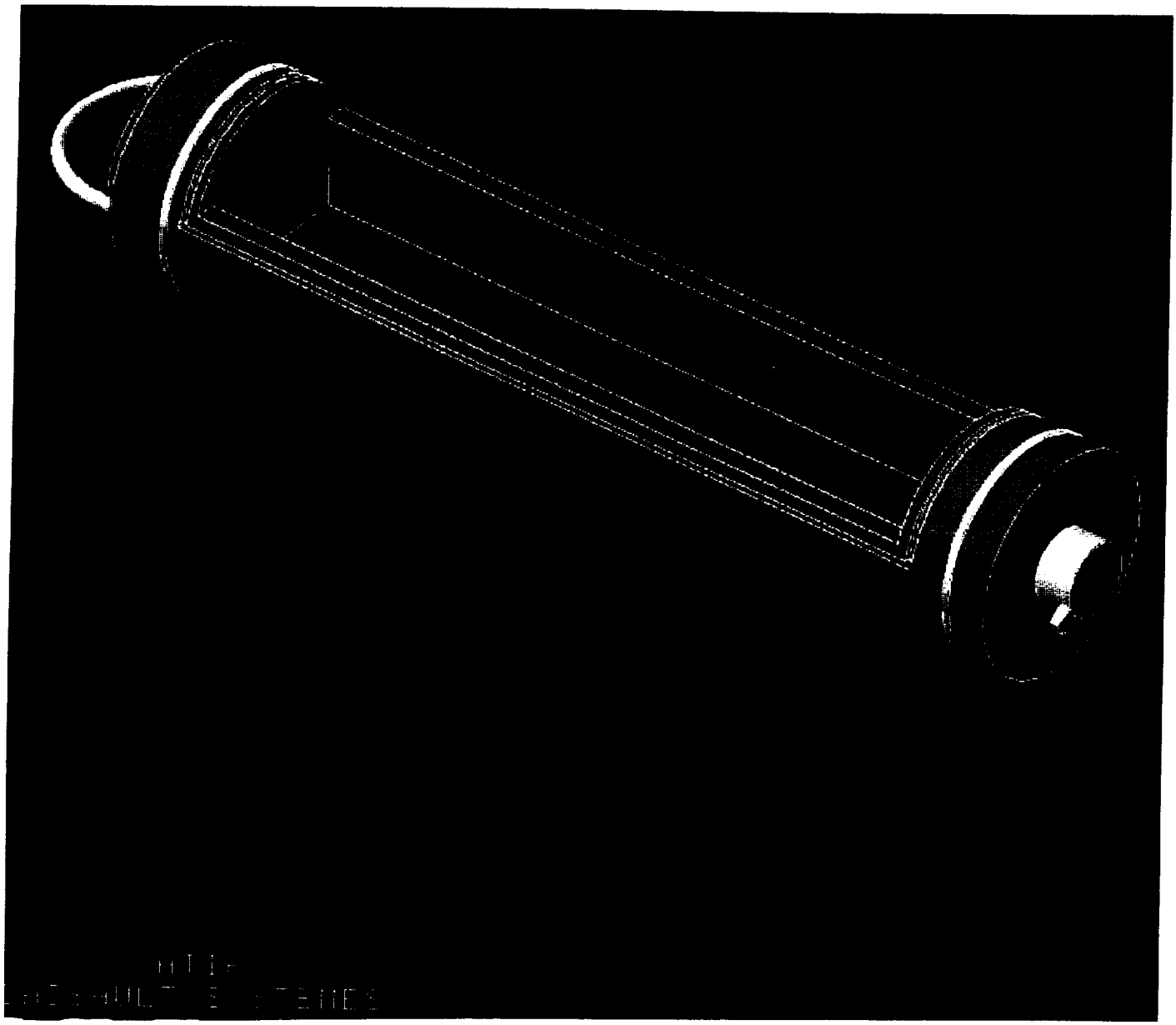

Figure 9.16 : Drawer Rendering

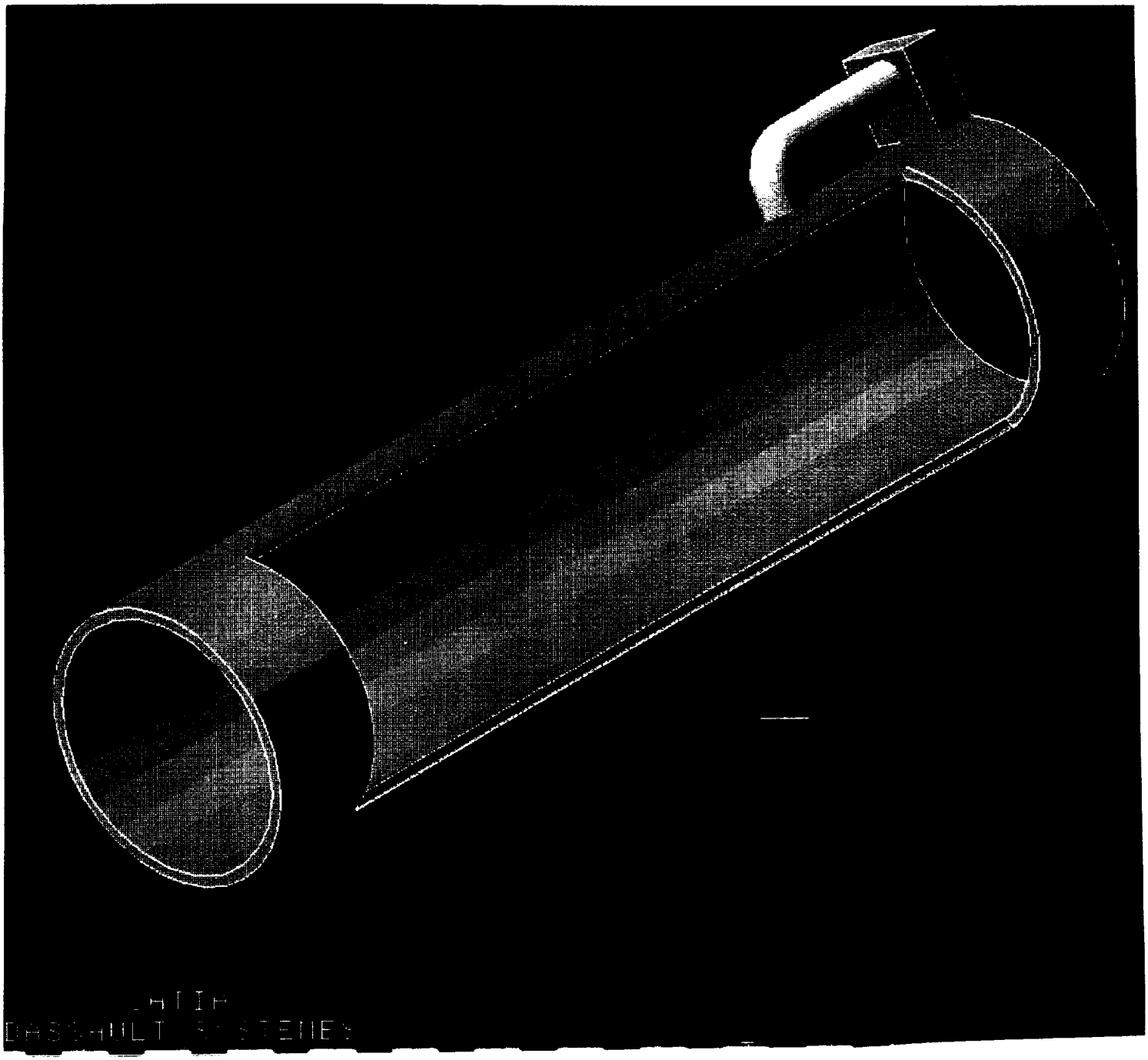

Figure 9.17 : Drawer Sleeve Rendering

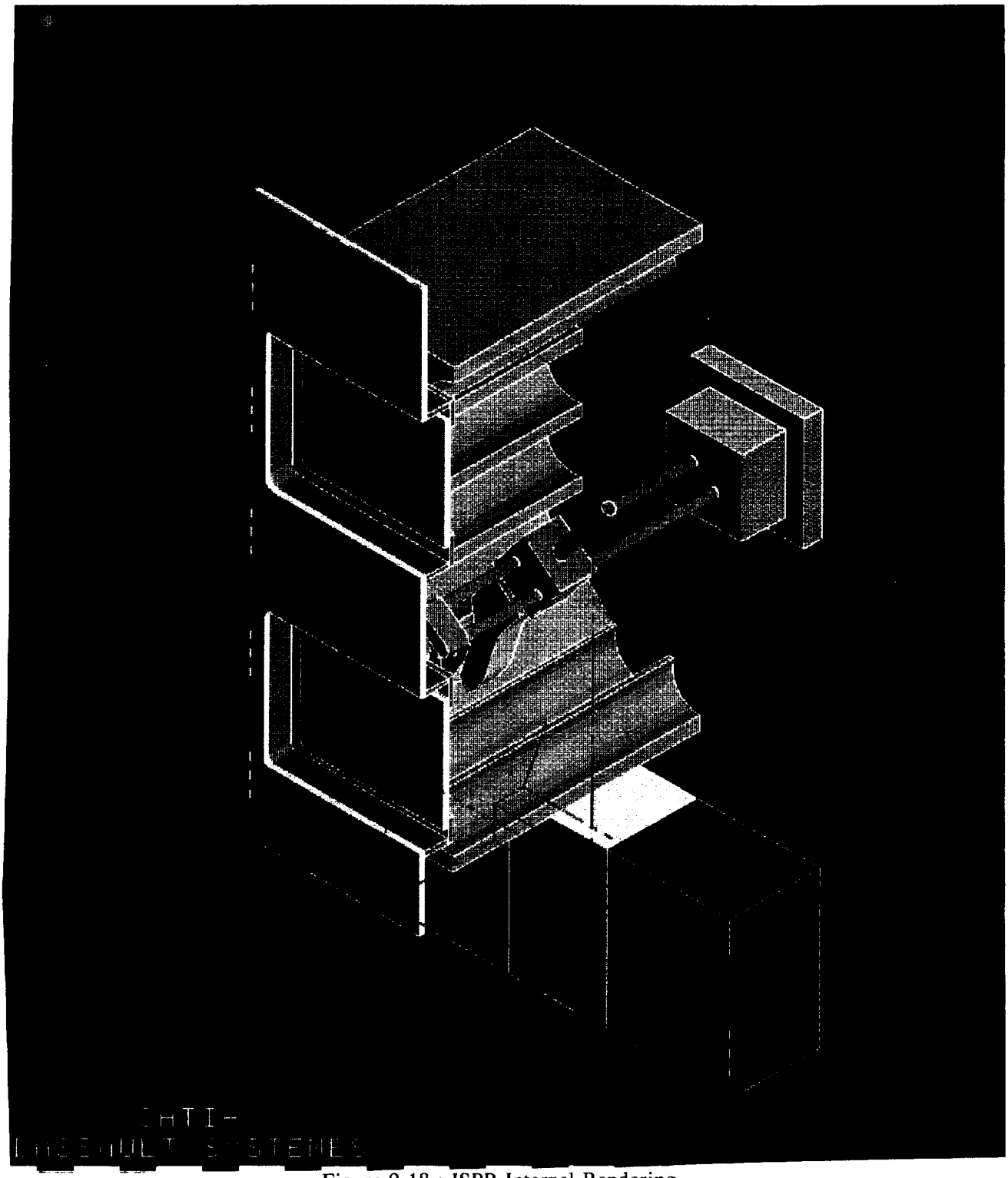

Figure 9.18 : ISPR Internal Rendering

9.8.2 Tables

Table 9.1 : Bill of Materials and Cost Estimates - Human Interface

Precision Measurements Inc.				
Reference Number	**Part Number**	**Quantity**	**Price Ea. ($)**	**Description**
1	6061	6 ft^2	TBD	0.5 in Al Plate
2	6061	32 ft^2	TBD	0.25 in Al Plate
3	6061-T6511	35 ft	TBD	Extruding Al Pipe (6" OD)
4	6061-T6512	35 ft	TBD	Extruding Al Pipe (6.5" OD)
5	8210B27	1	334	Electronic Brass Valve
6	249-7871-331-504	1	763	LED Light
7	81951	1	9.48	Electronic Switch
8	Cb-1047 D20	1	47.75	Electronic Timer

Table 9.2 : Bill of Materials and Cost Estimates - Data Management

Ref Num	Part Number	Quantity	Price Ea ($)	Description
Workhorse Catalog : Keithley Data Acquisition - Volume 24 - 1991				
1	WH-CRO-03	6	75	3 ft Long, Round, Shielded, Interface Cable
2	WH-PCDB-PAR	1	450	PC Bus Parallel Driver Board, Non-isolated, 25 Pin, Data Transfer
3	WH-PWR-100/NA	5	750	System Power Supply, 100 Watt
4	WH-CH-7	5	775	Card Rack and Backplate, 7 Slots for I/O
5	WH-CIB-PAR	5	425	Parallel Interface Board
6	WH-ME	5	50	Mounting Ears
7	WH-TC-16	9	825	16- Channel Thermocouple Input Board
8	WH-P-40CJC	9	125	I/O Terminal Panel, Temperature Sensing Element and Isothermal Panel on Board
9	WH-AIN-16	1	875	16 Channel Analog Input Multiplexer
10	WH-AEX-32	4	500	32 Channel Analog Expander
11	WH-S-80	4	110	I/O Terminal Panel, 5mm Screw Terminals
12	WH-AO-8	17	1100	8 Channel Analog Output Boards
Computer Catalog : CompuAdd Express - Spring 1993				
13	2950	1	2195	486DX2, 66MHz, 170MB, Intel Vendor
Optics Catalog : Anixter Wiring Systems Catalog - 1992-1993				
14	370-947-FDDI-36	1	45	6 ft Stranded Multi-fiber Cable (Indoor)
Electrical Connections Catalog : Anixter Wiring Systems Catalog - 1993-1994				
15	9J-2403-000B	1	600	800 ft Beldfoil, Sheilded, 3 Pair, Plenum-Paired Cable

Table 9.4 : Bill of Materials and Cost Estimates - Environmental Control

Precision Measurements, Inc.				
Reference Number	**Part Number**	**Quantity**	**Price Ea. ($)**	**Description**
1	TBD	2.93 m	TBD	72.5 Fe, 22 Cr, 5.5 Al Wire (0.02 mm dia.)
2	TBD	0.038 m	450	Constantine Wire (per chamber)
3	TBD	0.038 m	750	Copper Wire (per chamber)

9.8.3 Calculations

The heat transfer that takes place inside the chamber may be approximates by 1-D heat transfer analysis. All energy generated by the heating wire will be transferred radially to the crystal, and then down the chamber to the exposed end (the end is exposed due to the length needed for the end effector to grasp the chamber). The exposed end is modeled as a fin undergoing convective heat transfer to the flowing air around the cylinder. Al surface area of the chamber, except for the exposed end, is perfectly insulted by the alumina silica that stores the chambers (4). Refer to the glossary which follows for the definitions and units of all of the variables used. Elementary geometric equations will not be shown.

A_{ch} = cross-sectional area of chamber (m^2)
A_{hc} = cross-sectional area of heating wire (m^2)
A_{fac} = cross-sectional area of facility through which air is forced (m^2)
D_{ch} = diameter of chamber (m)
D_{hc} = diameter of heating wire (m)
h = convective heat transfer coefficient for exposed cylinder and moving air (W/m^2K)
K = degrees Kelvin
K_{air} = thermal conductivity of air (W/mK)
K_{fin} = equivalent thermal conductivity of exposed end of chamber (W/mK)
K_{poly} = thermal conductivity of polyethylene (W/mK)
K_{rub} = thermal conductivity of stopper (W/mK)
K_{water} = thermal conductivity of solution (W/mK)
L_1 = length of pedestal on which heating wire is wrapped (m)
L_2 = defined fraction of chamber length (m)
L_3 = defined fraction of chamber length (m)
L_4 = defined fraction of chamber length (m)
L_{exp} = length of chamber exposed to moving facility air (m)
Lhc = length of heating wire (m)
m = constant for use in heat transfer from fins (m^{-1})
n = number of active experimental sites
Nu = Nusselt number for air
v_{air} = kinematic viscosity of air (m^2/s)
P_{ch} = circumference of chamber (m)
P_{req} = total power requirement of environmental control system (W)
Pr = Prandtl number of air
q_{dot} = average heat generation at site with maximum crystal temperature (W)
q_{WORST} = actual heat generation during operation at site (W)
Q = volume flow rate of air through facility (m^3/s)
Q_{dot} = cooling load on central unit (W)
Q_{gen} = thermal energy supplied by inefficiencies of facility equipment (W)
r_1 = defined radius of chamber (m)
r_2 = defined radius of chamber (m)
r_3 = defined radius of chamber (m)
r_4 = defined radius of chamber (m)
r_5 = defined radius of chamber (m)
r_6 = defined radius of chamber (m)
r_7 = defined radius of chamber (m)
r_8 = defined radius of chamber (m)
r_{10} = defined radius of chamber (m)

R_1 = defined axial resistance inside chamber (K/W)
R_2 = defined axial resistance inside chamber (K/W)
R_3 = defined axial resistance inside chamber (K/W)
R_4 = defined axial resistance for exposed end of chamber (K/W)
R_{acc} = thermal resistance between facility and cabin air (K/W)
R_{bot} = thermal resistance between facility and air to the bottom (K/W)
R_{hc} = minimum electrical resistivity of heating wire (ohm*m)
R_{rad} = thermal resistance between heating wire and crystal (K/W)
R_{rear} = thermal resistance between facility and air to the rear (K/W)
R_{sides} = thermal resistance between facility and air to the sides (K/W)
R_{top} = thermal resistance between facility and air to the top (K/W)
Re = Reynolds number for air
T_a = temperature of ambient facility air (K)
T_{acc} = temperature of the cabin (K)
T_b = base temperature of exposed end of chamber (K)
T_{bot} = temperature of air to the bottom of the facility (K
T_{crys} = maximum temperature at which crystals is grown (K)
T_f = film temperature between chamber end and moving air (K)
T_{hc} = operational temperature of heating wire (K)
T_{rear} = temperature of air to the rear of the facility (K)
T_{sides} = temperature of air to the sides of the facility (K)
T_{top} = temperature of air to the top of the facility (K)
V = voltage (Volts)
V_a = velocity of moving air (m/s)

In Section 9.8.1, Figure 9.10 shows the chamber dimensions that were used in the calculations.

L_3 and L_4 may be determined in the following way:

$$L_3 = 0.0152 - L_{exp}$$

$$L_4 = L_{exp}$$

V_a may be calculated from Q and A_{fac}:

$$V_a = \frac{Q}{A_{fac}}$$

R_1, R_2, R_3, and R_4 are thermal resistances along the length of the chamber. They are calculated by treating the different parts of the chamber as parallel circuits:

$$R_1 = \sqrt{\frac{\pi}{L_1} * (K_{air}(r_1^2 + r_3^2 - r_2^2) + K_{poly}(r_2^2 + r_4^2 - r_1^2 - r_3^2))}$$

R_3 and R_4 take a similar from.

$$R_2=\frac{\pi}{L_2}*(K_{air}(r_1^2+r_5^2-r_4^2)+K_{poly}(r_2^2+r_4^2+r_6^2+r_8^2+r_{10}^2-r_1^2-r_3^2-r_5^2-r_7^2-r_9^2)+K_{rub}(r_3^2+r_9^2-r_2^3-r_8^2)+K_{water}(r_7^2-r_6^2))$$

Rrad is based on cylindrical resistance. It will determine the temperature of the heating wire:

$$R_{rad}=\frac{Ln(r_4/r_3)}{2\pi L_1 k_{poly}}$$

The reynolds number for the flowing air may be calculated the following way:

$$Re=\frac{V_a D_{ch}}{v_{air}}$$

The Nusselt number may be calculated, knowing the Reynolds Number:

$$N=0.3+\frac{0.62Re^{1/2}Pr^{1/3}}{(1+(\frac{0.4}{Pr})^{2/3})^{1/4}}*(1+\frac{Re}{282000})^{5/8})^{4/5}$$

Now that the Nusselt number is known, h may be calculated:

$$h=\frac{K_{air}Nu}{C_{ch}}$$

If the exposed end of the cylinder were considered a fin, it would have a thermal conductivity of:

$$K_{fin}=\frac{L_4}{R_4\pi r_{10}^2}$$

Knowing this, a constant used for fin calculations may be computed:

$$m=\sqrt{\frac{hP_{ch}}{K_{fin}A_{ch}}}$$

For Simplicity, it is wise to define two new variables:

$$X=\sqrt{hP_{ch}K_{fin}A_{ch}}$$

and
Algebraic manipulation of the fin equation yields the following formula:

At this point, all the variables have been solved. For cooling load computations, it is best to use the q_{dot}

$$Y=\frac{\sinh(mL_{exp})+\frac{h}{mK_{fin}}\cosh(mL_{exp})}{\cosh(mL_{exp})+\frac{h}{mK_{fin}}\sinh(mL_{exp})}$$

$$q_{dt}=XY\frac{T_{crys}-T_a}{1+XY(R_2+R_3)}$$

The value of D_{hc} is input by the designer. Knowing this, L_{hc} may be determined:

$$L_{hc}=\pi(0.00511+0.5D_{hc})\frac{L_1}{D_{hc}}$$

Now, the required heating wire resistivity for steady state operations may be calculated:

$$R_{hc}=\frac{V^2A_{hc}}{q_{dt}L_{hc}}$$

However, the probability of successfully achieving steady state operations is almost zero, given the imperfections of the model. Therefore, the heating wire must have a lower resistivity that is needed, so that the wire may be activated and deactivated.
The actual R_{hc} is that of the selected Fe-Cr-Al alloy. When it is operating, the actual q_{dot} is given by the following equation:

$$q_{WORST}=\frac{V^2A_{hc}}{1455x10^{-9}L_{hc}}$$

from this value, The may be computed:

$$T_{hc}=T_{crys}+q_{WORST}R_{rad}$$

The fin base temperature id calculated by simple axial resistance:

$$T_b=T_{crys}+q_{dt}(R_2+R_3)$$

The film temperature at the end of the chamber and the air passing over the end is given by the following formula:

$$T_f=\frac{T_b-T_a}{\cosh(mL_{exp})+\frac{h}{mK_{fin}}\sinh(mL_{exp})}+2T_a$$

value rather that the q_{worst} value:

$$Q_{dt}=nq_{dt}+\frac{T_{tp}-T_a}{R_{tp}}+\frac{T_{bot}-T_a}{R_{bot}}+\frac{T_{sides}-T_a}{R_{sides}}+\frac{T_{acc}-T_a}{R_{acc}}+\frac{T_{rear}-T_a}{R_{rear}}$$

Finally, total average power consumption is determined by the following relation (COP of cooling unit assumed to be 2.5):

$$P_{req}=\frac{Q_{dt}}{2.5}+nq_{dt}+Q_{gen}$$

For a complete list of all computed results, see section 9.8.2, Table 9.3